Open-Framework Chalcogenide Materials -from Isolated Clusters to Highly ordered Structuresand their Photocalytic Applications

Beatriz Silva-Gaspar, Raquel Martinez-Franco, Gerhard Pirngruber, Antoine Fécant, U. Diaz, A. Corma

Open-Framework Chalcogenide Materials - from isolated clusters to highly ordered structures - and their photocalytic applications

B. Silva Gaspar,[†,‡] R. Martinez Franco,[‡] G. Pirngruber,[‡] A. Fécant,[*,‡] U. Diaz,[†] and A. Corma[*,†]

†*Instituto de Tecnología Química, Universitat Politècnica de València-Consejo Superior de Investigaciones Científicas, Avenida de los Naranjos s/n, E-46022 Valencia, Spain*

‡*IFP Energies nouvelles, Rond-point de l'échangeur de Solaize, 69360 Solaize, France*

E-mail: antoine.fecant@ifp.fr; acorma@itq.upv.es

Abstract

Photocatalytic processes are regarded as a sustainable and environmental-friendly way to attenuate mankind's strong dependence on fossil fuels, which are the main responsibles for high pollution levels in our planet. Metal microporous chalcogenides, due to band structure, bandgap value and highly reduced charge carrier's residence time within the crystal lattice, are probably more suitable for photocatalysis than metal oxides, the most used photocatalysts. This review, besides updating the existing literature, intends to expand on the possibilities of these materials. This review is divided into two parts. The first part will focus on materials science, more specifically on presenting the main chalcogenide clusters and materials that are made up by such clusters: structures analogous to zeolites and ultimately hybrid materials. To finish the section, three alternatives of synthesis that have been investigated recently are presented. The second part will focus on photocatalysis, in particular the application

of these materials for the production of solar fuels by H_2O photodecomposition and CO_2 photoreduction, and the degradation of organic pollutants. This review concludes by presenting the challenges of these materials and future perspectives for their synthesis and use as photocatalysts.

Contents

1 Introduction

The 20th century was marked by the rapid increase in world population, energy consumption and the emergence of new technologies, particularly in the transport sector and electrical appliances, making mankind dependent on the burning of fossil fuels. Such dependence of fossil fuels has enabled the enormous development of the countries in the western world. However, today mankind is facing the consequences associated with its exploitation, namely the reduction of available reserves and the harmful effects of their use, such as pollution and the emission of greenhouse gases. Although the direct cost of energy to the consumer is relatively low compared to other essential goods, the secret cost, the energy externalities, associated with the negative impact that its discovery, exploitation, distribution and consumption as well as the consequences on human health due to environmental pollution, is paid by society as a whole. One of the greatest externalities is the increase in greenhouse gas emissions. Although the amount of carbon emitted from anthropogenic sources is lower than the naturally exchanged between the biosphere and the atmosphere, this increase is enough to artificially alter the climate.[1–3]

The energy provided by the sun, about 120 000 TW of electromagnetic radiation, far exceeds the current energy needs of mankind. Solar energy has enormous potential as an

economical, abundant and clean energy source. However, it cannot be used directly. Since solar energy is diffuse and intermittent, the conversion of solar energy into useful energy should also involve concentration and storage. Nowadays, it is possible to find commercially available technologies that allow the thermal use of solar energy for water or home heating and for the production of electricity through photovoltaic panels.[1]

Recently, intensive research has been carried out in the area of photocatalysis in order to produce solar fuels. The first compound found to show photocatalytic activity was TiO_2 in 1972[4] and, since then, different ways to increase photocatalytic performance have been investigated. Different materials, such as metal oxides, metal and oxy-nitrides, metal chalcogenides, alkali metal base, polyoxometalate-based strucutres, with sometimes very specific combined structural arrangements between materials such as Z-scheme systems or others with interfaces forming Schottky barriers and organic materials, are being investigated for use as photocatalysts.[5–16] Among the materials presented, the metal oxides, metal chalcogenides and their composites stand out.[17]

The vast majority of oxides show high values for the optical band gap and can only absorb radiation in the UV region. Bearing in mind that only 5% of the solar spectrum is made up of UV radiation and about 43% of the visible radiation, the synthesis of materials with band gaps more adapted to solar radiation becomes essential to meet high yields of conversion, especially for the solar-to-fuel route.[18] Metal chalcogenides comprise a viable alternative to metal oxides, as they have a band gap more suitable for solar radiation.[19] It is already possible to find in the literature reference to the use of metal chalcogenides as photocatalysts in processes of pollutants degradation but also for the production of fuels.[20–28]

Microporous materials have, over time, attracted enormous interest in both scientific and technological fields. Since they allow the interaction with atoms, molecules and ions at the surface but also at the bulk, these materials have innumerable applications, namely in gas separation, ionic exchange and petrochemical industries.[29] Since the applications of these materials are closely related to their topology and chemical composition, intense research

has been carried out on the synthesis of new materials. According to Zheng et al.[30] there are several advantages in using crystalline microporous materials as active photocatalysts. The open framework architecture helps, due to the high surface area, increase the number of active sites, but is also likely to reduce the electron-hole recombination rate since it reduces the average carrier path to reach the surface of the catalysts particle where the reaction occurs. However, oxide based porous materials are mainly insulators (typically silica or silica-alumina), presenting limitations for applications involving photon absorption. Thus, in order to expand such applications, the synthesis of porous materials with semiconducting properties became desirable.[31] In particular, while the conduction band of transition metal oxides and transition metal sulfides materials is primarily derived from the metal s orbitals, the valence band is primarily derived from oxygen $2p$ orbitals for transition metal oxides[32] and for transition metal sulfides it derives from sulfur $3p$ orbitals,[33] allowing substantially narrowed bandgaps for the latter.

Recently, porous chalcogenides materials have received special attention, as they combine the presence of an open framework with semiconductivity, thus making it possible to use such materials in optoelectronic devices, photocatalysis and fast ionic conduction materials.[34]

Although it is possible to find in the literature some reviews about metal chalcogenide materials, notably on metal sulfide nanostructures,[35–37] hollow nanostructures,[38] nanocrystals,[39] composites with graphene[40] and more recently on the application of metal sulfides on water splitting for H_2 production,[17] this review will focus on porous chalcogenides materials that have clusters as building blocks, because the most recent review on this subject is from 2013 and major developments have happened since then.[34,41,42] Therefore, besides updating the existing literature, this document intends to expand on the potential applications of these materials.

This review is divided into two parts. The first part will focus on materials science, more specifically on presenting the differences between microporous oxides and microporous chalcogenides, followed by the presentation of the main clusters that constitute these materi-

als. It then focuses on the materials that are made up by such clusters: structures analogous to zeolites and ultimately hybrid materials. To finish the section on materials science, three alternatives of synthesis that have been investigated recently are presented. The second part will focus on photocatalysis, in particular the application of these materials to the production of solar fuels and the degradation of pollutants.

2 Cluster-based Chalcogenide Materials

The term "chalcogen" was first used in 1930 by Werner Fischer and derived from the Greek words $\chi\alpha\lambda\kappa\acute{o}\zeta$, copper, and $\gamma\epsilon\upsilon\upsilon\acute{\omega}$, giving birth. By definition, this term refers to the elements of group 16 of the periodical table - oxygen, sulfur, selenium, telurium and polonium. However, it is generally used to treat all the elements of this group except oxygen, since the chemistry of this element was generally discussed in separate chapters in common chemical inorganic textbooks.[43,44] Hence, in order to be consistent with the classification used by other authors, when the word "chalcogen" or its derivatives are used, it is referring to the elements of group 16, excluding oxygen.

The main difference between oxygen and the other elements of group 16 is the presence of vacant d orbitals. The heavier elements can use these orbitals in bonding, so their coordination number is not limited to four nor their valence limited to two, as it is in oxygen.[44,45] Open framework chalcogenides present themselves as a particular system, since both cations and anions in the framework tend to adopt a tetrahedral coordination. In the case of zeolites or zeotype materials, only metal cations tend to adopt a tetrahedral coordination while oxygen atoms generally adopt a bi- or tricoordination.[46] This tetrahedral arrangement allows the formation of clusters that are not observed in oxygen-based materials.[42]

Therefore, it is observed that chalcogenide materials with an open framework present as building units M_xS_y clusters, where M is a metal cation, generally from Groups 12-14 (such as Zn, Cd, Ga, In, Ge and Sn), instead of TX_4 tetrahedra that can be found in zeolite or

zeolite-like materials. One of the immediate consequences of using M_xS_y clusters instead of the TO_4 is the increase pore size.[47]

Given that the framework consists of clusters, which can be seen as large artificial atoms, an extra structural level associated with each cluster arises, allowing to fine tune the material properties.[42,46] Of the many known clusters,[48] the tetrahedrally shaped clusters stand out.

Since the discovery in 1989 by Bedard et al.[49,50] of microporous sulfides through hydro(solvo)thermal methods, intense research has been done in order to obtain new materials with controlled chemical compositions and architectures, so that their physical and chemical properties are better adapted to a desired application.[51]

2.1 Clusters

Open framework chalcogenides are crystalline materials consisting of clusters that are connected by chalcogen bridges or metal ions. The porous volume is usually occupied by organic or inorganic components. The clusters that constitute these structures, due to their dimensions, are on the quantum dots scale. These materials have properties that depend on their dimensions, in particular the electronic structure and electronic properties.[42,48] Considering that the periodic arrangement of clusters can be seen as dots and the cavities as antidots, these materials allow the study of the interactions between individual dots and, due to the regular distance between them, the interdot coupling.[52] The electronic properties become particularly valuable as most of these clusters are semiconductors with a bandgap and band structures suitable for the visible region.

These clusters, which are essentially made up of metals and chalcogen atoms, can be synthesized from a wide variety of reactions. The simplest one is the association, in the appropriate proportions, of metal cations and chalcogen anions in solution. Since both components can achieve different oxidation states, it is still possible to obtain these clusters from a redox reaction using a metal reductant and a chalcogen oxidant. With these two techniques, non-molecular structures are usually obtained, that is, structures constituted by

the infinite connection between atoms into 1-, 2- or 3-dimensions.[48]

The clusters, after formed, can connect, originating open frameworks. These frameworks can be seen as decorated nets. A decorated net is a net where an atom was replaced by a cluster, while maintaining the connection pattern.[53] Figure 1 presents some examples of topologies presented by 3-dimensional structures. It is observed that the most common topology in this family of materials is the diamond topology, simple or double interpenetrated. Interpenetration refers to two or more nets, with the same or different chemical composition, chained to each other.[54]

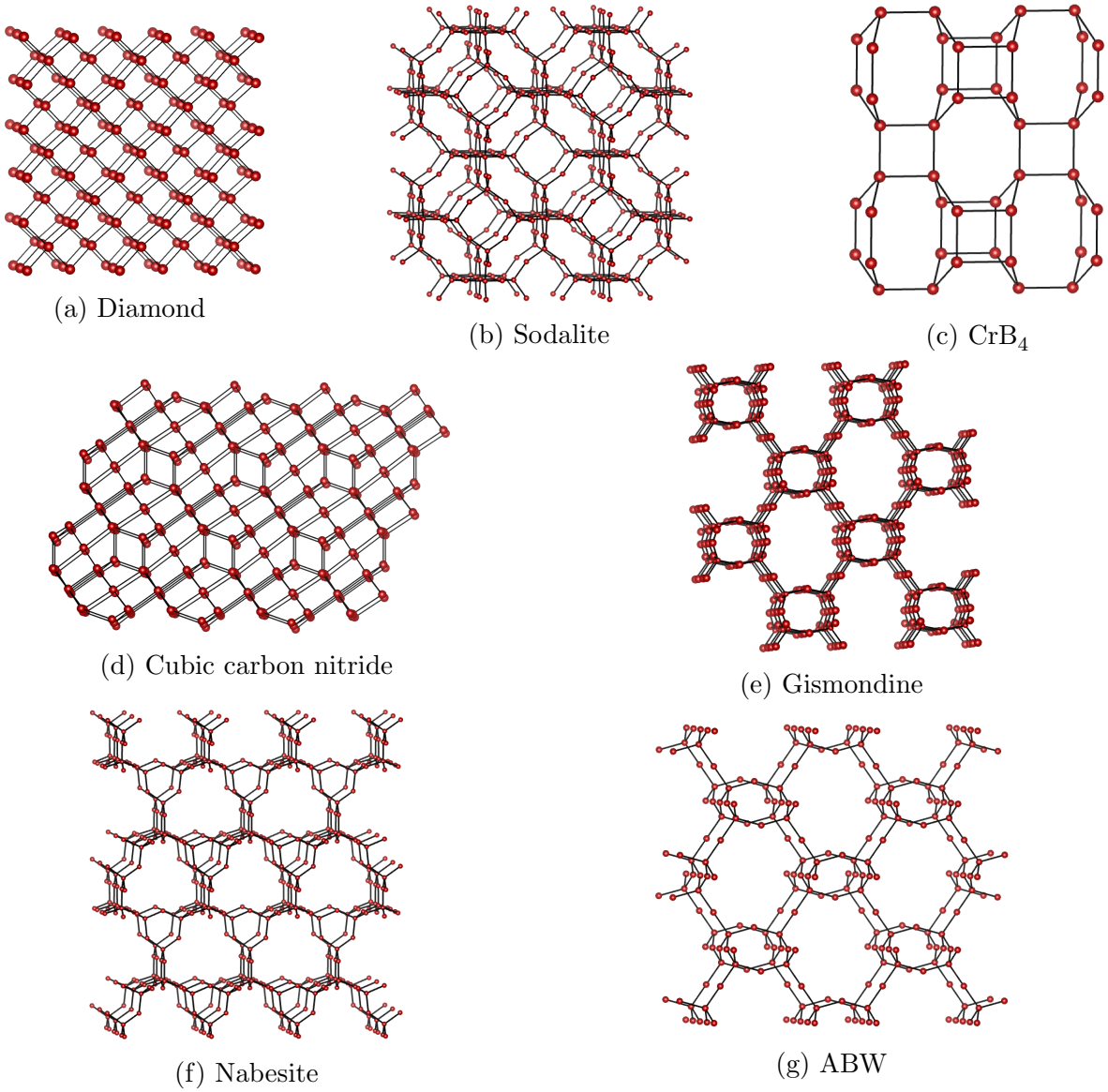

(a) Diamond (b) Sodalite (c) CrB_4

(d) Cubic carbon nitride (e) Gismondine

(f) Nabesite (g) ABW

Figure 1: Representation of diamond (D), sodalite (SOD), CrB_4, cubic carbon nitride (C_3N_4), gismondine, nabesite (NAB) and ABW topologies

2.1.1 Tetrahedral Clusters

This type of cluster is the most common building unit in open framework chalcogenide materials. They are usually composed of cations from groups 12 to 14, and may also have other elements such as Fe, Mn, Co, Cu or Li.

There are different types of tetrahedron clusters, namely supertetrahedral Tn, super supertetrahedral T$_{p,q}$, pentasupertetrahedral Pn, capped supertetrahedral Cn, oxyclusters

and a combination between tetrahedral and octahedral features in the same cluster, the TOn series.

2.1.1.1 Supertetrahedral Clusters Tn

The most common and simplest series of tetrahedral clusters is entitled supertetrahedral clusters. Tetrahedral clusters are fragments of the cubic ZnS-type lattice and denoted as Tn by Li et al.,[55] where n represents the number of metal layers. Figure 2 shows the diagrams of different Tn clusters for n=2, 3, 4, 5.

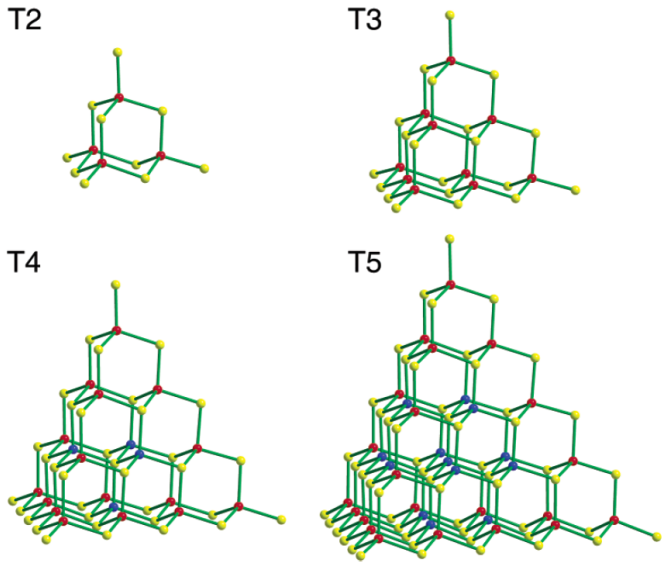

Figure 2: Diagrams for different Tn clusters (n = 2, 3, 4 and 5) where the red balls represent the cations and the yellow balls the anions. In clusters where two types of cations coexist, the blue balls represent the divalent cations[46]

The number of cations in a Tn cluster is given by $t_n = n(n+1)(n+2)/6$. The number of anions per cluster is given by $t_{n+1} = (n+1)(n+2)(n+3)/6$. The formulas for discrete Tn (n = 2-6) clusters are M_4X_{10}, $M_{10}X_{20}$, $M_{20}X_{35}$, $M_{35}X_{56}$ and $M_{56}X_{82}$, respectively. Taking into account that in a continuous network of clusters the four vertices of the supertetrahedron are shared with another supertetrahedron, the final composition of the structure is M_xX_y, where x= t_n and y= $t_{n+1} - 2$.

Regarding coordination, all cations have a coordination equal to 4. The same is no longer true for anions. They may have a coordination of 2 if they are at the vertices of the cluster, coordination of 3 if they are on the face of the cluster, or coordination of 4 if they are within the cluster. The number of anions with 2-coordination is given by $6n-4$, with 3-coordination given by $2(n-1)(n-2)$ and with 4-coordination is given by $(n-3)(n-2)(n-1)/6$. Table 1 shows the number of cations and anions present in an isolated Tn cluster or when it participates in a network, as well as the number of anions with coordination 2, 3 and 4. It is observed that anions with 4-coordination only exist for n greater or equal to 4. In order to ensure the compliance with Brown's equal valence rule,[56] the 4-coordinated chalcogen atoms are only bonded to divalent cations in order to ensure that the four bonds have a bond valence of 1/2, thus explaining the need to use divalent cations to obtain clusters with n greater or equal to 4. The number of divalent cations in the cluster as a function of n is given by $t_n - 6n + 8$.[52,57]

Table 1: Composition of Tn clusters

Cluster Tn	t_n	t_{n+1}	**Number of Cations x**	**Number of Anions y**	**Anion coordination**		
					2	**3**	**4**
1	1	4	1	2	2	0	0
2	4	10	4	8	8	0	0
3	10	20	10	18	14	4	0
4	20	35	20	33	20	12	1
5	35	56	35	54	26	24	4
6	56	84	56	82	32	40	10

As the size of the cluster increases, the overall negative charge increases, making it difficult to stabilize clusters with higher dimensions.[42] Therefore, only structures consisting of clusters up to n = 6 are known.

It is observed that the presence of low-valence cations in M^{3+}-S system promotes the formation of larger-sized clusters and high-valence cations promotes the formation of smaller clusters. When only trivalent cations are present it is common to obtain T3 clusters.

2.1.1.1.1 T2 and T3 chalcogenide based materials

In 1994 Yaghi et al.[58] presented the first synthesis of an open framework microporous sulfide based on Ge containing the T2 Ge_4S_{10} cluster as building unit and using $(CH_3)_4NHS$. The material obtained has the formula $[(CH_3)_4N]_2[MnGe_4S_{10}]$ and presents a noninterpenetrating framework with a diamond topology. The crystalline structure is based on the presence of T2 Ge_4S_{10} clusters which are connected by MnS_4 tetrahedra (see Figure 3). In order to obtain the 3-dimensional structure it was necessary to add mono or divalent cations, such as Mn, Cu,[58–60] Ag,[61] Fe[58] or Cd[58] which will be responsible for connecting the different building units, hence avoiding the formation of a layered material.

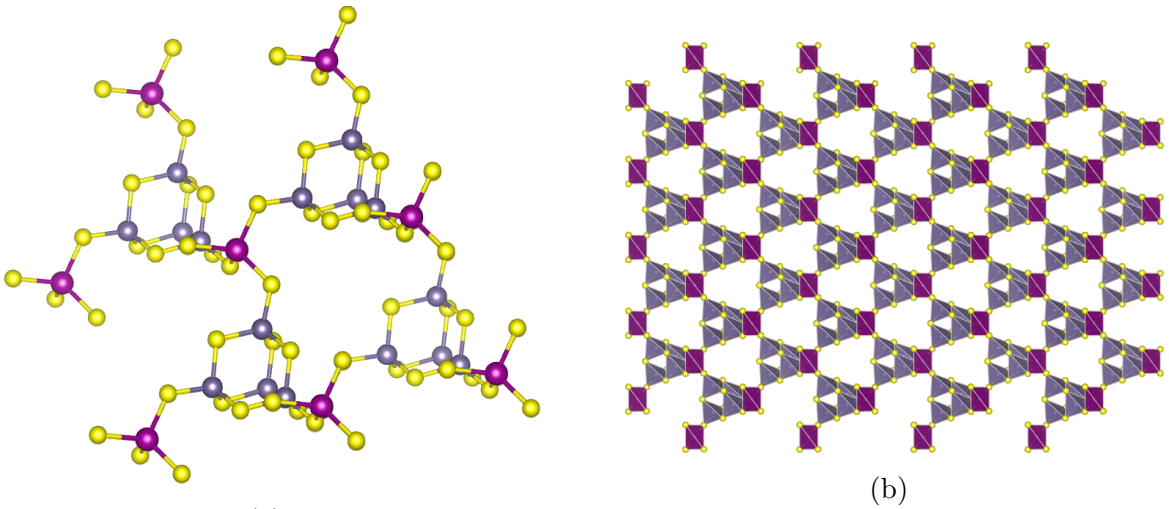

(a) (b)

Figure 3: (3a) Representation of the connection of the T2 Ge_4S_{10} clusters through MnS_4 tetrahedra. (3b) Structure of $MnGe_4S_{10}{\cdot}2\,(CH_3)_4N$ where the organic part was not presented (Mn - pink; Ge - gray, S - yellow)[58]

Also based on the T2 Ge_4S_{10} cluster, Cahill et. al[62] obtained a material entitled QUI-MnGS-1 with a diamond lattice. Although QUI-MnGS-1 is also based on the Ge_4S_{10} cluster, the presence of MnS_4 tetrahedral is not observed. The connection between the Ge_4S_{10} clusters is made by sulfur atoms at the vertices through a sulfur bridge. It was observed that it is possible to eliminate part of the structure directing agent (SDA) through calcination, at a temperature between 240°C and 360°C without destroying the framework. At temperatures

above 360°C the structure collapses.

Another interesting structure was synthesized by Zheng et al.[63] A laminar material was obtained, designated as UCR-28, constituted by alternating T2 $Ge_3S_9Zn(H_2O)$ clusters and simple $ZnS_3(H_2O)$ tetrahedrons (see Figure 4). The cluster of this material can be seen as a traditional T2 cluster where one of the tetrahedrons has been replaced by $Zn(H_2O)$. In UCR-28, the $Zn(C_6N_4H_{18})(H_2O)$ complex ion is used as SDA instead of an organic amine or pure organic cations.

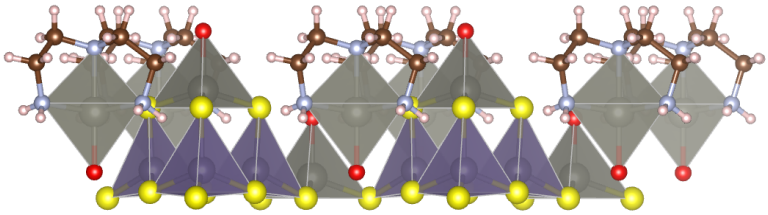

(a)

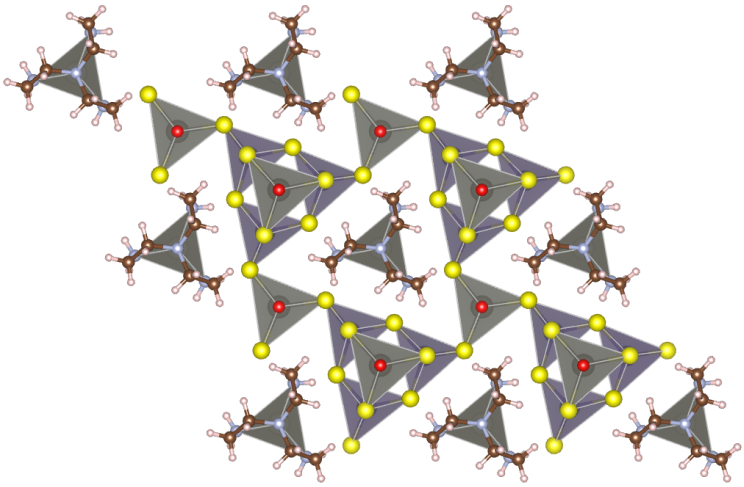

(b)

Figure 4: (4a) Side and (4b) top views of UCR-28 (H - pink, Ge - dark purple, S - yellow, Zn - dark gray, N - light gray, C - brown, O - red)[63]

In the Ge-S system the largest synthesized cluster is type T2. This is justified by the fact that the cations' charge is too high to satisfy the coordination environment of a tricoordinated anion that exists for clusters bigger than n =2. The number of known 3-dimensional frameworks is low, perhaps because fully connected M^{4+}-S frameworks would be neutral, not allowing the electrostatic interaction with a SDA.[46,64]

The chemical system In-S has been extensively studied by Cahill et al.[47,65] Several materials with different dimensions, from isolated clusters to 3-dimensional frameworks, based on the T2 In_4S_{10} and T3 $In_{10}S_{20}$ clusters were obtained. As for the materials based on the T3 clusters, it was concluded that such cluster could be obtained over a range of SDAs, and the presence of water played a key role in defining the final topology of the material, but not on the type of cluster formed (see Table 2). When using dimethylamine (DMA) or diethylamine (DEA) as SDA, a 3-dimensional structure is obtained (see Figure 5a). When the SDA used is the DEA and water exists in the initial gel, a laminar structure is obtained instead (see Figure 5b). Therefore, it can be said that the SDA is not the only determining factor for the final topology of the material.

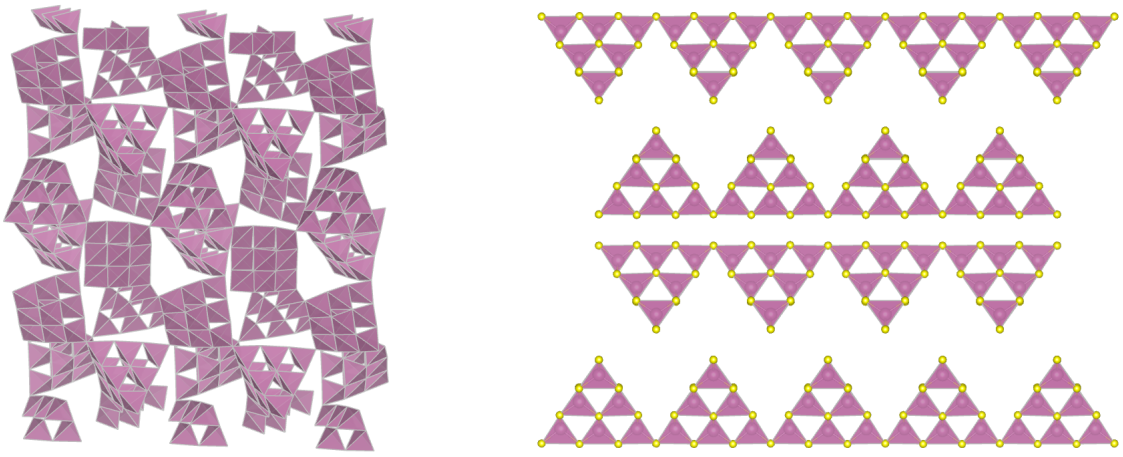

(a) (b)

Figure 5: Representations of (5a) DEA-InS-SB1 and (5b) DEA-InS-SB2 where the organic component was not presented (In - pink, S - yellow)[47]

Li et al.[55,66] also synthesized 3-dimensional microporous solids based on In, which presents the T3 clusters as building units in its structure. Three crystalline structures, ASU-31 (see Figure 6a), ASU-32 (see Figure 6b) and ASU-34 (see Figure 6c) were obtained, because different types of SDA were used.

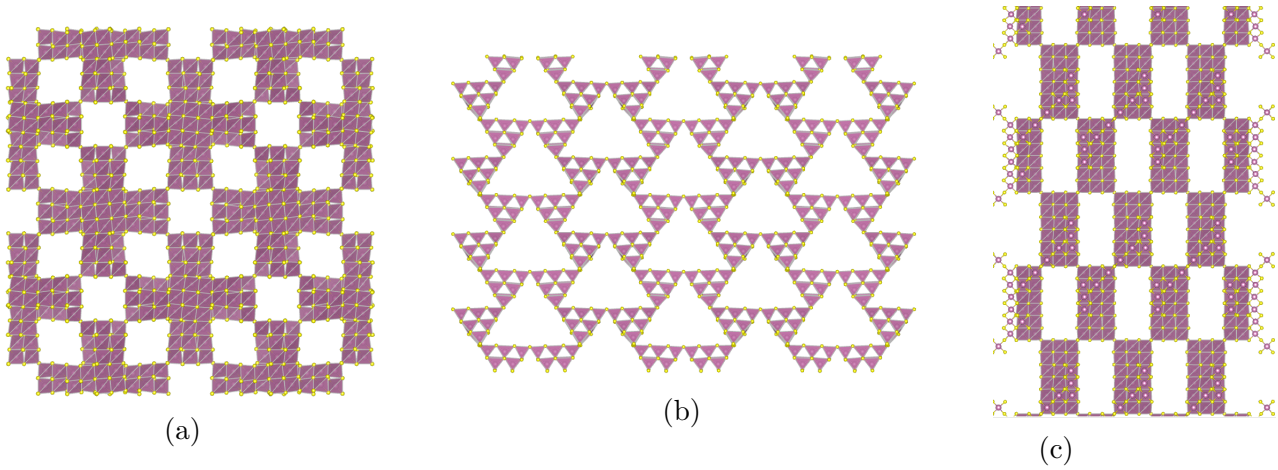

(a) (b) (c)

Figure 6: Representations of (6a) ASU-31, (6b) ASU-32 and (6c) ASU-34 where the organic component was not present (In - pink, S - yellow)[55,66]

Comparing the structures obtained by Cahill[47,65] and Li[55,66] (see Table 2), the structures synthesized by the first exhibited an interpenetrated framework. This type of framework occurs when the pore size is too large to support the framework. This is not the case with the structures obtained by Li, since the SDAs allowed the obtention of giant cavities.

Table 2: Different materials based on the T3 $In_{10}S_{20}$ cluster and their gels compositions and final topology (adapted from Ref.[47])

Material	**SDA**	**Gel composition (mol)**				**Cluster**	**Structure**	**Interpenetration**	**Ref.**
		In	S	Organic	H_2O				
DMA-InS-SB1	DMA[1]	1	2,3	4,4	16,6	T3	3D - DD[2]	Yes	[65]
DEA-InS-SB1	DEA[3]	1	2,3	6,8	trace	T3	3D - DD[2]	Yes	[47]
DEA-InS-SB2	DEA[3]	1	2,3	3,4	14,0	T3	2D	No	[47]
ASU-31	HPP[4]	1	2,5	n/a[5]	n/a[5]	T3	3D - SOD[6]	No	[55]
ASU-32	DPM[7]	1	2,5	n/a[5]	n/a[5]	T3	3D - CrB_4[8]	No	[55]
ASU-34	HMA[9]	1	2,5	n/a[5]	n/a[5]	T3	3D - CrB_4[8]	No	[66]

[1] Dimethylamine. [2] Double Diamond. [3] Diethylamine. [4] 1,3,4,6,7,8-hexahydro-2H-pyrimido[l,2-a]pyrimidine. [5] n/a - not available. [6]Sodalite (see Figure 1b). [7] Dipiperidinomethane. [8] (see Figure 1c). [9] Hexamethyleneimine.

Normally in this class of materials the different clusters are connected via a sulfur bridge, where the sulfur presents a sp^3 hybridization. Wu et al.[67] were able to obtain a molecule compound with an ethane-like conformation where two T3-InS clusters are connected by a sulfur that exhibits a sp hybridization. It was the first time that the stabilization of a linear sulfur was made by N-H$\cdots$S hydrogen-bonding interactions instead of metal-S multiple

bonds or steric hindrance from the ligand. Looking at Figure 7, one can see that three protonated 1,5-diazabicyclo[4.3.0]non-5-ene (DBN) molecules are surrounding the connection mode between the two T3 clusters.

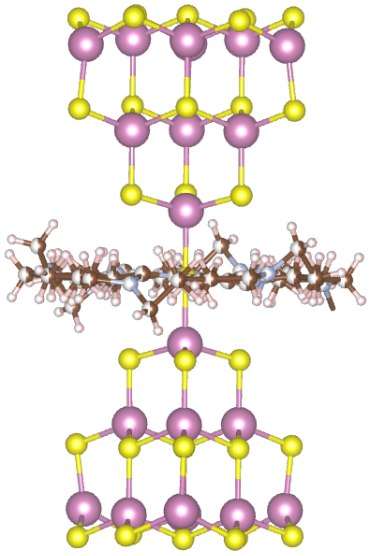

Figure 7: Molecular compound obtained by Wu et al.[67] (In - pink, S - yellow, C - brown, N - nitrogen, H - white)

The Ga-S system was also studied. Zheng et al.[68] having obtained for the first time a structure based on the T3 $Ga_{10}S_{18}$ cluster, called UCR-7. Depending on the SDA used, they were able to obtain a structure based on cluster T3 $Ga_{10}S_{17,5}(S_3)_{0,5}$, known as UCR-18, that presented a polysulfide linkage between the clusters which had not yet been observed (see Figure 8).

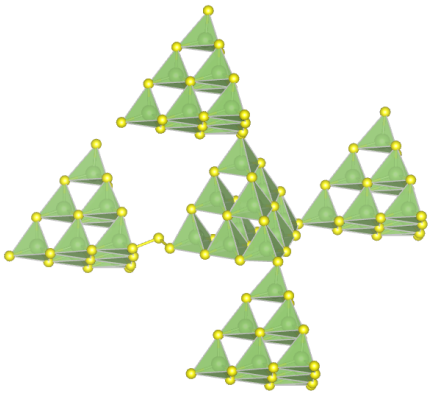

Figure 8: Representation of the connection mode between the clusters of the UCR-18 structure (Ga - green, S - yellow)[68]

When using 1-(2-aminoethyl)piperazine (AEP) as a SDA in the Ga-S system, clusters connected by a polysulfide bridge are obtained. However, when the same SDA is used in the In-S system, a structure where the clusters are connected through the common bisulfide bridge is obtained instead. According to Zheng et al.,[68] this situation is explained by the different sizes between Ga and In. Due to the small size of Ga when compared with In, a contraction of the framework occurs, making it more difficult to accommodate the AEP molecule. Thus, the presence of the polysulfide bridge allows the expansion of the framework, contrary to its natural contraction due to the presence of Ga instead of In.

More recently, a 3-dimensional interrupted structure based on the combination of Sn, In and S and using 3,5-dimethylpiperidine as SDA has been synthesized.[69] A structure is considered to be interrupted when the clusters that constitute it are only connected to three other clusters, instead of four (see Figure 9a). The obtained material, entitled SCU-36, has as framework based on 3-connected T2 clusters and has a *etc* topology (see Figure 9b). Other interesting features about SCU-36 is the presence of extra-large channels, consisting of 36-MR, and a very low framework density. As for the exchange properties of the material, after 12 hours of exchange with CsCl the N_2 absorption is negligible. When the time of exchange or the CsCl concentration were increased, the crystal structure collapsed.

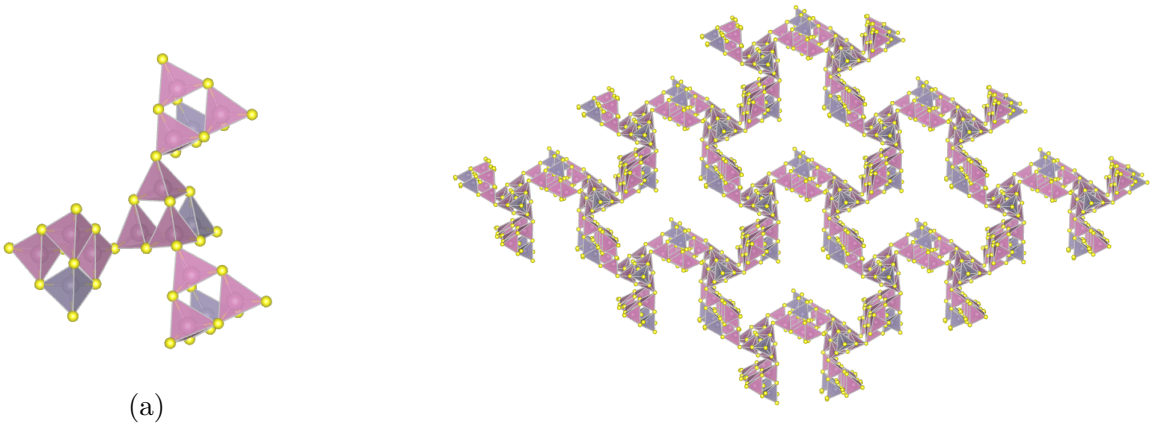

(a) (b)

Figure 9: Representations of (9a) an interrupted framework and of (9b) SCU-36 where the organic component was not present (In - pink, Sn - gray, S - yellow)[69]

Based on the same chemical system, 2-dimensional structures were later obtained.[70] Such materials, entitled SOF-23 and SOF-24 (see Figure 10), are based on the presence of interrupted T3-InSnS clusters but present several connection modes between the different clusters. Regarding the organic part, responsible for counterbalancing the negative charge of the framework, SOF-23 presents a combination between 1,8-diazabicyclo[5.4.0]-7-undecene (DBU) and $(CH_3)_2NH$, where the last species results from the decomposition of DMF during the the solvothermal synthesis. As for SOF-24, it also presents 1,8-diazabicyclo[5.4.0]-7-undecene (DBU) and (R)-()-2-amino-1-butanol (AB) on its extraframework space.

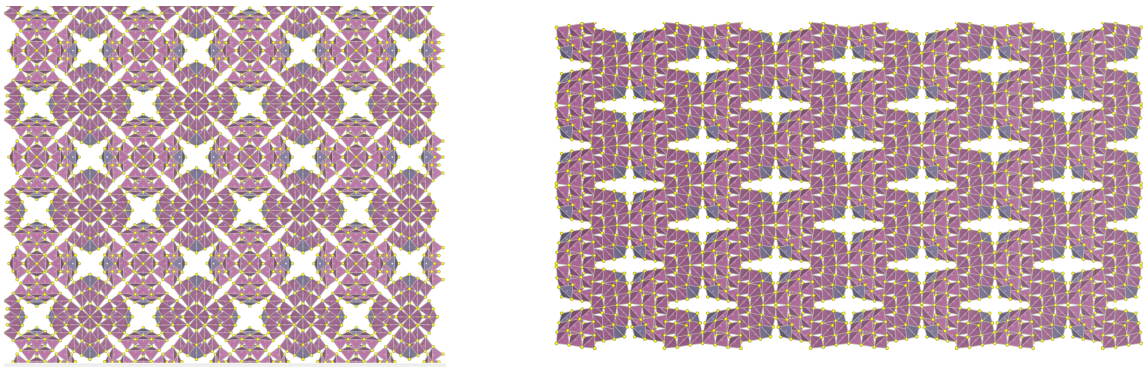

(a) (b)

Figure 10: Representations of (10a) SOF-23 and (10b) SOF-24 where the organic component was not present (In - pink, Sn - gray, S - yellow)[70]

According to Wu et al.,[70] when partial replacement of In by Sn occurs, the high negative charge of corner sites of clusters decreases, increasing the possibility for the formation of interrupted structures.

Continuing the research to obtain more complex structures, Wang et al.[71] synthesized for the first time a structure based on the extended spiro-5 unit, which are expanded through the fusion of five T3-InSnS clusters. The obtained compound, entitled SOF-27, exhibits for the first time a NAB topology (see Figure 1f). Comparing the structure obtained with nabasetie, the only known natural zeolite with the NAB structure, the ring size is increased three times due to the use of T3 clusters instead of TO_4 tetrahedra.

Turning to selenium-based materials, there is a reduced number of crystalline 3-dimensional selenium-based frameworks. The first known structure[72] is based on the T2 cluster Ge_4Se_{10}, where the addition of divalent metal cations is required to connect the different clusters, in order to achieve a 3-dimensional framework with an analogous structure to that obtained by Yaghi et al.[58]

Continuing the search for larger clusters, the first T3 cluster based on the In-Se system was obtained by Wang et al.[73] Later, Xue et al.[74] were able to obtain a family of compounds also based on the In-Se which presented polyselenides bridges as a way to connect the different clusters.

As for the Ga-Se chemical system, the first 3-dimensional open frameworks based on T3 clusters as building units were first obtained by Bu et al.[75] Two different materials were obtained: OCF-6 and OCF-13. The first one presents a diamond topology and a ring size of 18 T atoms while the second one presents a CrB_4 topology and a ring size of 24 T atoms. The synthesized structures present non-interpenetrating frameworks while the ones obtained for the Ga-S system are all interpenetrating nets. As for the synthesis conditions, the existence of water promotes the crystal growth while in the Ga-S system the synthesis must be held in a non-aqueous medium.

Table 3: Different materials based on the T3 $Ga_{10}X_{20}$ (X = S, Se) cluster and their gel compositions and final topology

Material	SDA	Gel composition (mol)					Cluster	Structure	Interpenetration	Ref.
		Ga	S	Se	Organic	H_2O				
UCR-7-GaS-TETA	TETA[1]	n/a[2]	n/a[2]	-	n/a[2]	-	T3	3D	Yes	[68]
UCR-7-GaS-TAE	TAE[3]	n/a[2]	n/a[2]	-	n/a[2]	-	T3	3D	Yes	[68]
UCR-7-GaS-DBA	DBA[4]	n/a[2]	n/a[2]	-	n/a[2]	-	T3	3D	Yes	[68]
UCR-18-GaS-AEP	AEP[5]	1	3,3	-	8,6	-	T3	3D	Yes	[68]
-	DEA[6]	1	2,1	-	33,0	-	T3	3D - DD[7]	Yes	[76]
OCF-6-GaSe-TMDP	TMDP[8]	1	-	2,5	4,9	152,9	T3	3D - D[9]	No	[75]
OCF-13-GaSe-DPM	DPM[10]	1	-	2,5	5,2	207,5	T3	3D - CrB_4[11]	No	[75]

[1] Triethylenetetramine. [2] n/a - not available. [3] Tris(2-aminoethyl)amine. [4] Di-n-butylamine. [5] 1-(2-aminoethyl)piperazine. [6] Diethylamine. [7] Double Diamond. [8]4,4'-trimethylenedipiperidine. [9]Diamond (see Figure 1a). [10]Dipiperidinomethane. [11] CrB_4 (see Figure 1c).

Recently, through the use of antimony, an ion that presents a non-tetravalent coordination, it was possible to obtain $Ga_{56}Sb_{16}S_{136}$ and $In_{36}Sb_6S_{75}$ superclusters that are based on the assembly of T3 clusters.[77]

The supercluster $Ga_{56}Sb_{16}S_{136}$ (see Figure 11a) can be seen as four T3 $Ga_{10}S_{20}$ clusters, sixteen GaS_4 tetrahedra and sixteen SbS_3 trigonal pyramids. Four GaS_4 tetrahedra are combined, presenting an arrangement similar to an adamantane cage. This adamantane-type arrangement is connected to four SbS_3 trigonal pyramids, generating a unit with the formula $Ga_4Sb_4S_{16}$. Each $Ga_4Sb_4S_{16}$ unit is connected to three T3 clusters, therefore presenting an interrupted Sb site (see Figure 11b).

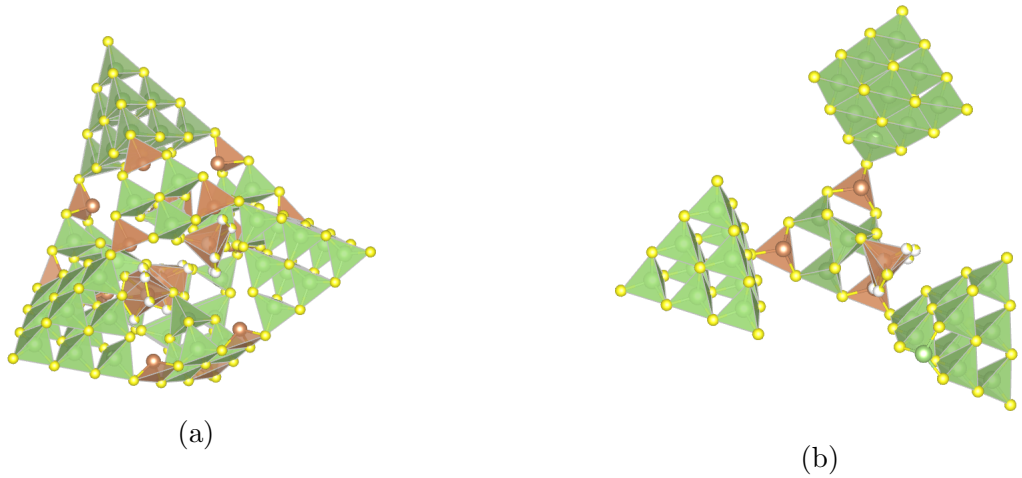

(a) (b)

Figure 11: (11a) $Ga_{56}Sb_{16}S_{136}$ supercluster and (11b) connection mode between the $Ga_4Sb_4S_{16}$ unit with each T3 cluster (Ga - green, Sb - brown, S - sulfur)[77]

As for the second supercluster, the $In_{36}Sb_6S_{75}$, it is composed by 3 $In_{10}S_{20}$ T3 clusters and a $In_6Sb_6S_{24}$ unit (see Figure 12). It is the $In_6Sb_6S_{24}$ unit responsible for connecting with the other superclusters. Each $In_6Sb_6S_{24}$ links with other three T3 clusters from three different supercluster by a Sb-S bond.

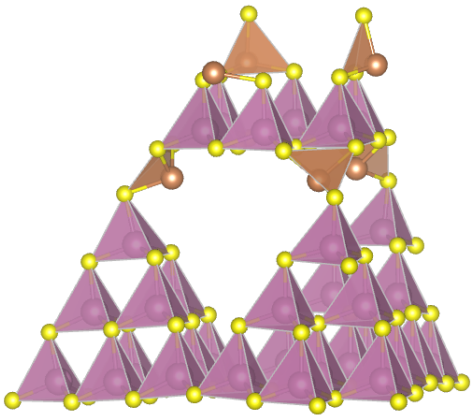

Figure 12: Representation of $In_{36}Sb_6S_{75}$ supercluster (In - pink, Sb - brown, S - yellow)[77]

Two new structures, MCOF-31 and MCOF-32, were obtained with these superclusters. MCOF-31, composed by the $Ga_{56}Sb_{16}S_{136}$ cluster, presents a 2-dimensional interpenetrate framework. As for MCOF-32, it presents a 3-dimensional framework with a *pcu* topology.

Regarding tellurium, obtaining structures with this element is the most challenging, since tellurium presents low reactivity and tellurides are environmentally unstable. Although examples of structures with Te are found in the literature, the majority do not present clusters as building units.[78] The first material based on T2 Ge/Sn-Te clusters was obtained by Tsamourtzi et al.[79] Following these works, Zhang et al[80] obtained the first material based on T2 In-Te clusters. The material obtained has a 2-dimensional chiral structure (see Figure 13) and the T2 clusters have a different composition. One of the Te of the cluster was substituted by ethylenediamine (see Figure 14). This organic component has a terminal position, not making any connection with other clusters.

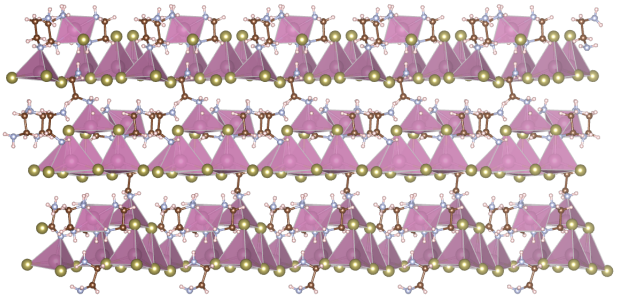

Figure 13: Representations of the layered material obtained by Zhang et al. (In - pink, N - gray, Te - dark green, H - light pink, C - brown)[80]

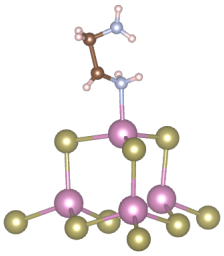

Figure 14: Representations of cluster that forms the structure obtained by Zhang et al. (In - pink, N - gray, Te - dark green, H - light pink, C - brown)[80]

2.1.1.1.2 Supertetrahedral clusters with n >3

The need to obtain structures with large pores has led to the development of structures composed by Tn clusters with n greater than 3, since the size of the ring is increased n times, thus leading to structures with a highly open framework.[75] Although Tn are the most commonly used type of clusters, they have limitations in their use. The first is the way to connect the different clusters. Generally, the connection between two clusters is made through bi-coordinated chalcogen bridge. When using this type of clusters, the formed structures tend to be interpenetrated, in order to reduce the potential energy and stabilize the structure, leading to a reduction in pore size and pore volume.[81,82] Another difficulty that arises is the drastically increase of negative charges with increasing n, making it difficult to synthesize clusters with large dimensions. Although the metal cations are always coordinated with four anions, the same cannot be said for anions at the surface. Thus, as the cluster size

increases, so does the number of underbonded anions, contributing to the huge increase in the global negative charge of the cluster.[83]

The first material based on a T4 cluster was synthesized in 2001 by Li et al.[57] This interpenetrating structure is formed by clusters of the type $In_{16}Cd_4S_{35}$, where Cd^{2+} presents a fundamental role in obtaining such structure. It is due to the addition of the divalent cation that the local charge balance at the core tetrahedral anion is achieved. Continuing the research on the synthesis of structures based on T4 clusters, Bu et al.[81] managed to synthesize a structure where a sulfur atom was connecting three T4 clusters.

Wang et al.[84,85] were able to synthesize a family of T4-based 3-dimensional sulfides as well as using transition metals, such as Fe and Co, to join the different T4 clusters into a 2-dimensional framework. Taking into account the mentioned materials (see Table 4), it is possible to obtain the structure of CrB_4 from a diverse range of SDAs, provided they contain a piperazine ring. However, the cubic carbon nitride and UCR-1 topologies are more rigid, since they can only be obtained from di-n-butylamine and 4,4'-trimethylenedipiperidine, respectively, as SDA. It is also interesting to note that when using 1,2-diaminocyclohexane as a SDA in the chemical systems In-Fe-S or In-Co-S the final material presents a 2-dimensional structure instead of a 3-dimensional structure.

Table 4: Different materials based on T4 $In_{16}X_4S_{35}$ (X = Zn, Cd, Fe, Co, Mn) cluster and their gel compositions and final topology

Material	SDA	Gel composition (mol)				Cluster	Structure	Interpenetration	Ref.
		In	S	X	Organic				
CdInS-44	BAPP[1]	1	2,5	0,3	4,3	$In_{16}Cd_4S_{35}$	3D - CrB_4[2]	Yes	[57]
UCR-8FeInS-DBA	DBA[3]	n/a[4]	n/a[4]	n/a[4]	n/a[4]	$In_{16}Fe_4S_{35}$	3D - C_3N_4[5]	No	[81]
UCR-8CoInS-DBA	DBA[3]	n/a[4]	n/a[4]	n/a[4]	n/a[4]	$In_{16}Co_4S_{35}$	3D - C_3N_4[5]	No	[81]
UCR-8ZnInS-DBA	DBA[3]	1	3,5	0,4	15,1	$In_{16}Zn_4S_{35}$	3D - C_3N_4[5]	No	[81]
UCR-8CdInS-DBA	DBA[3]	n/a[4]	n/a[4]	n/a[4]	n/a[4]	$In_{16}Cd_4S_{35}$	3D - C_3N_4[5]	No	[81]
UCR-1CdInS	TMDP[6]	1	2,9	0,3	3,9	$In_{16}Cd_4S_{35}$	3D - UCR-1[7]	No	[84]
UCR-1ZnInS	TMDP[6]	n/a[4]	n/a[4]	n/a[4]	n/a[4]	$In_{16}Zn_4S_{35}$	3D - UCR-1[7]	No	[84]
UCR-1MnInS	TMDP[6]	n/a[4]	n/a[4]	n/a[4]	n/a[4]	$In_{16}Mn_4S_{35}$	3D - UCR-1[6]	No	[84]
UCR-1CoInS	TMDP[6]	n/a[4]	n/a[4]	n/a[4]	n/a[4]	$In_{16}Co_4S_{35}$	3D - UCR-1[7]	No	[84]
UCR-5ZnInS-1	BAPP[1]	n/a[4]	n/a[4]	n/a[4]	n/a[4]	$In_{16}Zn_4S_{35}$	3D - CrB_4[2]	No	[84]
UCR-5ZnInS-2	AEPP[8]	n/a[4]	n/a[4]	n/a[4]	n/a[4]	$In_{16}Zn_4S_{35}$	3D - CrB_4[2]	No	[84]
UCR-5ZnInS-3	ATMP[9]	n/a[4]	n/a[4]	n/a[4]	n/a[4]	$In_{16}Zn_4S_{35}$	3D - CrB_4[2]	No	[84]
UCR-5MnInS	BAPP[1]	n/a[4]	n/a[4]	n/a[4]	n/a[4]	$In_{16}Mn_4S_{35}$	3D - CrB_4[2]	No	[84]
UCR-5CoInS	BAPP[1]	n/a[4]	n/a[4]	n/a[4]	n/a[4]	$In_{16}Co_4S_{35}$	3D - CrB_4[2]	No	[84]
-	DACH[10]	1	2,0	0,5	132,9	$In_{16}Fe_4S_{35}$	2D	No	[85]
-	DACH[10]	1	4,0	0,5	149,5	$In_{16}Co_4S_{35}$	2D	No	[85]

[1]1,4-bis(3-aminopropyl)piperazine. [2]CrB_4 (see Figure 1c). [3]Di-n-butylamine. [4] n/a - not available. [5]Cubic carbon nitride (see Figure 1d). [6]4,4'-trimethylenedipiperidine. [7]UCR-1 topology (see Figure 15). [8]1-(2-aminoethyl)piperazine. [9]4-amino-2,2,6,6-tetramethylpiperidine. [10]1,2-diaminocyclohexane.

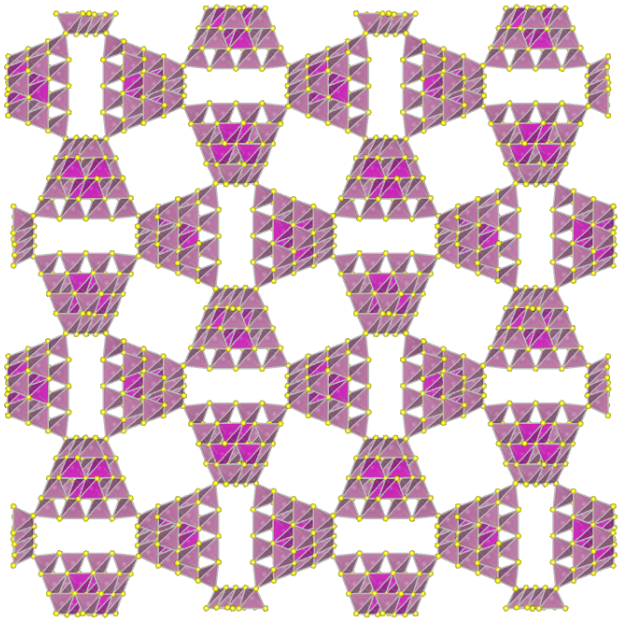

Figure 15: Representation of the UCR-1 structure (In - pink, Cd - mangenta, S - yellow)[84]

Now replacing In with Ga, Zheng et al.[68] were able to synthesize a structure based on the T4 $Ga_{16}Zn_4S_{35}$ clusters with the same structure, UCR-5, as the materials previously obtained by Wang et al.,[84] by using BAPP as a SDA. Continuing the study of materials

containing Ga, Bu et al.[75] obtained a material based on the Ga-Zn-Se system that does not present an interpenetrating framework by using TMDP as SDA.

Wu et al.[83] managed to synthesize a family of materials based on the complex Sn-Ga-M-X (M = Mn, Cu, Zn; X = S, Se) chemical system. It was found that in the systems under study, there was a phase transformation from a 3-dimensional interpenetrated diamond framework composed of T4 clusters, OCF-5 (see Figure 16a), to isolated and highly stable T4 clusters, OCF-40 (see Figure 16b). It was observed that OCF-5 has highly disordered dipiperidinomethane (DPM) molecules and OCF-40 highly ordered protonated piperidine. Thus, it is assumed that the driving force controlling the transformation of OCF-5 into OCF-40 is the gradual decomposition of DPM into piperidine, which causes the dissolution of OCF-5 and subsequent formation of OCF-40. When pyridine is used as SDA instead of DPM, only OCF-40 is obtained. In this system, the SDA does not influence the type of cluster obtained, but rather the dimension of the material obtained. It is also referred that in order to obtain large clusters, the relative concentrations of the cations involved must be carefully controlled. The cations involved have distinct functions. The cations M^{2+} or M^{+} serve to counterbalance the charge requirements of the anions at the cluster core and the high-valence cations, M^{4+} and M^{3+}, serve to stabilize the unbound anions at the cluster surface.

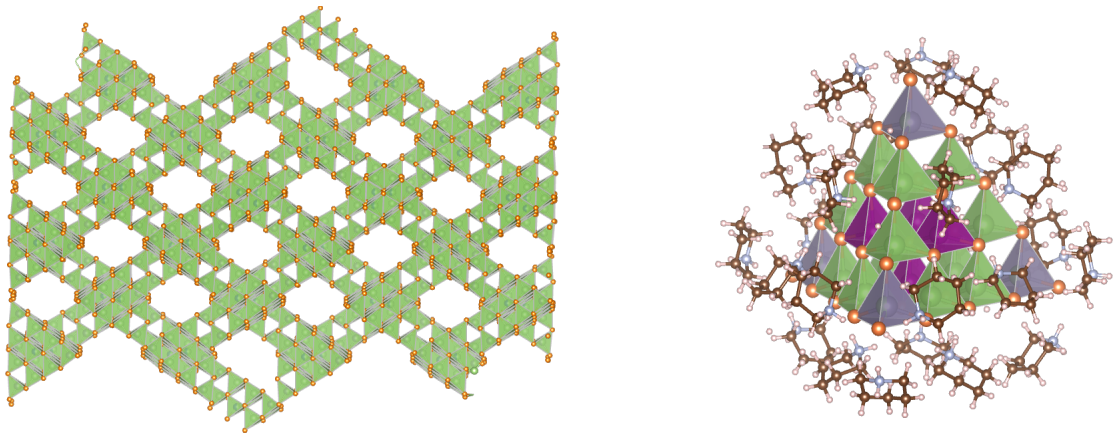

(a) (b)

Figure 16: Representations of (16a) OCF-5 and (16b) OCF-40 obtained by Wu et al. (Ga - green, N - light gray, Se - orange, H - light pink, C - brown, Sn - gray)[83]

It is well known that the doping of a material is used to tune its electronic properties. Wu et al.[86] evaluated how the doping of the chemical system Ga-Zn-Se by Sn or S or changing the amine type can influence the electronic properties of such T4 cluster based materials. The starting gel consisted of $Ga(NO_3)_3$, $Zn(NO_3)_2$, Se and H_2O. Four different SDAs, 1,5-diamino-2-methylpentane (DAMP), 4,4'-trimethylenedipiperidine (TMDP), piperidine (PR) or N-ethylcyclohexanamine (ECHA), were evaluated and for each SDA doping with Sn (by adding $SnCl_2$), S (by adding dimethylsulfoxide - DMSO) and dual doping with Sn and S was also evaluated. The experimental results of the different forms of doping are represented schematically in Figure 17.

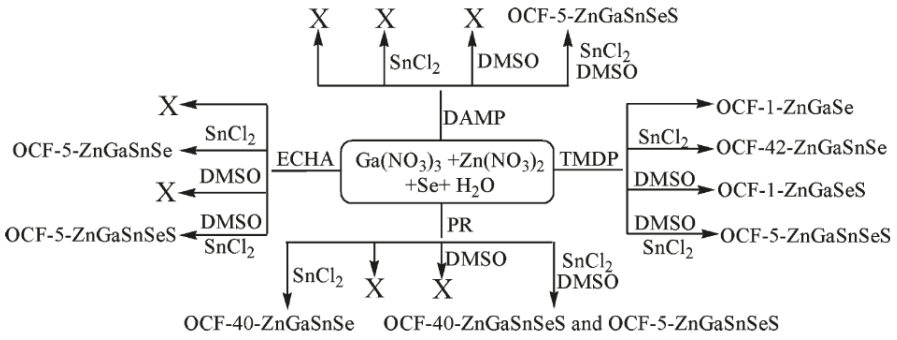

Figure 17: Scheme of the different forms of doping as well as the experimental results obtained (X means no crystalline product is obtained)[86]

Taking into account Pauling's valence rule[87] and Pearson's hard and soft acid base theory,[88] the core anion should be surrounded by Zn^{2+} and the corner sites should be occupied by high valence cations. Such rules dictate the distribution of the different ions on the cluster. It was observed that the core Se^{2-} is easily replaced by S^{2-} and partial replacement of the Se^{2-} at the face sites by S^{2-} is observed. The doping with Sn^{4+}, which will substitute the Ga^{3+} at the corner sites, suppresses the doping by S^{2-} because it has a bigger affinity for Se^{2-}. Comparing the consequences of the doping on the charge of the cluster, doping with S^{2-} does not affect it while doping with Sn^{4+} reduces the global charge of the cluster. Therefore, organic amines with lower charge density induce more Sn^{4+} doping on the corner sites of the cluster. The doping also affects the cluster size. Taking into account ionic radii and bond distances, doping with Sn increases the size of the cluster and doping with S decreases it. No doping or only doping with S, while using TMDP leads to OCF-1 (material previously study by Bu et al.[75]). For all used amines, OCF-5 (see Ref.[83] for more information regarding the topology) is obtained when both Sn and S doping is used. When only Sn doping is used, OCF-5, OCF-40 or OCF-42 (OCF-42 is a 3-dimensional structure composed by the combination of T2 and T4 clusters[89]) can be obtained, depending on the organic amine used.

Recently, by controlling the $M^{4+}/M^{3+}/M^{+}$ ratios and selecting a suitable SDA it was possible to obtain a 3-dimensional structure, entitled MCOF-3, where the T4-CuGaSnS clusters were connected by a single-Cu^{+}-ion (see Figure 18).[90] Comparing the MCOF-3' gel composition with OCF-40', there was an increase of Cu^{+}/Sn^{4+} ratio, which favors the connection between clusters being made by Cu^{+}, and the usage of a superbase, 1,5-diazabicyclo[4.3.0]non-5-ene (DBN), instead of piperidine as SDA. Regarding topology, MCOF-3 presents a three-fold interpenetrating diamond framework.

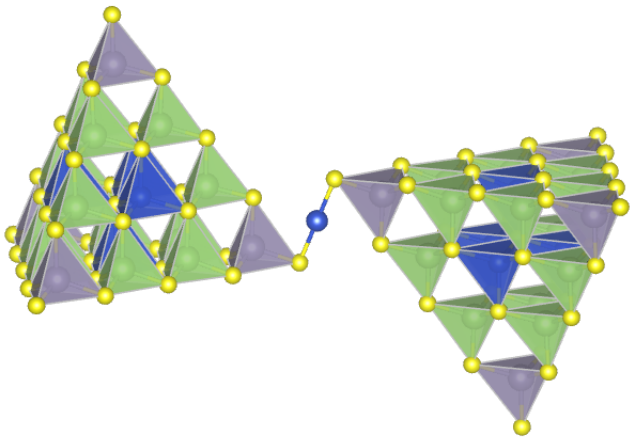

Figure 18: Mode of connection between the T4 clusters present on MCOF-3 (Sn - gray, Ga - green, Cu - blue, S - yellow)[90]

All 3-dimensional structures based on T4 clusters composed by three different metals have diamond as topology, regardless of the SDA used.

The first synthesized T5 cluster had a missing core atom.[91] As there is no core atom, there are no sulfur atoms with 4-coordination, so the existence of divalent cations is not necessary. Thus, it is possible to achieve large-sized clusters without the need to incorporate divalent cations in the structure, provided that the clusters have at least one missing core atom. Other structures based on pseudo T5 clusters were synthesized. Su et al.[92] managed to obtain a layered structure based on pseudo T5 cluster $In_{28}Cd_6S_{56}$. The synthesized structure has a lower Cd content than the expected for a T5 cluster, as the theoretical $In_{22}Cd_{13}S_{54}$ cluster is unstable due to the high negative charges.

To synthesize a true T5 cluster it was necessary to add Cu to the In-S system, obtaining a cluster with the formula $In_{30}Cu_5S_{54}$.[93] With this type of clusters it was possible to synthesize two distinct structures, one with a 2-dimensional framework, entitled UCR-16 (see Figure 19a), and another with a 3-dimensional framework, the UCR-17 (see Figure 19b) while using 4,4-trimethylenedipiperidine (TMDP) as SDA. Both structures are obtained in the same batch, with UCR-16 as the dominant phase.

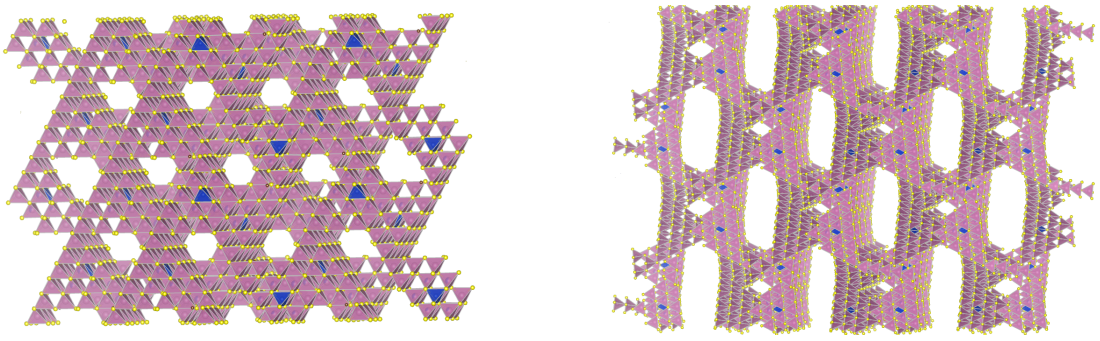

(a) (b)

Figure 19: Representations of (19a) UCR-16 and (19b) UCR-17 obtained by Bu et al. where the organic part is not presented (In - pink, Cu - blue, S - yellow)[93]

Wu et al.,[94] in order to study the insertion of dopants in specific places at atomic scale, obtained for the first time isolated T5 clusters. For that, a pseudo T5 cluster was first synthesized, entitled ISC-10, based on In-Cd-S system. It was also observed that, when the amount of Cd in the precursor gel increases, a 2-dimensional framework is obtained, entitled OCF-43, composed by the same clusters as in ISC-10. After obtaining the ISC-10, diffusion of Cu to the void of the cluster is performed, originating a T5 cluster composed by In-Cu-Cd-S. It was observed that even a small amount of Cu is enough to cause big differences on the photoelectric properties of the materials. The doping of ISC-10 by Mn^{2+} was also evaluated.[95] After the doping with Mn^{2+} there is a strong red emission that is not observed in the typical semiconductor materials doped with Mn^{2+}.

From the T5 clusters obtained so far only the combination M^{3+}/M^{2+} has been observed to be possible.

Some years after the synthesis of a true T5 cluster, a T6 cluster was obtained (see Figure 20).[96] In order to achieve a cluster of that size without adding organic ligands to stabilize the negative charges, a mixed metal strategy is used, in order to have some high valence cations at the corners of the cluster that allow the reduction of the global charge. In order to achieve that, the ratio M^{2+}/M^{3+} of an ideal T6 cluster should be one. In the obtained T6-based 2-dimensional structure (see Figure 21), named OCF-100, all Zn ions are located at the core or at the faces of the cluster and the edges are occupied by In^{3+}. As for the SDAs used

during OCF-100 synthesis, 3,5-dimethylpiperidine (DMP) and diethylenetriamine (DETA) were utilized.

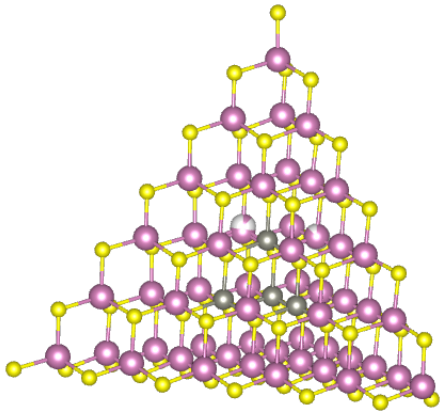

Figure 20: Representation of a T6 cluster (In - pink, Zn - black, S - yellow)[96]

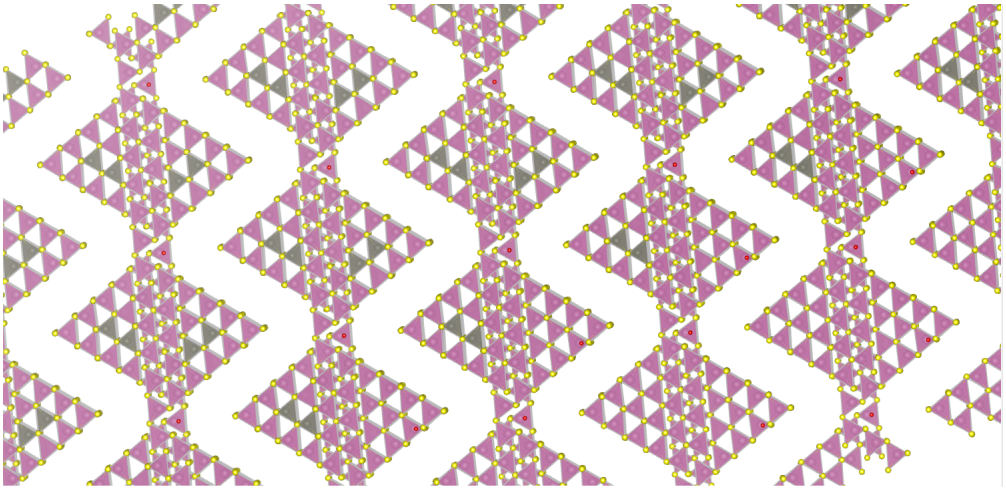

Figure 21: Representation of OCF-100 obtained by Xue et al. where the organic part is not present (In - pink, Zn - black, S - yellow)[96]

2.1.1.2 Super-supertetrahedral Clusters $T_{p,q}$

It was observed that in some cases four Tn clusters were organized in a polyhedra structure, giving rise to a supertetrahedron, called $T_{p,q}$, which means that Tp clusters are organized in a Tq cluster using a X^{2-} as a linkage between the clusters.[97] Figure 22 shows a representation of a $T_{3,2}$ cluster.

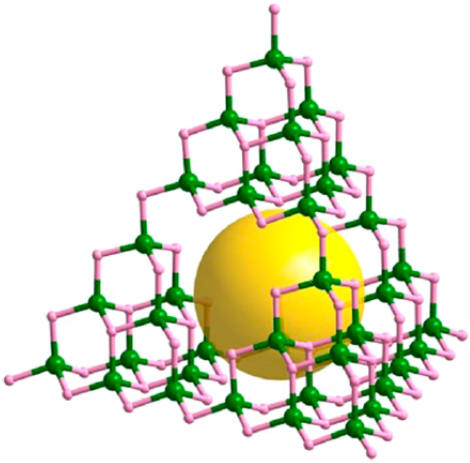

Figure 22: Representation of a $T_{3,2}$ cluster (In or Sn - green, S - pink)[98]

The first time such structure was obtained was by Li et al.[99] The synthesized structure consists in the presence of T2 clusters organized in a T4 cluster, thus leading to the presence of $T_{4,2}$ units with the composition $Cd_{16}In_{64}S_{134}$. When an ionic exchange was performed in order to attempt the substitution of the organic part with inorganic cations, no exchange was observed, revealing strong ionic forces between the organic agent and the crystal.

Continuing the work to obtain structures based on this type of clusters, Wang et al.[97] obtained a structure based on the infinite arrangement of T5 clusters, i.e. that presents a structure based on $T_{5,\infty}$ (see Figure 23a). The material obtained, entitled CIS-11, is an example of the super supertetrahedral arrangement for the Cu-In-S chemical system. In order to obtain the $T_{5,\infty}$ arrangement, it is observed that the corner sulfur atom has a coordination of 4, responsible for connecting four T5 clusters, being the first time such connection between clusters is observed. CIS-11 could be obtained by using different SDAs. When dibutylamine (DBA) is used as SDA, crystals with higher morphology and crystallinity are obtained. By using isopropylcyclohexylamine (iPcHA) it is possible to obtain a higher synthetic yield. Some years later, another structure was obtained, entitled CIS-27, also based on the arrangement of T5 clusters into a $T_{5,\infty}$ crystal, but by using 3, 5-dimethylpiperidine (DMP) as SDA instead of DBA or iPcHA.[100] CIS-27 presents a different connection mode between the different T5 clusters when compared to CIS-11 (see Figure 23b). For each

group of four T5 clusters, three are connected through a 3-coordinated sulfur atom and the remaining T5 cluster is connected to just one cluster.

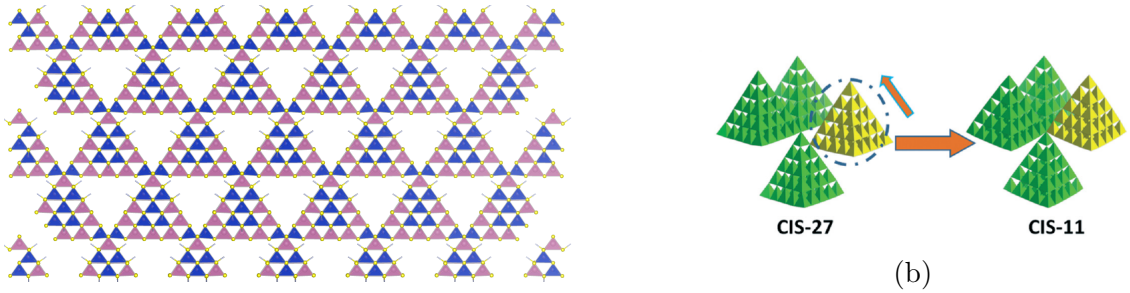

(a) (b)

Figure 23: (23a) Representation of a $T_{5,\infty}$ crystal (In - pink, Cu - blue, S - yellow).[97] (23b) Comparison of the different connection modes between CIS-11 and CIS-27[100]

A material was then obtained, entitled ITF-9, based on the T4 In-Zn-S clusters which were geometrically arranged to form a $T_{4,\infty}$ crystal.[101] ITF-9 presents a single-diamond topology and after an ionic exchange with Cs^+ to eliminate the SDA, the structure maintains its crystallinity. The stability of ITF-9 was also compared with UCR-1 and UCR-8. Both materials consist of T4 clusters, but the mode of connection between the clusters is different (see Table 4). In UCR-1 the clusters are connected through a bicoordenated sulfur bridge and in UCR-8 the clusters are connected through a tricoordenated sulfur bridge. Although the ITF-9 maintains its diffraction pattern after the ion exchange at room temperature, the intensity of the peaks associated with the UCR-1 and UCR-8 structures decrease drastically. When the ion exchange is performed at a higher temperature, ITF-9 is able to maintain its structure. The same is not true for UCR-1 and UCR-8, occurring the collapse of the structures.

2.1.1.3 Pentasupertetrahedral Clusters Pn

Another example of tetrahedral clusters are the penta-supertetrahedral clusters Pn. Each Pn cluster can be seen as an assembly of four Tn tetrahedrally distributed into the four faces of one anti-Tn cluster. An anti-Tn cluster is a Tn cluster where the positions of cations and

anions are exchanged. P1 (see Figure 24) and P2 (see Figure 25) clusters can be found as building blocks in a wide variety of open frameworks. Comparing to a Tn cluster of the same order, a Pn cluster has larger dimensions. For that reason, it is harder to prepare materials that use Pn clusters as building units.[46,64,102]

The number of cations in a Pn cluster is given by $t_n = [4n(n+1)(n+2)/6] + [(n+1)(n+2)(n+3)/6]$ and the number of anions is given by $x_n = [4(n+1)(n+2)(n+3)/6] + [n(n+1)(n+2)/6]$ (see Table 5).

Table 5: Composition of Pn clusters

Cluster Pn	t_n	x_n
1	8	17
2	26	44
3	60	90

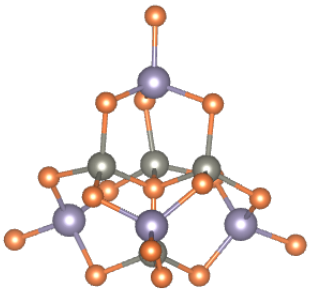

Figure 24: Representation of P1 cluster (Se - orange, Zn - gray, Sn - dark purple)[103]

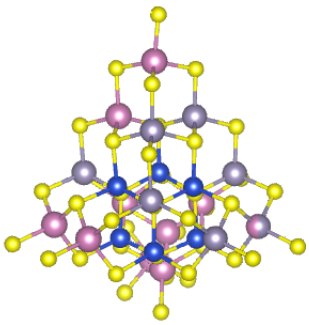

Figure 25: Representation of P2 cluster (In - pink, Cu - blue, S - yellow)[104]

A P1 cluster consists of four T1 MX_4 clusters and one anti-T1 XM_4 at the core, resulting in a P1 cluster with the composition M_8X_{17}.[102] Zimmermann et al.[105] and Dehnen et al.[103] obtained P1 clusters of the type $M_4Sn_4Se_{17}$ (M = Zn, Mn, Co). A 3-dimensional structure was then obtained based on the $Cd_4Sn_3Se_{13}$ cluster, which derives from $Cd_4Sn_4Se_{17}$, originating a polar open-framework.[106] The extra-framework is occupied by K^+ cations which can be exchanged with other cations such as Li^+, Na^+ or Rb^+, while maintaining the structure of the material.

Continuing the research to obtain P1 clusters, Palchik et al.[107] obtained clusters based on sulfur instead of selenium, presenting the chemical formula $M_4Sn_4S_{17}$ (M = Zn, Mn, Co, Fe). Also based on the $Zn_4Sn_4S_{17}$ cluster, Manos et al.[108,109] obtained a 3-dimensional structure in which each cluster is connected to four Sn atoms through the four terminal sulfur atoms. In turn, each Sn atom is connected to four clusters. The connection of clusters through metal centers is somewhat rare when it comes to methods of connection between clusters. Regarding the topology of the structure, it is of the diamond type with three different sizes of cavities (see Figure 26a). Each cavity has a distinct chemical reactivity, since the distribution of K^+ cations is different in each one (see Figure 26b). Due to the difference in cavity chemical reactivity, the structure has a high Cs^+ selectivity, even in the presence of a major excess of Li^+, Na^+, K^+ or Rb^+. In the absence of Cs^+, the structure has a high ion-exchange capacity for NH_4^+, comparable to that of natural zeolites.

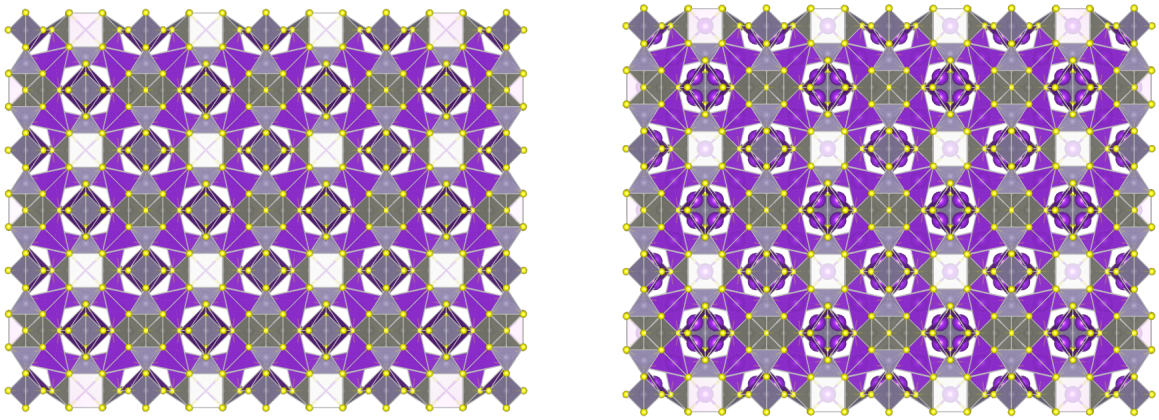

(a) (b)

Figure 26: Representation of the structure obtained by Manos et al.,[108,109] (26a) without and (26b) with the presence of K^+ (Zn - gray, K - purple, S - yellow)

As for 3-dimensional structures based only on P2 clusters (see Figure 25), Lv et al.[104] were able to synthesize such structures, entitled it MCOF-1 (see Figure 27a) and MCOF-2 (see Figure 27b). Both materials are based on a combination of Sn-In-Cu. MCOF-2 presents an interrupted open framework, which is somewhat peculiar for these type of structures. As for the SDA used to obtain these structures, it results from a combination of (R)(-)-2-amino-1-butanol (2-AB) and 1,8-diazabicyclo[5.4.0]-7-undecene (DBU). Both structures collapse after an ion exchange with Cs^+.

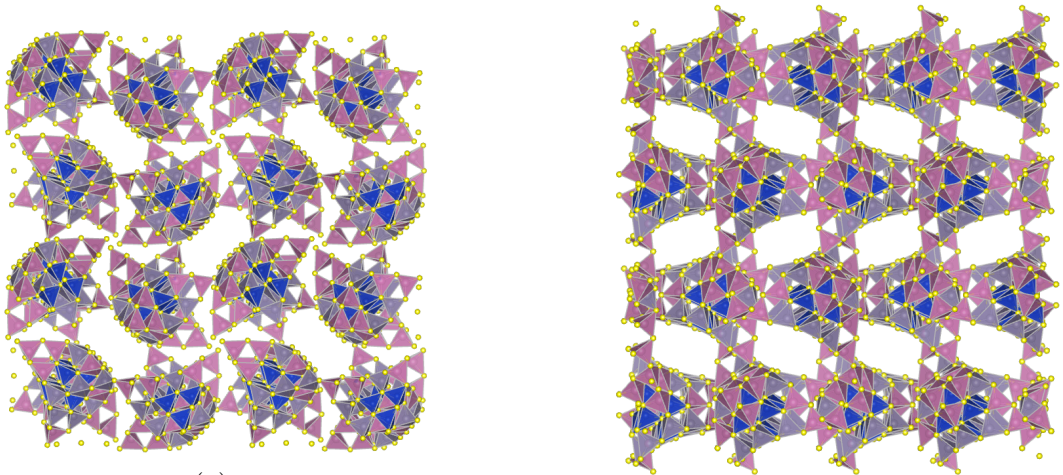

(a) (b)

Figure 27: Representation of the structures (27a) MCOF-1, with a chiral *srs*, and (27b) MCOF-2, with a double diamond topology (Sn - gray, In - pink, Cu - Blue, S - yellow)[104]

Another example of a 3-dimensional structure composed by P2 clusters is MCOF-4.[90] This material is composed by P2-CuGaSnS clusters interconnected by Cu^+ cations, being the first time that this combination of metals is used in this family of clusters and the connection between them is not made by a bisulfide bridge.

As can be seen, most of the structures obtained are isolated clusters, and there is no example of a laminar structure composed by this type of clusters.

2.1.1.4 Capped Supertetrahedral Clusters Cn

A third example of tetrahedral clusters is the Capped Supertetrhaedral series Cn. Each Cn clusters consists of Tn clusters covered by a shell of atoms. Each face of the individual Tn cluster is covered by the bottom atomic sheet of a T$(n+1)$ cluster and each corner covered by a metal-chalcogenide group. Thus, the stoichiometry of a M_xX_y type Cn cluster is equal to $x = [n(n+1)(n+2)]/6 + [4(n+1)(n+2)]/2 + 4$ and $y = [(n+1)(n+2)(n+3)]/6 + [4(n+2)(n+3)]/2 + 4$ (see Table 6).[46] Representations of clusters C1 and C2 can be found in Figures 28 and 29 respectively.

Table 6: Composition of Cn clusters

Cluster Cn	x	y
1	17	32
2	32	54
3	54	84

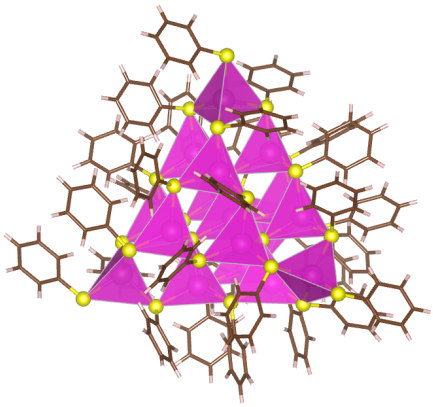

Figure 28: Representation of C1 cluster (Cd - pink, C - carbon, S - yellow)[110]

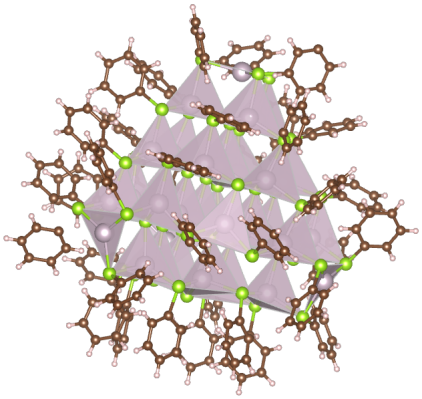

Figure 29: Representation of C2 cluster (Se - green, H - light pink, Hg - gray)[111]

Lee at al.[112] obtained for the first time a C1 cluster with the composition $S_4Cd_{17}(SPh)_{28}$. Later, a 3-dimensional double interpenetrated diamond structure based on the C1 $Cd_{17}S_4(SCH_2CH_2OH)_{26}$ cluster[110] and a 3-dimensional polymeric complex based on $[S_4Cd_{17}(SPh)_{24}(CH_3OCS_2)_{4/2}]_n \cdot n\ CH_3OH$[113] were also synthesized.

The first material based on the C2 cluster, with the composition $Cd_{32}S_{14}(SC_6H_5)_{36}{\cdot}DMF_4$, was obtained by Herron et al.[114] Vossmeyer et al.[115] obtained a similar structure but with different organic parts. It was observed that the organic residue has a direct influence on the final architecture as well as on the optical properties of the final material. Other examples of materials based on the C2 cluster can be found in the literature. For example, Behrens et al.[116] obtain an unusual C2 cluster based on Hg-Se chemical system where the Hg atoms

adopt an almost trigonal planar coordination, and Eichhöfer et al.[111] synthesized the first manganese chalcogenide C2 clusters.

Within this series of clusters, another similar one appears, entitled Cn, m, that has the same chemical composition as a Cn cluster, but presents a different spatial arrangement of the corner atomic unit. The Cn, m cluster is obtained by rotating one of the atomic units by 60°. Each Cn cluster has four atomic units and each one can be rotated independently, giving rise to four distinct series (m corresponds to the number of atomic units rotated).[46]

Zheng et al.[117] obtained the first example of clusters of this series. The cluster $Cd_{54}S_{32}(SPh)_{48}(H_2O)_4$ and $Cd_{32}S_{14}(SPh)_{40}$ are the first examples of C3, 4 (see Figure 30) and C2, 2 (see Figure 31), respectively. It was also observed that it is possible to dope the C3, 4 clusters obtained with Fe or Co.

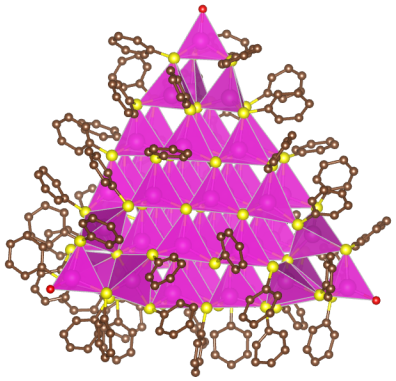

Figure 30: Representation of C3, 4 cluster (Cd - pink, C - carbon, S- yellow)[117]

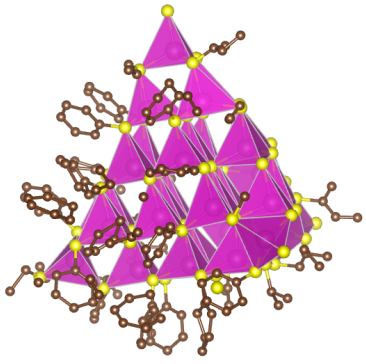

Figure 31: Representation of C2,2 cluster (Cd - pink, C - carbon, S- yellow)[117]

It can therefore be concluded that clusters of this series have not yet been obtained

without the presence of an organic component and that the materials obtained are only the result of the combination M^{2+}-X (X = S, Se). With the exception of the materials synthesized by Behrens et al.[116] and Eichhöfer et al.,[111] all the others have in their composition Cd, a chemical element known for its toxicity.

2.1.1.5 Oxyclusters

The addition of oxygen atoms to the clusters is a technique used to obtain large clusters, since it allows the diffusion of the bond valence associated to the chalcogen anions. It is thus possible to obtain Tn clusters with $n > 2$ with only tretavalent metals.[118] Regarding more practical applications, metal chalcogenides may present stability problems, namely when used as photocatalysts. Therefore, it is expected that the formation of oxycluster-based structures will have a superior stability, being able to maintain the electronic properties, such as adequate band structures and favorable absorption on the visible region.[119]

The first isolated $Sn_{10}O_4S_{20}^{8-}$ oxycluster (see Figure 32) was obtained in 1975 by Schiwy et al.[120] Later, Kaib et al.[121] obtained the same isolated anion but using Li insatead of Cs as a counter cation. Due to the replacement of Cs by Li, the water content is about 2,5 times higher that of the structure with Cs.

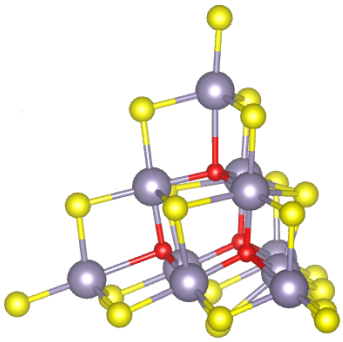

Figure 32: Representation of the T3 $Sn_{10}O_4S_{20}$ oxycluster (Sn - gray, O - red, S - yellow)[121]

Parise et al.[122] obtained for the first time a 3-dimensional structure with a 4-connected

porous system using as building units the clusters previously obtained by Schiwy et al.[120] The material obtained, designated as TETN-SnOS-SB2, presents a two-interpenetrating network, a topology analogous to cristobalite and $HN(CH_3)_3^+$, decomposed from TETN used during the synthesis, occupying the channels (see Figure 33). Continuing the research to obtain structures based on the T3 $Sn_{10}O_4S_{20}^{8-}$ cluster, the same research team obtained a layered material, entitled TMA-SnOS-SB3.[123] It was observed that it is possible to obtain the TETN-SnOS-SB2 or TMA-SnOS-SB3 structures from the analogous non-oxygen frameworks. Although the source of oxygen is not known, one possible hypotheses for the origin of this element is the decomposition of the water used as a solvent in the gel.

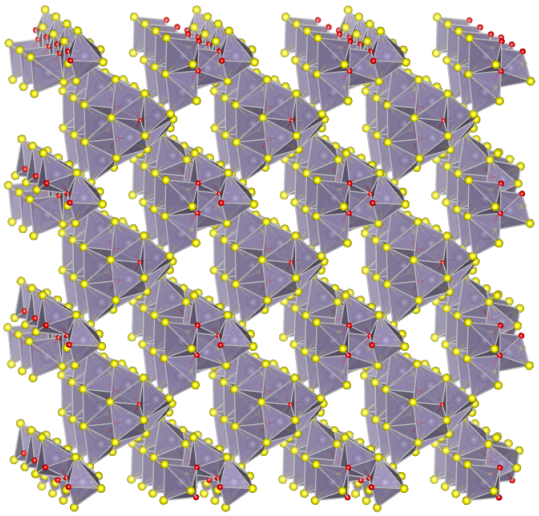

Figure 33: Representation of the structure TETN-SnOS-SB2 where the organic part $HN(CH_3)_3^+$ is not shown (Sn - gray, O - red, S - yellow)[122]

Huang et al.[118] obtained for the first time a material composed of T4 $Sn_{20}O_{10}S_{34}$ oxyclusters (see Figure 34). Such material presents a two fold interpenetrating diamond framework and maintains its structure in an environment with a pH from 1 to 13 for a period of one week. When an attempt was made to eliminate the organic compounds present in the porous system by ion exchange with Cs^+, it was observed that the porosity of the sample did not change.

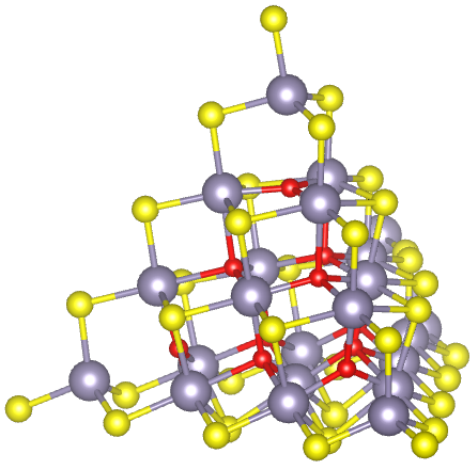

Figure 34: Representation of the T4 $Sn_{20}O_{10}S_{34}$ oxycluster (Sn - gray, O - red, S - yellow)[118]

Regarding the In-Sn-O-S chemical system, Zhang et al.[124] obtained a 3-dimensional material based on the pseudo T4 $In_4Sn_{16}O_{10}S_{34}$ oxycluster (see Figure 35) for the capture of heavy metals. Regarding topology, this material presents a two-fold interpenetrated 3-dimensional framework analogue to cristobalite.

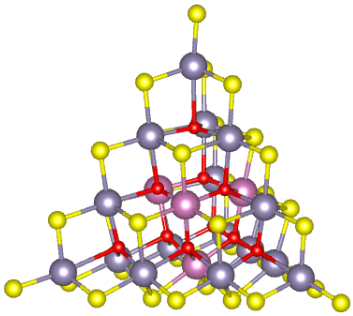

Figure 35: Representation of the pseudo T4 $In_4Sn_{16}O_{10}S_{34}$ oxycluster (Sn - gray, O - red, In - pink, Zn - pink, S - yellow)[124]

Zhang et al.,[125] in order to develop a catalyst for oxygen reduction reaction, obtained isolated Ge-Zn P1 oxyclusters doped by Mn (see Figure 36). The clusters obtained are more stable than the traditional P1, due to the replacement of S^{2-} with OH^- at the four corners of the cluster.

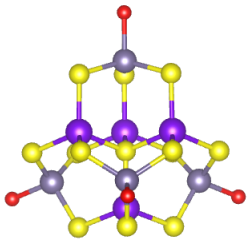

Figure 36: Representation of the P1 oxycluster (Ge - gray, O - red, Mn - purple, S - yellow) [125]

As for the Ga-O-S system, Vaqueiro et al. [76] were successful in obtaining a 3-dimensional structure based on a T3 cluster where the terminal sulfur was substituted by an oxygen atom. The connection between the clusters is made by an unusual polysulphide linkage and it is the first time that the linkage of these types of clusters is made through a O^{2-} bridge.

Aharia et al. [126] studied the Sn-Se chemical system. It was observed that there is a change of phases between a $TMA_2Sn_3Se_7$ laminar material to a $TMA_2Sn_5Se_{10}O$ 3-dimensional material (where TMA represents tetramethylammonium, the SDA used). What differentiates the achievement of the different phases are temperature and synthesis time. It was observed that for two days of synthesis, a laminar monocyclic phase is the only phase present. On the fourth day of synthesis, three distinct phases coexist: two laminar orthorombic and monocyclic phases and a third unknown phase. On the seventh day of synthesis there is a fourth phase associated with a 3-dimensional tetragonal material which becomes the only phase present after sixteen days of synthesis. The 3-dimensional material (see Figure 37) consists of T2 $Sn_4Se_{10}O$ clusters with the oxygen atom located at the center (see Figure 38).

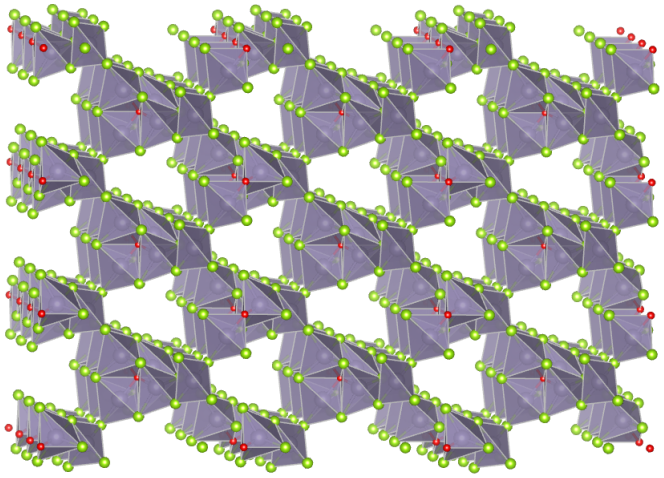

Figure 37: Representation of $TMA_2Sn_5Se_{10}O$ 3-dimensional material (Sn - gray, O - red, Se - green)[126]

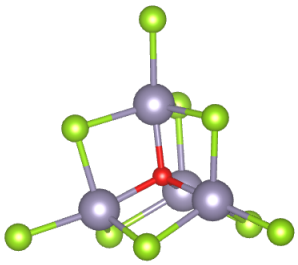

Figure 38: Representation of $TMA_2Sn_5Se_{10}O$ 3-dimensional material building unit (Sn - gray, O - red, Se - green)[126]

Continuing the research in obtaining selenium-based materials, Lin et al.[119] prepared a material based on the T3 $Sn_{10}O_4Se_{20}$ cluster while using N-(2-aminoethyl)ethanolamine (AEAE) as SDA. The structure synthesized, entitled OCF-61-SnOSe, can be deconstructed into three levels of organization. The primary building unit is the $SnSe_4$ tetrahedron. The next structural level would be to obtain a T3 $Sn_{10}Se_{20}$. However, its formation is unfavorable, as it is an unstable structure due to the excessively high bond valence due to Sn^{4+}. Thus, a T3 $Sn_{10}O_4Se_{20}$ is formed, where four adamantane-type cages surround O^{2-} groups, being the secondary building unit. The tertiary building unit is the formation of the super-supertetrahedral cluster. Four T3 $Sn_{10}O_4Se_{20}$ are connected through bicoordinated Se^{2-} but also through a dimeric $Sn_2Se_6^{4-}$, originating a T2 cluster (see Figure 39). Therefore, OCF-

61-SnOSe can be characterized by the presence of the super-supertetrahedral $T_{3,2}$ cluster which presents a honeycomb layered structure.

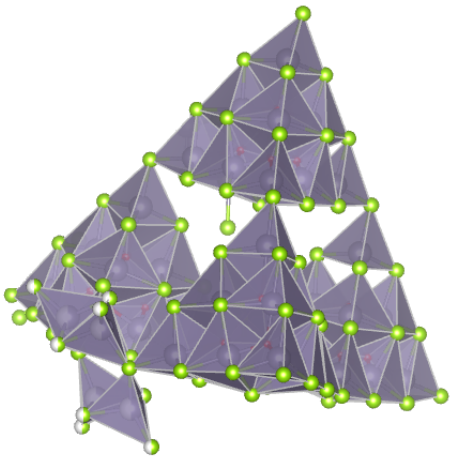

Figure 39: Representation of the unusual building unit present in OCF-61 (Sn - gray, O - red, Se - green)[119]

2.1.1.6 TOn clusters

TOn differs from Tn, Cn to Pn cluster series so far presented, as they result from the combination of tetrahedral and octahedral bonding features in the same cluster. Such clusters result in the combination of a NaCl-like octahedral core covered by a ZnS-like tetrahedral shell.

The first example of a structure based on this type of clusters was obtained by Wu et al.[127] This structure, entitled OCF-41, is made up of In-S TO2 clusters. The TO2 cluster consists of an $In_{10}S_{13}$ octahedral core which presents four four T2 In_4S_{10} clusters on the corners, and four hexagonal In_3S_3 rings on the faces (see Figure 40). OCF-41 presents a 2-dimensional structure where the TO2 clusters are connected through dimeric $In_2S(H_2O)_2$ units.

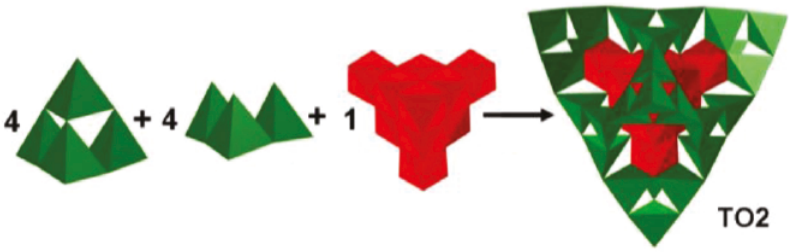

Figure 40: TO2 cluster composed by four T2 clusters, four hexagonal rings and an octahedral core[127]

Due to the high negative charge associated with the TO2 cluster it is difficult to counterbalance it using the usual SDAs, thus limiting the construction of structures with high dimensions. One of the methodologies used by Wang et al.[128] to obtain a 3-dimensional structure using TO2 clusters as building units was through the introduction of high-valence metal cations. Two 3-dimensional structures, entitled SOF-25 and SOF-28, based on Sn-In-S TO2 clusters and using R-(-)-2-amino-1-butanol (2-AB) and 1,8-diazabicyclo[5.4.0]-7-undecene (DBU) as SDAs were obtained. Both materials present a double (see Figure 41a) and triple interpenetrated diamond framework (see Figure 41b), respectively.

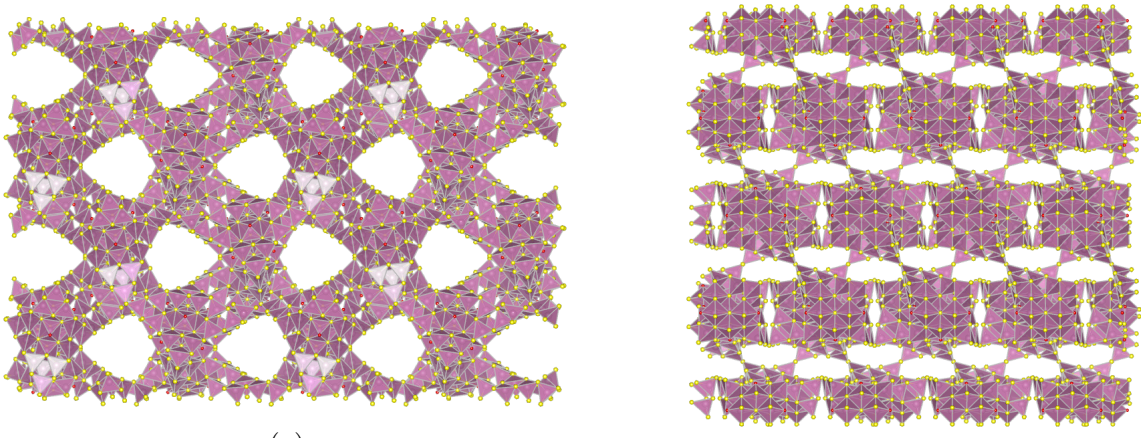

(a) (b)

Figure 41: Representation of (41a) SOF-25 and (41b) SOF-28 materials (In - gray, O - red, S - yellow)[128]

2.1.1.7 Structures with different series and types of combined clusters

Examples of structures consisting of only one type of cluster as a building unit were presented. However, it is possible to have materials composed by more than one type of cluster. Thus, by increasing the complexity and diversity of these systems, it is possible to synthesize materials with physical and chemical characteristics adapted to a specific application.

Starting with the Tn clusters, there are four types of clusters, thus it is possible to have six different combinations: T2-T3, T2-T4, T2-T5, T3-T4, T3-T5 and T4-T5. The biggest challenge in synthesizing structures based on different Tn clusters is the phase separation, ending with two distinct structures containing only one type of cluster.

Han et al.[129] synthesized for the first time a compound that consisted on the presence of Sn-Ga-S T2 cluster and the uncommon Sn-S-O T3 cluster, adopting a PtS type topology.

The first example of a T2-T4 combination is presented by Wu et al.[89] The synthesized structure, OCF-42, results in a combination of $M^{4+}/Ga^{3+}/Se^{2-}$ T2 cluster and $Ga^{3+}/Zn^{2+}/Se^{2-}$ T4 cluster by using 4,4'-trimethylenedipiperidine (TMDP) as SDA. The structure is not constituted through the alternation of the two types of clusters. Each T2 cluster is connected to four T4 clusters (see Figure 42a) and each T4 cluster is connected to one T2 cluster and three T4 clusters (see Figure 42b), thus obtaining a T2/T4 framework ratio equal to 1:4.

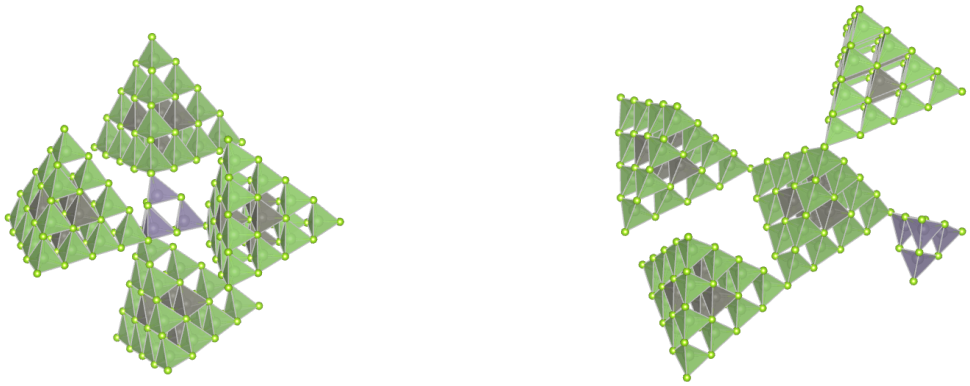

(a) (b)

Figure 42: Different modes of connection in OCF-42: (42a) one T2 cluster connecting four T4 and (42b) one T4 clusters connecting one T2 cluster and three T4 clusters[89]

As for the T2-T5 combination, Wang et al.[130] managed to obtain such structure, designated CIS-52, through the combination of Ge-In-Cu-S. The starting system was In-S and

the addition of Cu favors the formation of T5 clusters, while the presence of Ge favors the formation of T2 clusters. In this case, the structure is composed through the alternation of clusters.

When Zheng et al.[68] obtained for the first time a structure based on the Ga-Zn-S T4 cluster system, it was also observed that by changing the SDA, an architecture based on the alternation of clusters type T3 and T4 is obtained, named UCR-19. Another example of a structure based on the presence of T3 and T4 clusters is presented in Ref.,[76] being the first example of the incorporation of Co on the Ga-S system.

The 3-dimensional structure synthesized by Wang et al.[91] where, for the first time a pseudo-T5 cluster was obtained, is based on the alternation of the pseudo T5 cluster with T3 clusters. Another example of a 3-dimensional structure composed by the combination T3-T5 clusters is the material obtained by Zhang et al.,[131] named IOS-35. In such material the T3 clusters are composed by In and S and the T5 clusters are oxyclusters, presenting a combination of In, O and S.

A material with the combination T4-pseudo-T5 was first obtained by Wang et al.[132] Such structure, OCF-45, presents a non-interpenetrated diamond topology and it is based on the In-Mn-S chemical system. OCF-45 presents a large extraframework volume and windows aperture due to the non-interpenetrating topology and the presence of big clusters size. For the elimination of the SDA, a simple ion exchange with Cs^+ can be done. However, a small shift of the diffraction peaks towards lower angles can be observed, since with the elimination of the large organic species the crystalline framework tends to shrink.

As for structures based on different clusters, Zhang et al.[133] manage to synthesize a material, entitled HCF-1, which was composed by P1 and T2 clusters of the chemical system In-S, presenting a 2-dimensional framework. Following these works, a 3-dimensional structure based on $T_{3,2}$ and T3 clusters from the Sn-In-S chemical system was obtained.[98] In such structure, SOF-2, each $T_{3,2}$ clusters is connected to four T3 clusters.

Of all the observed combinations, it should be noted that no material has yet been

obtained that results from the combination of M^{4+} and M^{2+} metals.

2.1.2 Non Tetrahedral Clusters

Due to the tetrahedral coordination of Tn, Pn and Cn clusters series, these units become the ideal candidates for the construction of open frameworks. However, the number of clusters available is limited. Moreover, clusters in the Pn and Cn series tend to maintain their isolated form rather than forming open frameworks. It is therefore advisable to create other series of clusters in order to complement the cluster-based chalcogenide open frameworks.[128]

2.1.2.1 Semi-cube Clusters

Regarding this type of clusters, two possible compositions stand out: Sb_3S_6 (see Figure 43) and Sn_3S_4 (see Figure 44).[47]

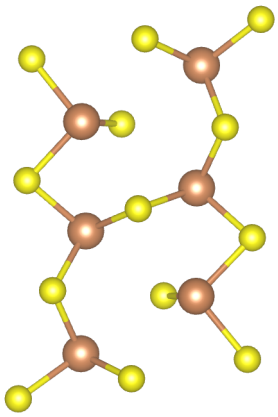

Figure 43: Representation of Sb_3S_6 building units[134]

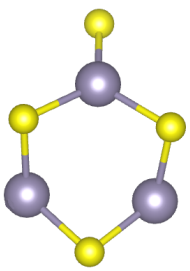

Figure 44: Representation of Sn_3S_4 building unit[135]

Parise et al.[136] obtained for the first time a layered material based on the Sb_3S_6 cluster. When tetramethylammonium ion is used as a SDA, a 3-dimensional structure is obtained.[137] Research continued into this chemical system, using large tertiary amines in order to try to produce materials with larger cavities.[134] When tetrapropylammonium hydroxide or triethylenetetramine is used, no 3-dimensional materials are obtained, but 1-dimensional and 2-dimensional structures, respectively.

The materials obtained by Bedard et al.[49,50] in 1989 are the first examples of layered materials composed by the semicube Sn_3S_4 clusters. Next, Jiang et al.[135,138–141] have studied the Sn-S system, obtaining layered materials based on the periodic arrangement of Sn_3S_4 clusters. Two types of layered materials were obtained: SnS-1 and SnS-3. The difference between the two is based on the way the clusters are connected. SnS-1 presents a hexagonally shaped 24-atom rings (see Figure 45a) and SnS-3 (see Figure 45b) has elliptically shaped 32-atom rings.

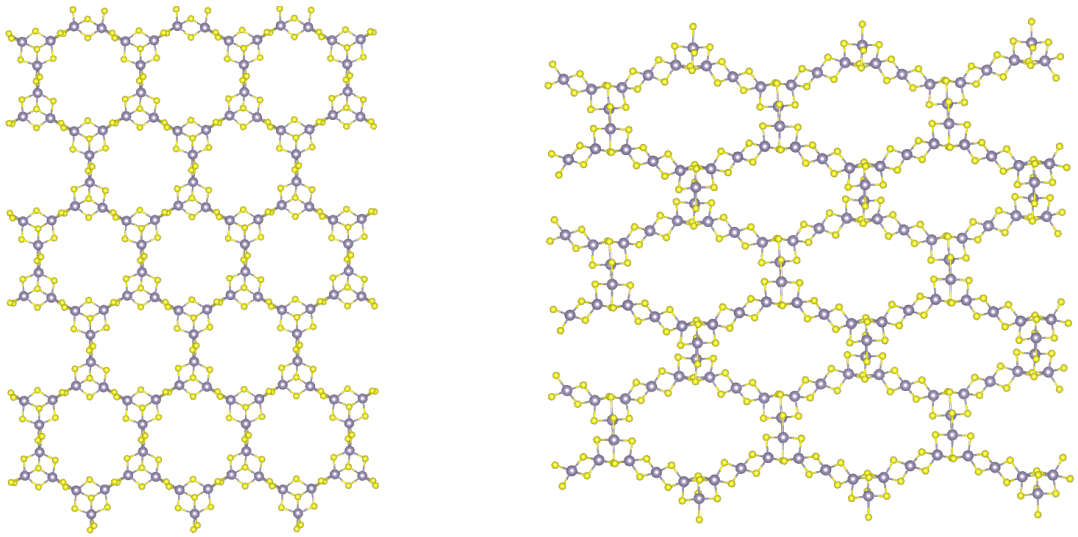

(a) (b)

Figure 45: Representation of (45a) SnS-1 and (45b) SnS-3 laminar structures where the organic part was not represented (Sn - gray, S - yellow)[135]

It has been observed that when using small size SDAs, such as tetrabutylammonium hydroxide, SnS-1 is obtained and with large size SDAs, for example tetrapropylammonium

or tetrabutylammonium hydroxides, originate SnS-3. Both structures have a surprising flexibility. In order to accommodate SDAs with different shapes or dimensions, the synthesized materials may undergo a certain degree of elastic deformation, changing the interlamellar spacings instead of forming a structure with a new topology. Another important characteristic of these materials is their thermal stability when removing the SDA used during their synthesis. SnS-1 was also subjected to an ion-exchange study. When tetramethylammonium hydroxide is located in the intralaminar space, it is possible to exchange part of the organic component with Na^+, Ca^{2+}, Co^{2+} or Ni^{2+}. However, the structure collapses when trying to exchange with Cu^{2+} or Ag^+.[142]

Bowes et al.[143] performed a more in-depth study of the SnS-1 structure. It was noted that it is possible to use tetramethylammonium (TMA), tert-butylammonium (TBA) or quinuclidinium (QUIN) as SDAs to obtain these structures. Such species occupy the interlaminar space, being responsible for counterbalancing the charge of the framework, but also to support it. The size and shape of the SDA is responsible for controlling the interlaminar distance, but also the thermal stability, and adsorption and sieving properties of the material. The SnS-1 structure is able, to a certain extent, to exchange with other species, occurring its swelling. When the species are too large, they are simply excluded, thus having a sieving effect. The substitution of sulfur by selenium was also evaluated. The analysis of diffraction data allows the conclusion that the structures of the materials $TMA_2Sn_3S_7$ and $TMA_2Sn_3Se_7$ are identical. However, an increase in lattice was observed due to the larger size of the selenium comparing to sulfur. It is also possible to obtain the SnS-1 structure from tris-2-aminoethylamine[144,145] or 1-(2-aminoethyl)piperidine,[145] thus showing the flexibility of this structure to accommodate different molecules into their interlayer space. Qi et al.[146] continued to study the ion-exchange properties of SnS-1. After exchanging with Cs^+ or Sr^{2+}, the material maintains its crystalline structure.

Switching to selenium-based materials, Han et al.[147] obtained 1-dimensional and 2-dimensional materials with the Sn_3Se_4 semicube cluster, using the alcohol C_2H_5OH as a sol-

vent. The laminar material has a honeycomb structure with elliptical holes with $Mn(en)_3^{2+}$ cations at the nanochannels. For the 1-dimensional structure, it can been represented as a an anionic zig-zag chain with $Ni(en)_3^{2+}$ located between the chains.

2.1.2.2 Icosahedral Clusters

As seen above, the presence of monocations such as Cu^+ [59–61] or Ag^+ [61] is restricted to connecting the clusters or to partially replacing the cationic sites of the tetrahedral clusters. With the increase in the content of monocations in the framework, new clusters emerge, where the icosahedral clusters stand out. This type of clusters has six connection modes, allowing the obtention of topologies that would not be possible with tetrahedron clusters. To obtain this type of icosahedral clusters, the presence of high valence cations with a tetrahedral coordination is essential, since it reduces the negative charge of the chalcogenide ions.[148] The monocation that has been the subject of most research is copper, originating a new family of materials such as copper-rich open-framework chalcogenides. Due to the high copper content in the structures, there is a reduction in the band gap value, making these materials promising when it comes to applications in the areas of photovoltaic and photocatalysis applications.[149]

The first examples of structures with icosahedral clusters as building units were obtained by Schimek et al.[150] The 3-dimensional structure obtained consists in the connection of Cu_8S_{13} icosahedral clusters through Sb atoms that assume a tetrahedral coordination with the sulfur atoms.

Following these works, Zhang et al.[151] obtained a material based on icosahedral clusters composed by Cu and S using Ge as a connection mode (see Figure 46).

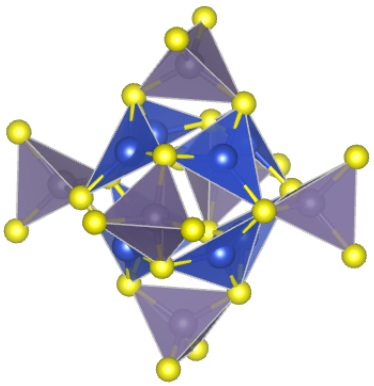

Figure 46: Representation of an icosahedral cluster (Ge - gray, Cu - blue, S - yellow)[151]

Regarding the structure, it can be seen as a cubic packing of Cu_8S_{12} icosahedral clusters that are connected in two directions by dimeric Ge_2S_6 units and on the other direction by GeS_4 (see Figure 47a). Comparing with 3-dimensional structures composed by T2 clusters with the same chemical elements, it can be observed that the architecture formed by icosahedral clusters presents a higher number of Cu than Ge. Continuing the research on this series of materials, it was possible to obtain structures also composed by Cu_8S_{12} icosahedral clusters that were only connected by GeS_4 units.[152] The structures obtained present the 3-dimensional topology of perovskite (see Figure 47b). Comparing the two materials, the structure that only presents as GeS_4 units as a link between the clusters needs only K^+ or Rb^+ instead of organic amines to stabilize the structure. A structure composed by Cu_8S_{12} icosahedral clusters connected in two directions through GeS_4 and in one direction by Ge_2S_6 dimeric unit was then obtained[153] (see Figure 47c). Comparing the three materials, the one that presents the biggest extraframework volume is the material that presents as a way of connecting the dimeric units Ge_2S_6 in two directions.[151] The material with the lowest extraframework volume is the one where the only form of connection between the clusters is by GeS_4.[152] This can be explained by the way clusters are connected: the more connections are made by Ge_2S_6 dimeric units, the more the framework will expand.

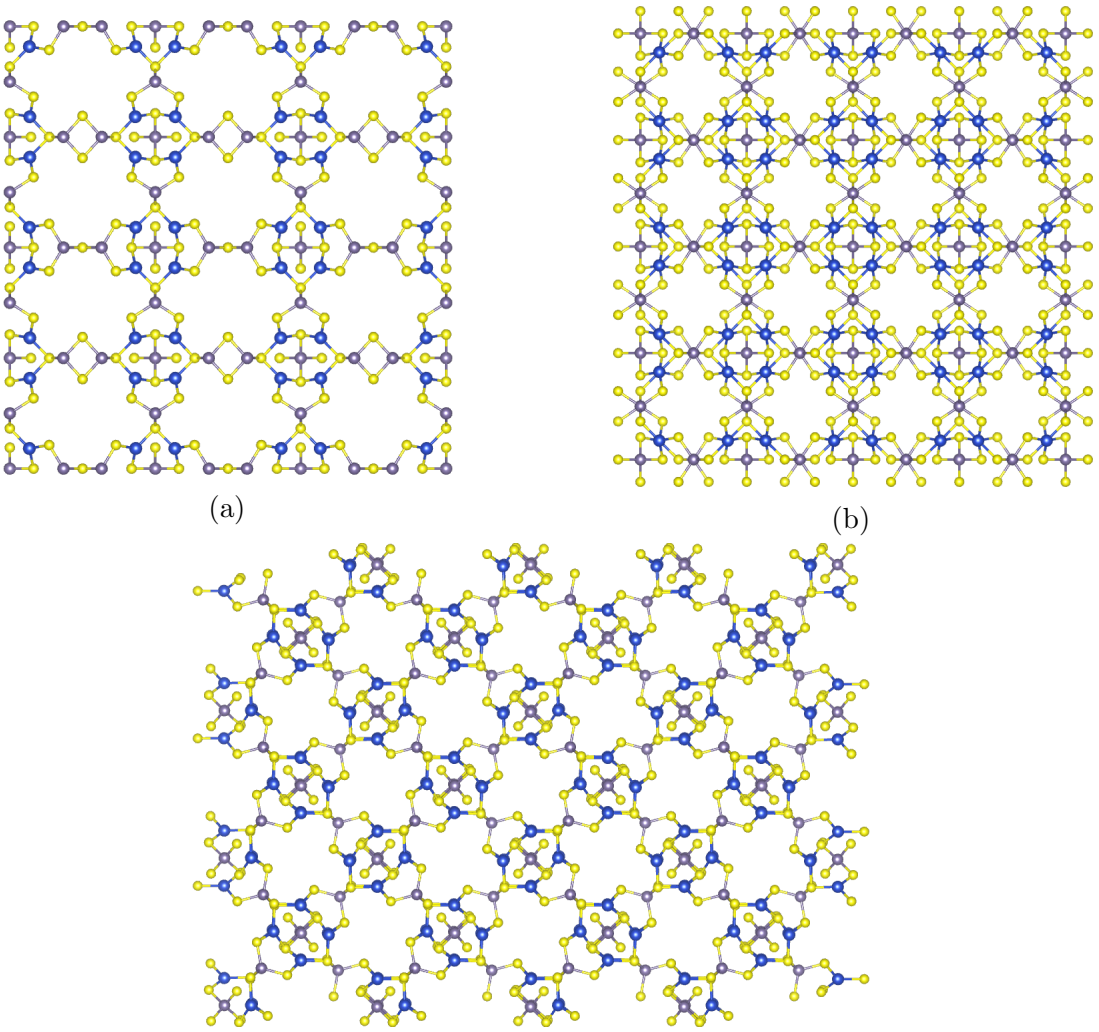

Figure 47: 3-dimensional structures composed by icosahedrons as building units but with different modes of connection between them. (47a) Clusters connected in two directions by dimeric Ge_2S_6 units and on the other direction by GeS_4.[151] (47b) Clusters connected in all directions by GeS_4 units.[152] (47c) Clusters connected in two directions through GeS_4 and in one direction by Ge_2S_6 dimeric unit[153] (Ge - gray, Cu - blue, S - yellow)

More recently, Tang et al.[154] have obtained a 3-dimensional structure composed of Cu_8S_{12} icosahedral clusters that are surrounded by Cu_8S_{16} rings. Such structure presents GeS_4 tetrahedra entrapped, being the first time tetrahedrons have not participated in the cluster connection.

It is possible to find in the literature materials that use Sn^{4+} instead of Ge^{4+} to connect the different clusters.[155,156] Due to the way the different clusters are connected, the material

obtained by Zhang et al.[155] presents a multiple channel system, something rare for a material with a cubic symmetry. Behrens et al.[156] also obtained a series of materials based on Cu_8S_{12} icosahedral clusters. In some materials obtained, it was observed for the first time the inclusion of Sn^{3+} in the cluster, being the first example of materials based on Cu_7SnS_{12} icosahedral clusters while still using Sn^{4+} as a connection between the clusters.

For selenium, the first series of 3-dimensional materials were obtained by Zhang et. al.[148] This series of materials are based on the presence of Cu_8Se_{13} icosahedral clusters that are connected by $AsSe_{13}$ tetrahedral units. Yang et al.[157] then obtained a 3-dimensional framework based on the presence of Cu_8Se_{13} icosahedral and Cu_4Se_6 octahedral clusters. Each icosahedron is connected to six tetrahedrons through six distorted $SnSe_4$ and each tetrahedron is connected to three icosahedrons through three $SnSe_4$ via sharing vertex and Se-Se bonds. Due to this method of connection, the material obtained presents (3,6)-connected *pyr* topology (see Figure 48). When trying to eliminate piperidine (PR), the organic SDA used during the synthesis, via ion exchange with Cs^+ or Na^+, it is not successful.

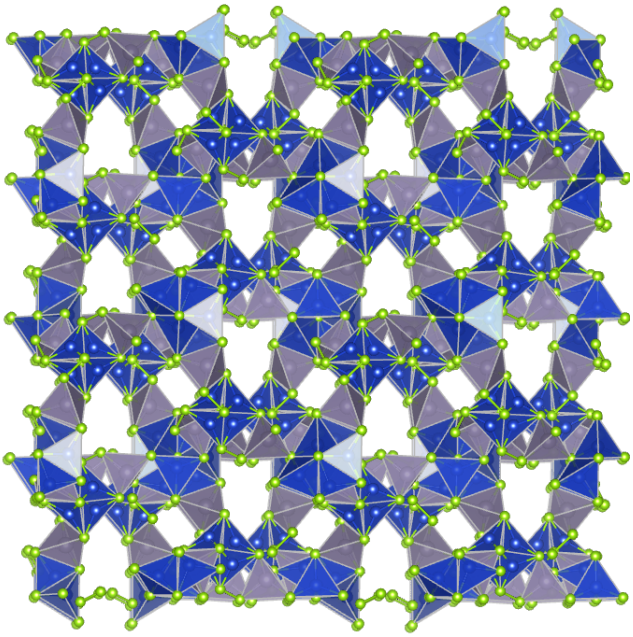

Figure 48: Representation of the structure obtained by Yang et al.[157] (Sn - gray, Cu - blue, Se - green)

Luo et al.[149] were able to obtain for the first time a family of materials where the icosa-

hedral clusters were connected only by Ge_2Se_6 or Sn_2Se_6 dimers. This was achieved by using SDAs with low charge density, such as piperidine (PR). As the only method of connection is via dimer, this family of materials has the highest extra framework volume (see Figure 49). It was also obtained for the first time a material composed by Cu_7GeSe_{13} clusters. Such materials have the *pcu* topology, analogue to the MOF-5 [1].

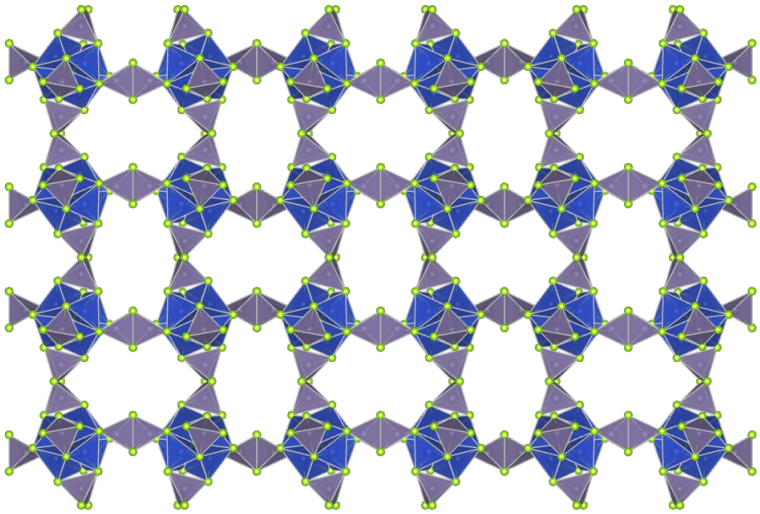

Figure 49: Representation of the structure obtained by Luo et al.[149] (Sn - gray, Cu - blue, Se - green)[149]

Another example of 3-dimensional materials consisting of Ge-Cu-Se are those materials obtained by Wang et al.[159] The framework of the first material consists of two types of clusters, Cu_8Se_{13} icosahedral and Cu_4Se_6 octahedral, which are connected through bridging with $GeSe_3(Se_2)$ units. Such connection mode between the clusters originates a material with a *pyr* topology. The second material can be seen as a 3-dimensional framework composed by Cu_8Se_{13} connected solely by Ge_2Se_6 dimers.

2.1.3 Final Considerations

As can be seen from the examples presented above, there is a great variability of materials composed by different combinations of chemical elements and type of clusters. The mate-

[1]MOF-5 is a metal-organic framework compound composed by tetrahedral $[Zn_4O]^{6+}$ units linked by arylcarboxylate ligants and it was obtained for the first time by Kaye et al.[158]

rials obtained can have different dimensions, from isolated clusters, 1-dimensional chains of clusters, laminar and 3-dimensional materials. Due to the use of M_xX_y clusters instead of TO_4 tetrahedron, materials with a superior pore opening are obtained.

The most common method of connection between clusters is through bichalcogeneos bridges. However, it is still possible to find examples of materials where clusters are connected through polychalcogeneos bridges, metals or even dimers. Evaluating the three chalcogens studied, S, Se and Te, sulfur is the most common chalcogen present in the studied materials. The number of structures with Se is quite small in relation to the number of structures constituted by S. In relation to the tellurium, because it is an element with low reactivity that generally gives rise to unstable structures, the number of known structures is even smaller.

For 3-dimensional materials, the typical topology is diamond, and most materials have an interpenetrated network, since it reduces the potential energy of the structure. As such, the extraframework volume, as well as the pore opening, tends to decrease.

Table 7 shows clusters synthesized so far with the simplest combination, i.e. clusters consisting of only one type of metal and one type of chalcogen.

Table 7: Clusters formed by only one type of metal and one type of chalcogen

	S	**Se**	**Te**
Ge	T2	T2	T2
Sn	Semicube	Semicube	T2
In	T2 T3 pseudo T5 & T3 TO2	T2 T3	-
Ga	T3	T3	-
Cu	Icosahedral	-	-

Regarding the combination Ge-S or Ge-Se, it is observed that the number of 3-dimensional structures obtained is reduced, often requiring the use of other metals, such as Mn, Cu, or

Ag to connect the different clusters. As for Sn-S or Sn-Se combinations, it is only possible to obtain laminar structures that have as building unit the semicube cluster. Two distinct laminar structures, SnS-1 and Sn-3, were synthesized and widely studied. Both structures are quite elastic, i.e. they can be obtained using a wide variety of SDAs. It is observed that when the SDA is altered, it will affect the intralaminar space, instead of obtaining a new topology. SnS-1 is obtained when large SDAs are used and SnS-3 is obtained when small SDAs are used.

It is also observed that M^{4+}-X^{2+} combinations originate small clusters, such as T2 and semicube clusters. In order to increase the size of the obtained clusters without the addition of other metals, oxygen is added to the system. Thus, it is already possible to find T3 and T4 clusters consisting of the Sn, O and S or Sn, O and Se.

Both in the Ga-S and Ga-Se system, the synthesized materials are composed of T3 clusters. It is observed that to obtain 3-dimensional structures composed by Ga and Se, the gels should not present water in their composition and the final structures are not interpenetrated. On the contrary, for the the Ga-S system, the gels should contain water in their composition and, until now, only interpenetrated 3-dimensional structures have been obtained.

Recently, materials containing copper, due to their electronic properties and band structure, have been investigated for applications in the area of photocatalysis and photovoltaics. In order to obtain clusters rich in this monocation, it is necessary to use a non-tetrahedron cluster, the icosahedron. Most of the synthesized materials that use this cluster as a building unit would require the addition of high-valence cations, such as Sn or Ge. However, it is already possible to find in the literature examples where the clusters are only composed and connected by units that contain Cu and S.

The In-S system presents the greatest diversity of clusters, obtaining clusters of type T2, T3 and TO2. As for the topology of the materials obtained, they may be isolated clusters, laminar or 3-dimensional, with a simple or interpenetrated net. Table 8 presents the main

characteristics of the materials synthesized.

Table 8: Different materials based on the In-X (X = S, Se) chemical system

Material	SDA	Gel composition (mol)					Cluster	Structure	Ref.
		In	S	Se	Organic	H_2O			
DPA-InS-ML	DPA[1]	n/a[2]	n/a[2]	-	n/a[2]	n/a[2]	T2	OD	[65]
Component 1	PR[3], DMF[4]	1	without	4,5	92,0	without	T2	3D - Int. D[5]	[74]
Component 2	3,5-DMPR[6], DMF[4]	1	without	4,5	47,6	without	T2	3D - D[7]	[74]
Component 3	1-MPR[8]	1	without	5,1	41,2	6,8	T2	3D - D[7]	[74]
DMA-InS-SB1	DMA[9]	1	2,3	without	4,4	16,6	T3	3D - DD[10]	[65]
DEA-InS-SB1	DEA[11]	1	2,3	without	6,8	trace	T3	3D - DD[10]	[47]
DEA-InS-SB2	DEA[11]	1	2,3	without	3,4	14,0	T3	2D	[47]
ASU-31	HPP[12]	1	2,5	without	n/a[2]	n/a[2]	T3	3D - SOD[13]	[55]
ASU-32	DPM[14]	1	2,5	without	n/a[2]	n/a[2]	T3	3D - CrB_4[15]	[55]
ASU-34	HMA[16]	1	2,5	without	n/a[2]	n/a[2]	T3	3D - CrB_4[15]	[66]
UCR-7-InS-TETA	TETA[17]	1	without	2,5	18,5	21,8	T3	3D - DD[10]	[73]
UCR-15-InS-DPM	DPM[14]	1	2,2	without	113,1	without	pseudo T5 & T3	3D - DD[10]	[91]
OCF-41-InS-DBU	DBU[18], acetonitrile	1,0	2,0	without	70,7	113,1	TO2	2D	[127]

[1] Dipropylamine. [2] n/a - not available. [3] Piperidine. [4] Dimethyl formamide. [5]Interrupted diamond. [6] 3,5-Dimethylpiperidine. [7] Diamond (see Figure 1a)
[8] 1-Methylpiperidine. [9] Dimethylamine. [10] Double diamond. [11] Diethylamine. [12] 1,3,4,6,7,8-hexahydro-2H-pyrimido[l,2-a]pyrimidine.
[13] Sodalite (see figure 1b). [14] Dipiperidinomethane. [15] (see figure 1c). [16] Hexamethyleneimine. [17] Triethylenetetramine. [18] 1,8-Diazabicyclo[5.4.0]undec-7-ene
[18] 1,8-Diazabicyclo[5.4.0]undec-7-ene

Looking first at the In-Se system, it is possible to obtain 3-dimensional structures composed by T2 clusters or T3 clusters. To obtain structures composed by T2 clusters it is necessary to use an SDA with a piridine ring and the use of another solvent, such as DMF, besides water. The UCR-7 structure, the only structure synthesized with T3 clusters so far, can be obtained, in addition to triethylenetetramine (TETA), by other SDAs, such as piperazine (PZ), 1,4-diazabicyclo[2.2.2]octane (DABCO), 2-(2-aminoethylaminoethanol) (AEAE) or 3-dimethylaminopropylamine (DMAPA). Thus, UCR-7 is a more elastic structure, since it can be obtained by a wider variety of SDAs. All structures are diamond-like topology. However, those composed of T2 are not interpenetrated, where one of them presents interrupted sites.

Moving to the In-S system, it is possible to obtain isolated clusters, laminar or 3-dimensional, simple or interpenetrated, structures. As previously discussed, water plays a key role in the final topology obtained, since for the same SDA used, different architectures can be obtained taking into account the water content present in the initial gel (DEA-In-SB1 vs. DEA-InS-SB2). Unfortunately, more information on the experimental methodology used to obtain ASU-32 is not publicly available, so it is not possible to compare it with the other

material where the same SDA was used, the UCR-15 structure.

By increasing the degree of complexity, it is possible to obtain structures where the clusters are composed of two types of metals (see Table 9).

Table 9: Clusters formed by two metals and sulfur

	S						
	In	**Cd**	**Fe**	**Co**	**Zn**	**Cu**	**Mn**
Ge	-	-	-	-	-	Icosahedral	-
Sn	TO2	-	P1	P1	P1	Icosahedral	P1
In	-	T4 pseudo T5 $T_{2,4}$	T4	T4	T4 T6 $T_{4,\infty}$	T5 $T_{5,\infty}$	-
Ga	-	-	-	T4 & T3	T4 T4 & T3	-	-

The addition of M^{2+} or M^{+} cations to an M^{3+}-X^{2-} system allows the obtained cluster size to be increased, from T3 to T4, T5 or T6.

When Zn or Co is added to the Ga-S system, it is possible to obtain structures composed by T4 clusters or by the combination of T4 and T3 clusters. T4 clusters are obtained in the presence of Zn when 1,4-bis(3aminopropyl)piperazine is used as SDA. However, when Zn is not present in the system, only T3 clusters are obtained, thus showing the importance of the presence of M^{2+} to obtain structures with larger clusters. When the SDA is replaced by triethylenetetramine (TETA), a structure consisting of alternating T3 and T4 clusters is observed. The structures composed by Ga-Zn-S are 3-dimensional with an interpenetrated structure. When there is the replacement of S with Se, it is possible to obtain 3-dimensional structures without being interpenetrated.

When inserting a M^{2+} or M^{+} cation in an M^{4+}-X^{2-} system, the size of the Tn type clusters is not increased. Clusters of type P1 and icosahedral are obtained, when M^{4+} is Sn, and only icosahedral when the cation of high valence is Ge.

The chemical system with the greatest diversity of clusters is, again, the one that contains

In in its composition. Table 10 systematizes the materials obtained in this chemical system.

Table 10: Different materials based on the In-X-S (X = Zn, Cd, Fe, Co, Mn) chemical system

Material	SDA	Gel composition (mol)				Cluster	Structure	Ref.
		In	S	X	Organic			
CdInS-44	BAPP[1]	1	2,5	0,3	4,3	T4	3D - CrB_4[2]	[57]
UCR-8FeInS-DBA	DBA[3]	n/a[4]	n/a[4]	n/a[4]	n/a[4]	T4	3D - C_3N_4[5]	[81]
UCR-8CoInS-DBA	DBA[3]	n/a[4]	n/a[4]	n/a[4]	n/a[4]	T4	3D - C_3N_4[5]	[81]
UCR-8ZnInS-DBA	DBA[3]	1	3,5	0,4	15,1	T4	3D - C_3N_4[5]	[81]
UCR-8CdInS-DBA	DBA[3]	n/a[4]	n/a[4]	n/a[4]	n/a[4]	T4	3D - C_3N_4[5]	[81]
UCR-1CdInS	TMDP[6]	1	2,9	0,3	3,9	T4	3D - UCR-1[7]	[84]
UCR-1ZnInS	TMDP[6]	n/a[4]	n/a[4]	n/a[4]	n/a[4]	T4	3D - UCR-1[7]	[84]
UCR-1MnInS	TMDP[6]	n/a[4]	n/a[4]	n/a[4]	n/a[4]	T4	3D - UCR-1[6]	[84]
UCR-1CoInS	TMDP[6]	n/a[4]	n/a[4]	n/a[4]	n/a[4]	T4	3D - UCR-1[7]	[84]
UCR-5ZnInS-1	BAPP[1]	n/a[4]	n/a[4]	n/a[4]	n/a[4]	T4	3D - CrB_4[2]	[84]
UCR-5ZnInS-2	AEPP[8]	n/a[4]	n/a[4]	n/a[4]	n/a[4]	T4	3D - CrB_4[2]	[84]
UCR-5ZnInS-3	ATMP[9]	n/a[4]	n/a[4]	n/a[4]	n/a[4]	T4	3D - CrB_4[2]	[84]
UCR-5MnInS	BAPP[1]	n/a[4]	n/a[4]	n/a[4]	n/a[4]	T4	3D - CrB_4[2]	[84]
UCR-5CoInS	BAPP[1]	n/a[4]	n/a[4]	n/a[4]	n/a[4]	T4	3D - CrB_4[2]	[84]
InFeS	DACH[10]	1	2,0	0,5	132,9	T4	2D	[85]
InCoS	DACH[10]	1	4,0	0,5	149,5	T4	2D	[85]
InCdS-1	TEA[11], TGA[12]	1	4,0	1	18	pseudo T5	2D	[92]
UCR-16CuInS	TMDP[6]	1	2,5	0,4	4,1	T5	2D	[93]
UCR-17CuInS	TMDP[6]	1	2,5	0,4	4,1	T5	3D - DD[13]	[93]
ICS-10-CdInS	DBN[14], PR[15]	1	5,4	0,4	30,6	pseudo T5	0D	[94]
OCF-43-CdInS	DBN[14], PR[15]	1	5,3	2,6	29,3	pseudo T5	2D	[94]
ICS-10-CuInS	DBN[14], PR[15]	1	5,6	0,2	30,6	pseudo T5	0D	[94]
OCF-100-ZnInS	DMDP[16]	1	12,4	2,1	47,1	T6	2D	[96]
OCF-99-ZnInS	DMDP[16]	1	4,9	0,7	18,5	T4	2D	[96]
CdInS-420	DBN[14], DEM[17]	1	5,0	3,4	17,3	$T_{2,4}$	0D	[99]
CIS-11-CuInS	DBA[3]	1	3,4	0,1	19,7	$T_{5,\infty}$	3D - D[18]	[85]
CIS-27-CuInS	DMDP[16]	1	3,4	0,1	26,4	$T_{5,\infty}$	3D	[100]
ITF-9-ZnInS	DMDP[16], Pyr[19]	1	9,7	0,7	120,7	$T_{4,\infty}$	3D - DD[18]	[101]

[1]1,4-bis(3-aminopropyl)piperazine. [2]CrB_4 (see Figure 1c). [3]Di-n-butylamine. [4] n/a - not available. [5]Cubic carbon nitride (see Figure 1d). [6]4,4'-trimethylenedipiperidine. [7]UCR-1 topology (see Figure 15). [8]1-(2-aminoethyl)piperazine. [9]4-amino-2,2,6,6-tetramethylpiperidine. [10]1,2-diaminocyclohexane. [11]Triethylamine. [12] Thioglycolic acid. [13] Double diamond topologie. [14]1,5-diazabicyclo[4.3.0]non-5-ene. [15]Piperidine. [16] 3,5-dimethylpiperidine.[17] 4-[2-(dimethylamino)ethyl]morpholine. [18] Diamond topology (see Figure 1a) [19]Pyrrolidine

Looking only at the materials consisting of T4 clusters, although they can be obtained with different SDAs, they all consist of the same type of cluster. In this system, the SDA influences the dimension and topology of the final material, but not the formation of the cluster.

For larger clusters, it is possible to obtain, with the same SDA, distinct structures based on the same cluster (UCR-16 vs. UCR-17). It is also possible to obtain, with the same SDA, clusters with different dimensions, by changing the relative concentrations of the reagents (OCF-100 vs. OCF-99). It is still possible to obtain, using the same SDA but different gel

compositions, the same type of clusters but originating structures with different dimensions (ISC-10 vs. OCF-43). Thus, the influence of the SDA, as well the gel composition, on type of cluster and final architecture of the material obtained seems to depend from system to system.

It was also observed that when a M^{4+} cation is inserted in a M^{3+}-X^{2-} system, there is the probability of interrupted structures forming, since the overall negative charge of the cluster decreases.

Finally, it is possible to obtain the same cluster with three types of metals and with two types of chalcogeneous. This diverse combination of chemical elements allows the costumization of the dimensions of the cluster, its band structure and electronic properties according to a specific application. When added to the In-S system Cu, will favor the formation of large clusters and the addition of Ge favors the formation of small clusters. Thus, it is possible to find in the Ge-In-Cu-S system a structure composed by the alternation of T2 and T5 clusters.

2.2 Zeolite Analogue Structures

Zeolites are an important family of microporous crystalline inorganic materials, with numerous applications, namely in adsorption and separation processes and in the petrochemical industry as catalysts. Zeolites present the general formula $A_{x/n}$-$[Si_{1-x}Al_xO_2]\cdot m\ H_2O$, where A is a metal cation with a valence n. Regarding their structure, two hundred and forty eight different architectures are known,[160] based on the connection through the vertices of the tetrahedrons TO_4, where T, can be Si or Al. It is possible to find numerous porous materials based on zeolites, where the T atom is replaced by other elements, such as Ga, Ge or P.[161] However, these materials, because they are TO_4-based, are insulating and therefore have limited applications in photo, electro and optical fields.

In recent years, chalcogenide-based semiconductor zeolite analogs have been synthesized, where the oxygen is replaced by another chalcogen (such S, Se or Te), and the T atom by

another metallic cation tetracoordinated. This strategy has been successful in obtaining semiconductor structures with high surface area and microporosity. However, the number of such structures with the IZA structure code remains small. Although there are many 3-dimensional microporous chalcogenide structures, as noted earlier, the presence of different anion coordination and the possible absence of tetravalent metal ions leads to the creation of non-zeolite structures.[162] As the size of the cluster increases, some characteristics appear that make the structure non-zeolite, such as anions with three or four coordination. Thus, the structures analogous to zeolites are generally based on T2 clusters, where metallic ions with high valence are used to balance the overall charge of the structure.[163]

The first reference to a material with an analogue structure to a zeolite is from 1997. The material obtained by Cahil et. al[164] consists on the presence of T2 Ge_4S_{10} clusters that are connected by Mn. Using 1,4-diazabicyclo[2.2.2]-octane as SDA it is possible to obtain an analogous structure to the Li-A (ABW, following the IZA code) zeolite where the SiO_4 and AlO_4 were substituted by MnS_4 and Ge_4S_{10}, respectively.

Zheng et al.[31] obtained a series of zeolite analogous materials based on the combination of M^{4+} and M^{3+} in the same Tn cluster. In order to synthesize clusters involving both cations and to avoid the formation of two types of clusters consisting only of M^{4+} or M^{3+}, Zheng et al. resorted to a synthesis in a non-aqueous medium in order to overcome such problem. The zeolite analogue materials obtained were designed through the triple replacement of O^{2-} by S^{2-} or Se^{2-}, Si^{4+} by Ge^{4+} or Sn^{4+}, and Al^{3+} with Ga^{3+} or In^{3+}. Any M^{4+}/M^{3+} combination is possible. Due to the different possible combinations, it is feasible to customize the physical properties of the final material, such as band gap, luminescence, pore size, surface area, ion exchange and chemical stability. The previously synthesized 3-dimensional structures generally have a low thermal stability, collapsing at temperatures below 300°C. In order to avoid such a situation, the M^{4+}/M^{3+} ratio should preferably be between 0,2 and 1,2. This is contrary to the Loewenstein's rule of stability of zeolites, which states that the M^{4+}/M^{3+} ratio should not be less than 1.[165]

All materials can be described as a network of Tn clusters composed of M^{4+}-M^{3+}-X^{2-}, which are connected to each other through the vertices by a bichalcogenide bridge. The different synthesized samples were grouped into four families: UCR-20, UCR-21, UCR-22 and UCR-23. Each family refers to materials with the same framework topology but different chemical compositions. UCR-20, UCR-21 and UCR-23 have as building units T2 type clusters while UCR-22 presents a pseudo-T4 cluster as building unit. Regarding topology, UCR-20 presents the sodalite framework (see Figure 50a), UCR-21 has a diamond structure (see Figure 50b), UCR-22 has two interpenetrating diamond conformations (see Figure 50c) and UCR-23 has a CrB_4 type topology (see Figure 50d). UCR-20 and UCR-21 have a large pore size, consisting of 12 T atoms, while UCR-22 and UCR-23 have an extra-large pore size, consisting of 24 and 16 T atoms respectively. The main characteristics of the different obtained materials are summarized in the Table 11.

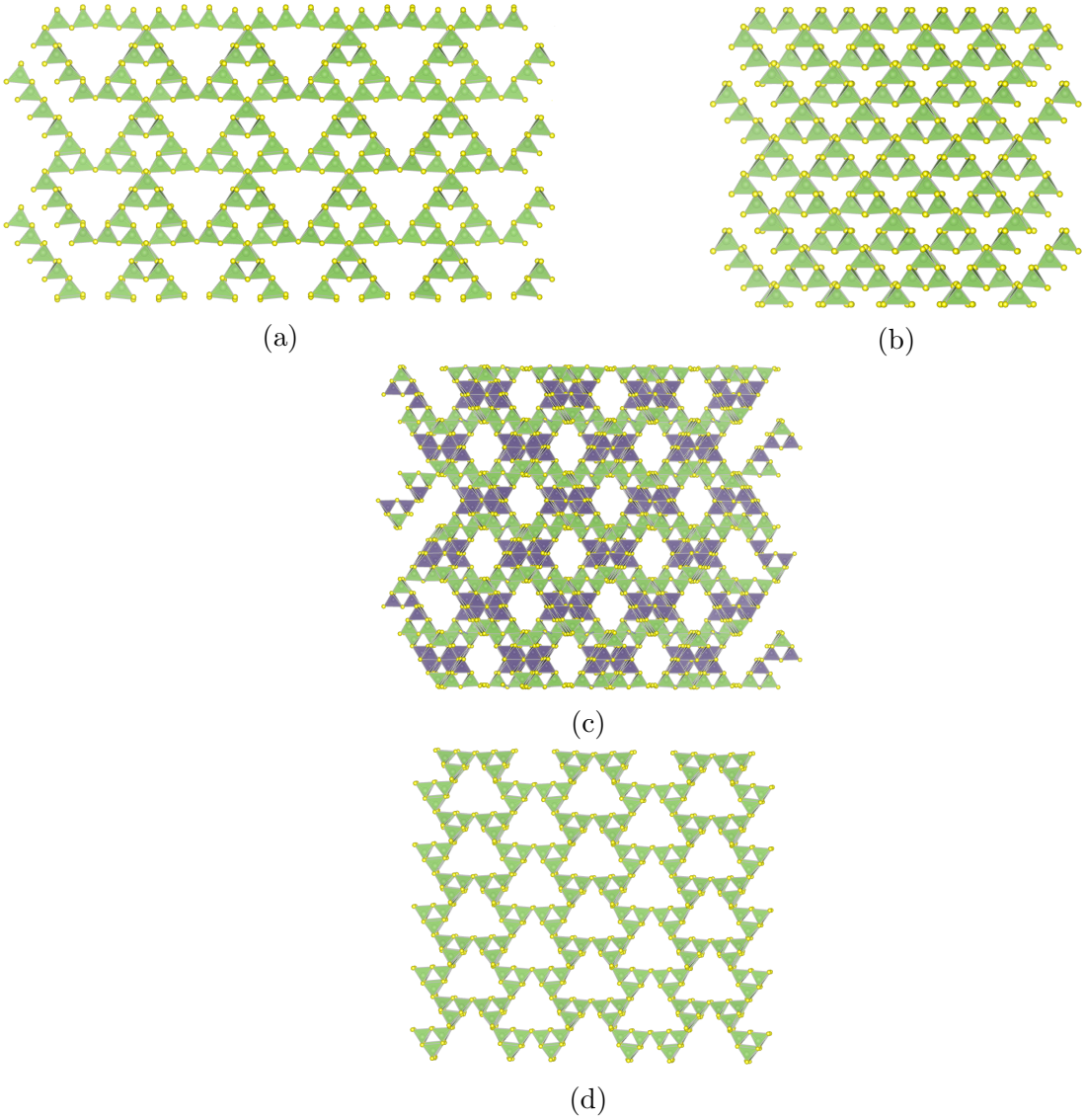

Figure 50: Representation of the different structures obtained by Zheng et al.[31] - (50a) UCR-20, (50b) UCR-21, (50c) UCR-22 and (50d) UCR-23 (Ga - green, Sn - grey, S - yellow)

The samples UCR-20GaGeS-AEP, UCR-20GaGeS-TAEA, UCR-20-InGeS-TMDP, UCR-20-InSnS-TMDP, UCR-21GaGeS-AEM, UCR-22InGeS-AEP, UCR-22GaSnS-AEP and UCR-23GaGeS-AEM were able to keep their structure after heating with air at 300°C for 1 hour. After a calcination at 350°C under a N_2 atmosphere, 77 % of the nitrogen and 81 % of the hydrogen were eliminated from UCR-20-GaGeS-TAEA without collapse of the structure. It was also observed that an ion exchange with CsCl is also able to eliminate the SDA. After the ionic exchange it was observed that the sample had a type I isotherm. As for the textural

properties, it presents a Langmuir surface area of 807 m^2/g, a micropore volume of 0,23 m^3/g and an average pore diameter of 9,5 Å. For the remaining samples, there is no reference to whether they have been subjected to a calcination under N_2 atmosphere, ionic exchange or other technique to eliminate the SDA present.

Table 11: Different zeolite analogue materials obtained by Zheng et al.[31] and their chemical composition, final topology and pore size

Material	**SDA**	**Composition**			**Cluster Composition**	**Structure**	**Pore Size**
		M^{4+}	M^{3+}	X^{2-}			
UCR-20-GaGeS-TAEA	TAEA[1]	Ge	Ga	S	$Ga_{2,67}Ge_{1,33}S_8$	3D - SOD[2]	12 T Atoms
UCR-20-GaSnS-TMDP	TMDP[3]	Sn	Ga	S	$Ga_{1,8}Sn_{2,2}S_8$	3D - SOD[2]	12 T Atoms
UCR-20-InGeS-TMDP	TMDP[3]	Ge	In	S	$In_3Ge_1S_8$	3D - SOD[2]	12 T Atoms
UCR-20-InSnS-TMDP	TMDP[3]	Sn	In	S	$In_{2,5}Sn_{1,5}S_8$	3D - SOD[2]	12 T Atoms
UCR-20-GaGeSe-TMDP	TMDP[3]	Ge	Ga	Se	$Ga_xGe_{4-x}Se_8$	3D - SOD[2]	12 T Atoms
UCR-21-GaGeS-APO	APO[4]	Ge	Ga	S	$Ga_{3,3}Ge_{0,7}S_8$	3D - D[5]	12 T Atoms
UCR-21-GaSnS-TAEA	TAEA[6]	Sn	Ga	S	$Ga_{2,32}Sn_{1,6}S_8$	3D - D[5]	12 T Atoms
UCR-21-InGeS-APP	APP[7]	Ge	In	S	$In_{1,84}Ge_{2,16}S_8$	3D - D[5]	12 T Atoms
UCR-21-InSnS-AEP	AEP[8]	Sn	In	S	$In_xSn_{4-x}S_8$	3D - D[5]	12 T Atoms
UCR-21-GaSnSe-TAEA	TAEA[6]	Sn	Ga	Se	$Ga_{2,47}Sn_{1,53}Se_8$	3D - D[5]	12 T Atoms
UCR-22-GaGeS-AEP	AEP[8]	Ge	Ga	S	$Ga_{3,33}Ge_{0,67}S_8$	3D - DD[9]	24 T Atoms
UCR-22-GaSnS-AEP	AEP[8]	Sn	Ga	S	$Ga_{2,13}Sn_{1,87}S_8$	3D - DD[9]	24 T Atoms
UCR-22-InGeS-AEP	AEP[8]	Ge	In	S	$In_{2,69}Ge_{1,31}S_8$	3D - DD[9]	24 T Atoms
UCR-22-GaSnSe-TOTDA	TOTDA[10]	Sn	Ga	Se	$Ga_{1,73}Sn_{2,27}Se_8$	3D - DD[9]	24 T Atoms
UCR-23-GaGeS-AEM	AEM[11]	Ge	Ga	S	$Ga_{2,67}Ge_{1,3}S_8$	3D - CrB_4[12]	16 T Atoms
UCR-23-GaSnS-AEM	AEM[11]	Sn	Ga	S	$Ga_{2,29}Sn_{1,71}S_8$	3D - CrB_4[12]	16 T Atoms
UCR-23-InGeS-AEM	AEM[11]	Ge	In	S	$In_{1,84}Ge_{2,16}S_8$	3D - CrB_4[12]	16 T Atoms

[1]Tris(2-aminoethyl)amine. [2]Sodalite (see Figure 1b). [3]4,4'-trimethylenedipiperidine. [4]dl-1-amino-2-propanol. [5]Diamond (see Figure 1a).
[6]Tris(2-aminoethyl)amine. [7]1-(3-aminopropyl)-2-pipecoline. [8]1-(2-aminoethyl)piperazine. [9]Double Diamond.
[10]4,7,10-trioxa-1,13-tridecanediamine. [11]N-(2-aminoethyl)morpholine. [12] (see Figure 1c).

Lin et al.[166] have managed to synthesize structures rich in Ge or Sn, thus managing the obtention of truly high silica zeolite analogous structures. It was observed that a small portion of divalent cations induce crystallization of Sn/Ge rich structures. Four different materials, CPM-120, CPM-121, CPM-122 and CPM-123 with different topologies were obtained. All the materials have as building units T2 clusters composed by M^{4+}-M^{2+}-X^{2-} and connected by a bichalcogenide bridge through the clusters vertices. The clusters of CPM-120 are organized to form the sodalite topology, obtaining the zeolite-type RWY framework. CPM-121 presents a non-interpenetrated diamond framework. Regarding CPM-122, it has a doubly-diamond framework. Finally, CPM-123 has a CrB_4 type structure, the same as the zeolite framework code BCT. The main characteristics of the different obtained materials

are summarized in the Table 12.

Table 12: Different zeolite analogue materials obtained by Lin et al.[166] and their chemical composition and final topology

Material	SDA	Composition			Cluster Composition	Structure
		M^{4+}	M^{3+}	X^{2-}		
CPM-120-ZnGeS	AEM[1]	Ge	Zn	S	$Zn_{0,81}Ge_{3,19}S_8$	3D - SOD[2]
CPM-121-ZnGeS	AEM[1], TBA[3]	Ge	Zn	S	$Zn_{0,93}Ge_{3,07}S_8$	3D - D[4]
CPM-122-ZnCdGeS	AEM[1], LTD[5], DBU[6]	Ge	Zn, Cd	S	$Zn_{0,65}Cd_{0,41}Ge_{2,9}S_8$	3D - DD[7]
CPM-123-ZnGeS	AEM[1], HA[8]	Ge	Zn	S	$Zn_{1,21}Ge_{2,79}S_8$	3D - CrB_4[9]
CPM-120-ZnSnSe	BPP[10]	Sn	Zn	Se	$Zn_{0,99}Sn_{3,01}Se_8$	3D - SOD[2]
CPM-120-CdSnSe	BPP[10]	Sn	Cd	Se	$Cd_{0,68}Sn_{3,32}Se_8$	3D - SOD[2]

[1]N-(2-aminoethyl)morpholine. [2]Sodalite (see Figure 1b). [3]Tributylamine. [4]Diamond (see Figure 1a). [5]2,6-Lutidine [6]1,8-diazabicyclo[5.4.0]undec-7-ene. [7]Double Diamond. [8]1-hexylamine. [9] (see Figure 1c).
[10]1,3-bis(4-piperidinyl)propane.

After the synthesis, due to the blocking of the porous system by the used SDAs, the samples show negligible gas adsorption. However, after exchange with Cs^+, the synthesized materials show an isotherm type I. For thermal stability, e.g. CPM-120-ZnGeS sample maintains structural and mechanical integrity when heated in air at 310°C for at least 1 hour, presenting itself as a thermally and chemically stable sample. Further studies have been conducted on the CPM-120-ZnGeS-AEM structure,[167] namely on its charge selectivity. After performing an ionic exchange with Cs^+, it was observed that the structure presents a selectivity towards cationic organic molecules, and can thus be used to respond selectively according to the charge properties of the compounds. It was also observed that this chalcogenide material presents, besides charge selectivity, size selectivity.

Wu et al.[168] were able to synthesize two zeolite analogue structures based on T2 clusters as building units, entitled SOF-20 and SOF-21, using a combination of In and Sn as the cations and a mixture of superbases as SDA. SOF-20 can be obtained with a mixture of 1,5-diazabicyclo[4.3.0]-5-nonene (DBN), N-aminoethylpiperazine (AEP) and N-(2-aminoethyl)ethanolamine (AEAE). Regarding SOF-21, this material can be synthesized when 1,8-diazabicyclo[5.4.0]-7-undecene (DBU), piperidine (PR) and N-(2-aminoethyl)ethanolamine (AEAE) are used as SDA. What differs these structures from those previously synthesized is

the inter-cluster bridging angle. Generally, the values of this parameter are between 104° and 110°. The SOF-20 structure has an inter-cluster bridging angle between 107° and 128° (see Figure 51a), hence having the largest bridging angle observed for a 3-dimensional chalcogenide framework. SOF-21 also presents a surprisingly high inter-cluster bridging angle, between 106° and 113° (see Figures 51b and 51c).

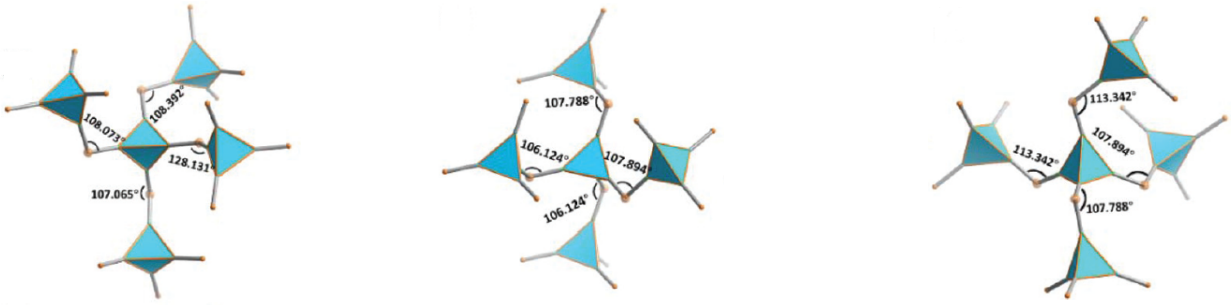

(a) (b) (c)

Figure 51: Connection mode, and its connection angle, between the clusters of (51a) SOF-20 and (51b and 51c) SOF-21 structures[168]

Looking now at the topology of the samples, the SOF-20 structure shows a non-interpenetrated gismondine net (see figure 1e), being the first time such topology is observed in this class of materials. Regarding SOF-21, it presents a twisted diamond topology, having an extra-framework volume slightly higher than the samples with a diamond topology of previously synthesized samples such as UCR-21 or CPM-121 (see Table 11 and 12 respectively). As for the porosity of the samples, although ion exchange with Cs^+ is generally used for the elimination of the SDAs, this technique proved ineffective for the SOF-20 sample, since the structure collapses after the ion exchange procedure. As for the SOF-21 sample, it does not collapse after the ion exchange with Cs^+. However, during the degassing process the structure collapses, thus not being possible to perform a gas adsorption experiment.

Lin et al.[162] synthesized a structure, by using piperidine (PR) as SDA, that presented ordered interrupted sites, allowing to precisely dope the material and to help the creation of extra-large pores. The structure, entitled CSZ-5, is composed of tetracoordinated In and bicoordinated Se making up a T2 cluster with a new boracite-related topology. Due to

the method of connection between the clusters, this structure presents a multiple channel system. On the <100> direction it is possible to find an aperture of 12-MR and on the <110> direction the aperture is 16-MR (see Figures 52a and 52b). It is possible, due to the presence of interrupted sites, to dope the structure in order to adapt the electronic structure and the photoelectric characteristics of the material to a specific given application (see Figures 52a and 52c to see the atomic doping).

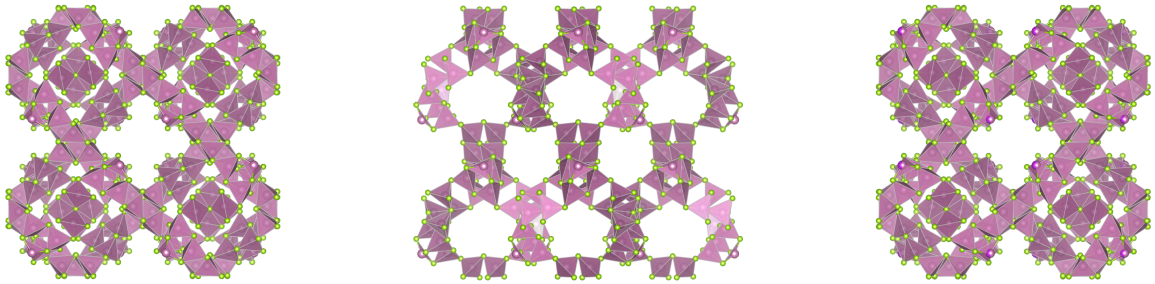

(a) (b) (c)

Figure 52: Different orientations of CSZ-9, (52a and 52b) before and (52c) after doping with Bi where the organic part ((In - pink; Bi - mangenta, Se - green)[162]

So far, zeolite-like structures are all made up of type T2 clusters and result from the combination of M^{4+}/M^{3+} or M^{4+}/M^{2+}. Chen et al.[169] were able to synthesize a structure analogue to a zeolite based on the system $M^{4+}/M^{3+}/M^{2+}$ still using the T2 clusters as building units. Starting with the precursor gels previously used by Lin et al.,[166] these were doped with Ga^{3+}, In^{3+}, Sn^{4+} or Cd^{2+}. Through progressive additions of Ga precursor into the gel, it is observed that it helps to improve the morphology of the CPM-120 crystals. A transition from irregularly block shaped crystals to regular rhombic-dodecahedron crystals is observed with the increase of Ga content. Regarding the location of Ga in the T2 cluster, it can occupy different positions, as it is shown that depending on the amount of Ga precursor added, it can substitute Ge or Zn. Ga will first substitute Ge and then it will replace Zn. For the addition of In, small quantities result in no uniform CPM-120 crystals being obtained. When the amount of In precursor increases, the formation of CPM-121 crystals is observed. After optimization of the experimental conditions, it was possible to obtain the CPM-121

structure where Ge and Sn coexist in the same cluster. The same was observed after the addiction of Cd, being possible to obtain the structure CPM-121 where Zn and Cd coexist in the same cluster. Figure 53 shows the main experimental results obtained.

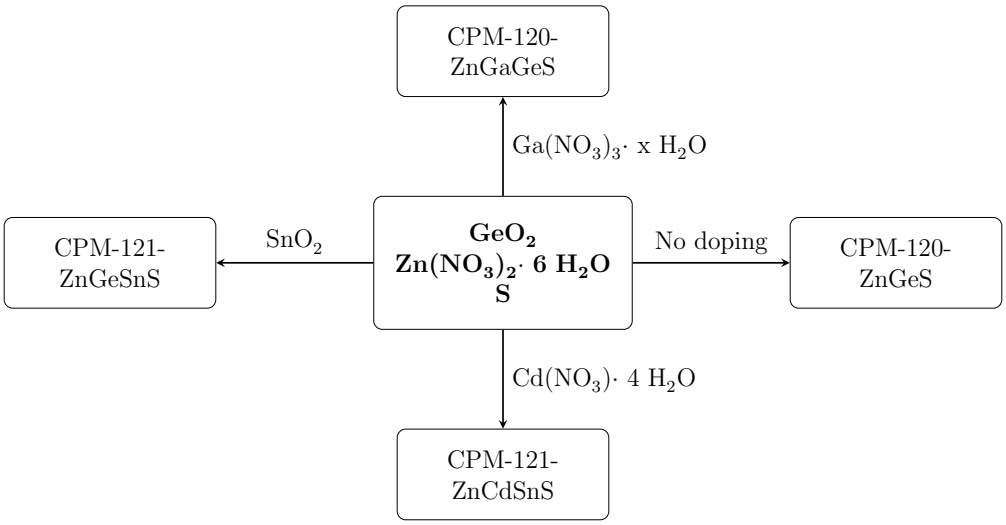

Figure 53: Scheme of the different forms of doping as well as the experimental results obtained in [169]

The stability of the structures after ion exchange with Cs^+ was also studied. It was found that the CPM-120 structure is much more stable than the CPM-121 structure, with a thermal stability up to 610°C and a highly porous framework.

Xue et al.[163] obtained for the first time zeolite analogous structures based on a combination of P1 and T2 clusters. The structures, entitled CSZ-9 and CSZ-10, are composed by In and S and present non-interpenetrating frameworks based on C_3N_4 and SOD typologies, respectively. When an attempt was made to perform an ion exchange with Cs^+ to eliminate the SDA (3,5-dimethylpiperidine - 3,5-DMP), the structures collapsed. Later, the same team of researchers obtained two new structures based on the In-Se chemical system.[82] These structures, entitled CSZ-11 and CSZ-12, result in a combination of P1 clusters with defects. CSZ-11 and CSZ-12 present non-interpenetrating frameworks and can be seen as extended *crb* (see Figure 54a) and *irl* (see Figure 54b) networks, respectively. In order to eliminate the SDA, an ionic exchange with Cs^+ was used. However, CSZ-11 collapses af-

ter the exchange and CSZ-12 only after the degassing procedure necessary to carry out N_2 adsorption measurements.

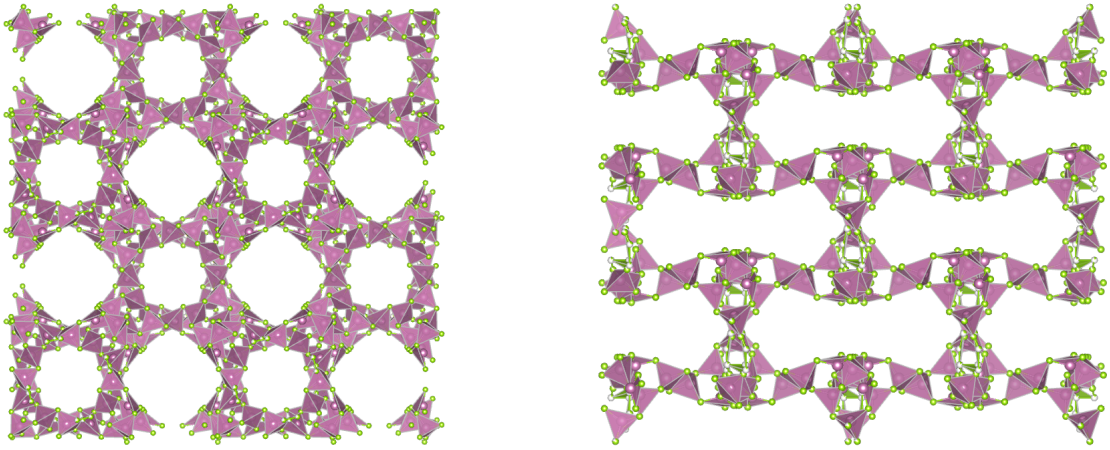

(a) (b)

Figure 54: Representation of the structures (54a) CSZ-11 and (54b) CSZ-12 (In - pink, Se - green)[82]

Several 3-dimensional cluster-based structures have been synthesized, as can be seen in the first section of this document. However, for a structure to be considered analogous to a zeolite it is necessary that it contains M^{4+} cations in its composition and the anions of the structure must present a coordination equal to two. In view of these definitions, structures analogous to zeolites are limited to small clusters, since, as seen above, with the increase in cluster size anions with different coordination numbers appear. Thus, most of the structures presented are clusters of type T2.

Of the different possible combinations of cations, the most similar to a zeolitic structure is the combination M^{4+}/M^{3+}, where M^{4+} can be Ge or Sn and M^{3+} Ga or In. It is also possible to find structures rich in M^{4+} cations, which are intended to be analogous to zeolitic structures rich in Si. It should be noted that in order to facilitate the crystallization of structures rich in M^{4+} cations, the addition of small quantities of M^{2+} cations is necessary. This technique, the addition of M^{2+} cations to M^{4+}-X^{2-} systems, is something that had already been done previously, namely in the first publication regarding the synthesis of a 3-dimensional structure based on the T2 Ge_4S_{10} cluster.

Although there are materials with a topology that correspond to an IZA approved topology, it is possible to obtain architectures that are not accessible through the use of TO_4 tetrahedrons, since the system under study has different physical and chemical characteristics from those presented by a more usual zeolitic system. It is possible to find examples of structures with more exotic structures, with multiple channels of different dimensions, large pores or with different pores openings.

One of the great problems of these structures is their low thermal stability. It was observed that, in order to overcome this problem, the M^{4+}/M^{3+} ratio should be lower than one, an observation that goes against the Löwenstein's rule,[165] which states that the M^{4+}/M^{3+} ratio should be higher than one. Although it has been shown that M^{4+}/M^{3+} ratios lower than one lead to an increase in the thermal stability of the structures, no justification has been provided so far for the violation of this rule.

Another issue associated with these structures is the difficulty of eliminating the SDA. The most commonly used technique for pore volume recovery is ion exchange with a cesium salt. Although this technique has the best results, several structures collapse when trying to eliminate the SDA.

2.3 Hybrid Materials

Up to now most of the structures presented are composed by inorganic clusters that are connected by bicoordinated chalcogens atoms. However, it is possible to connect the different clusters through organic ligands, thus opening the doors to new materials with new physical and chemical properties. Due to the synergistic effect between the organic and inorganic components, such hybrid materials have unique optic and photochemical properties.[48]

In 2010, Vaqueiro[41] published an extensive review on hybrid materials focused mainly on materials composed by clusters that had an organic component in their composition. Thus, although some examples of clusters with inorganic and organic components will be presented, the main focus will be on materials that present inorganic clusters connected through organic

ligands, particularly recent publications, and composite materials that combine inorganic clusters with other materials such as graphene.

2.3.1 Hybrid clusters

Several examples can be found in the literature of clusters that present in their composition inorganic and organic parts.

For structures composed by the simplest supertetrahedron, T2, different topologies and chemical compositions were obtained. It is possible to find examples of 1-dimensional,[170,171] 2-dimensional[172] or 3-dimensional[173,174] structures composed of T2 clusters that combine organic and inorganic components. For larger clusters, it is possible to find several examples of hybrid materials consisting of P1,[175,176] C1,[175,177] C2[178] and a combination of P1 and C1 clusters.[175] Some of the structures obtained have interesting characteristics, namely the presence of chiral quartz-type and moganite topologies,[175,176] remarkable photoelectric properties[177] or the use of metal-chelate dyes as SDA, thus obtaining materials with optically active guest species.[178]

The use of organic species is one of the strategies used to obtain isolated clusters, since the presence of the organic components allows the stabilization of the negative charges of clusters, especially in large clusters. Recalling that the Cn cluster series has not yet been obtained without the use of organic components. Wu et al.[179] obtained a family of isolated clusters, from T3 to T5, where the four corners of the clusters were connected to 1.5-diazabicyclo[4.3.0]non-5-ene or 1-methylimidazole organic compounds. Another example of isolated clusters that are stabilized due to the presence of organic molecules in the vertices is the T3 gallium sulfide obtained by Vaqueiro et al.[180]

2.3.2 Ordered organic-inorganic materials analogs to MOF's

According to IUPAC's definition,[181] a porous solid can be considered as a metal-organic framework (MOF) when it can be defined by a coordination network, i.e. a coordination

compound with repeated coordination units along 1-, 2- or 3-dimensions, with organic ligands and potential porosity. Rowseel et al.[182] maintains that, in addition, the solid should be highly crystalline, as this is the only way to establish important structure-property relationships. Porosity is one of the most important challenging aspects to develop of these materials as it allows, by analogy with zeolitic structures, their application in areas such as separation, ion exchange or catalysis.[183]

Currently, it is possible to find in the literature numerous materials composed of inorganic chalcogenide clusters that are connected by organic ligands. These materials, analogous to MOF's, may present a 1, 2- or 3-dimensional architecture.

Xie et al.[184] obtained 1-dimensional zig-zag structures composed of P1 clusters that are connected by dipyridyl ligands (see Figure 55a). Other examples of 1-dimensional hybrid materials composed by clusters of the Cn or Pn series were obtained by Zheng et al.[185] (see Figure 55b) and Zhang et al.[186] Evaluating the optical properties of the different materials obtained, Zheng et al.[185] observed that such materials present optical size-dependent properties. Larger clusters lead to a red shift into longer wavelengths in the optical absorption spectra and superlattices show a broader absorption spectra in comparison to discrete clusters. The materials obtained by Zhang et al.[186] used tetrahedral quadridentate linkers to connect the different clusters (see Figure 55c), for the first time.

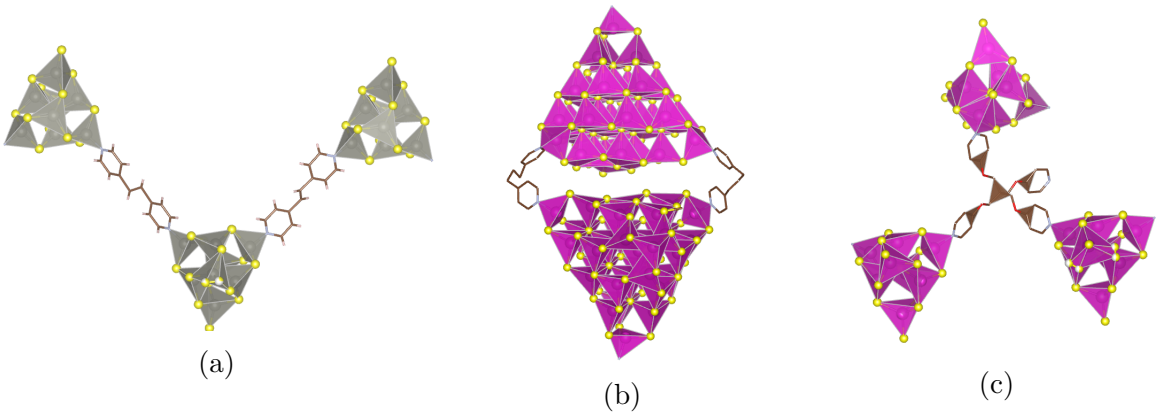

Figure 55: Representation of 1-dimensional structures obtained by (55a) Xie et al.,[184] (55b) Zheng et al.[185] and (55c) Zhang et al.[186] (Zn - gray, C - brown, S - yellow, Cd - pink, O - red)

For 2-dimensional structures, Zheng et al.[187] obtained layered materials consisting of cadmium Cn type clusters and Xu et al.,[188] also using cadmium, obtained a hybrid layered tellurium-based structure where T3 clusters were connected through 4,4'-trimethylenedipyridine organic compound. Continuing research on cadmium hybrid materials, Chen et al.[189] obtained a 2-dimensional structure where the cadmium sulfide C1 clusters are connected by tetrakis(imidazolyl)borate ligands. Vaqueiro et al.[190] obtained a 2-dimensional structure with a honeycomb topology composed by T3 Ga-S clusters which were connected through 1,2-di(4-pyridyl)ethylene. Subsequently, the same team of researchers obtained chiral nanotubes and a 2-dimensional structure where each T3 cluster is connected to other four T3 clusters.[191] Some years later, a new type of hybrid super-supertetrahedral cluster was obtained.[192] This new type of cluster is obtained when each vertice of the tetrahedron is replaced by a hybrid T3 cluster and the center of the tetrahedron is occupied by a T3 cluster. The five T3 clusters are connect through bipyridyl ligands forming a 2-dimensional framework with cross-shaped pores. Figure 56 shows a representation of the super-supertetrahedral obtained.

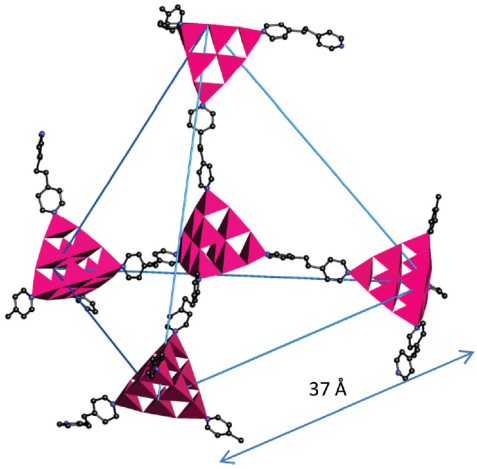

Figure 56: Representation of the super-supertetrahedral obtained by Vaqueiro et al.[192]

In the field of structures composed by oxyclusters, Yang et al.[193] obtained a laminar material, entitled IOS-1, composed by T5 In-O-S clusters that were connected by a carboxylate ligand thus presenting a honeycomb-like topology. Continuing the research, Yang et al.[193]

were able to obtain for the first time T5 oxycluster-based materials made be the combination of In, O and S. Two different structures, IOS-1 and IOS-2, were obtained. IOS-1 is a layered material where the clusters are connected by benzenetricarboxylate ligants and IOS-2 is a 3-dimensional structure where the clusters are connected by imidazolate linkers.

As for 3-dimensional structures, the structures obtained by Lee et al.[112] and Jin et al.[113] mentioned above are the first examples of 3-dimensional structures composed by a combination of inorganic clusters and organic ligands. Manos et al.[194] obtained a structure composed of T2 clusters where each cluster was connected through a methylamine ligand. Another interesting characteristic of the structure obtained is the presence of the $[Zn(H_2O)_4]^{2+}$ complexes as an extraframework species, acting as a SDA and counter cation. Wu et al.[195] were able to synthesize 3-dimensional 4-connected structures where T3 or T4 clusters are connected by imidazolate. The different structures obtained present an interpenetrating diamond topology and the negative framework charge is counterbalanced by Li^+ cations and protonated 1,8-diazabicyclo[5.4.0]undec-7-ene molecules. Using imidazolate as an organic ligand, Zhang et al.[196] obtained a 3-dimensional structure, designated by SCIF-11, where the different T3 clusters were connected through the usual bicoordenated sulfur or through imidazolate (see Figure 57a), being one of the first materials where the existence of connection through inorganic and organic components was observed. An interrupted 3-dimensional structure, named SCIF-12, consisting of T4 clusters connected through imidazolate (see Figure 57b) was also synthesized. Regarding the topology of synthesized materials, SCIF-11 presents a distorted double-interpenetrated diamond topology and SCIF-12 a 3,4-connected *ins* topology.

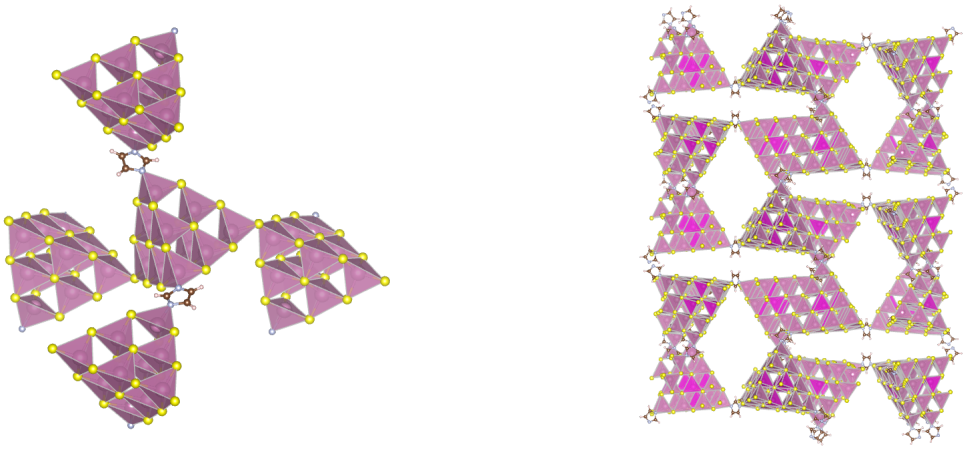

(a) (b)

Figure 57: Representation of (57a) SCIF-11 and (57b) SCIF-12 (In - pink, Cd - mangenta, S - yellow, C - brown, N - gray, H - light pink)[196]

For 3-dimensional structures composed by oxyclusters, a quartz chiral structure composed by T5 $In_{35}S_{48}O_8$ connected by imidazolate, named IOS-2, was synthesized by Yang et al.[193]

2.3.3 Composite hybrid materials

So far, materials consisting of clusters composed of organic and inorganic components or materials where inorganic clusters were connected by organic molecules have been presented. However, it is possible to find hybrid materials that consist of the coating of graphene, metals, TiO_2 or films with inorganic clusters. The presence of this heterojunction allows to improve the charge separation properties of the material, thus contributing to the increased efficiency of the hybrid material when it is used as a photocatalyst, for example.

Hou et al.[197] were able to deposit T4 Sn-Ga-Zn isolated clusters (previous obtained in[83]) on reduced graphene oxide sheets. Regarding the optical properties of the composite, it can be observed that there is a small red-shift on the absorption edge and an enhanced absorption intensity when compared to the isolated clusters. It is observed that the hybrid material composed by the clusters dispersed in graphene has a higher photocurrent density than isolated clusters, which means that the hybrid material has a greater capacity to generate and separate charges. It is also observed that the hybrid composite material presents a

higher stability against photo-corrosion than the isolated clusters. Therefore, the presence of graphene contributes to the improvement of the charge separation properties but also avoids photo-corrosion of the final material.

Li et al.[198] deposited T5 Cu-In-S clusters on a TiO_2 electrode to produce photo-electrodes. Another example of a hybrid material that results from the combination of inorganic clusters with TiO_2 is the TiO_2 nanochips doped with T5 In-Cd-S clusters.[199]

Liu et al.[200] explored the possibility of coating nobel metal substrates with Tn clusters in order to make the most of the semiconductor-metal heterojunction that forms. The noble metal chosen was silver in the shape of nanowires and the multimetalic T4 clusters with different metallic compositions obtained in Ref.[83] were selected for the clusters. Hu et al.[201] doped a $BiVO_4$ film with a T5 Cu-Ga-Sn clusters and evaluated the photochemical performance through the water splitting reaction.

It is also possible to find examples of materials that combine zeotype chalcogenide materials with metals or materials that presents organic molecules or nanoparticles confined into the cavities.

Using the zeolitic-type materials previously obtained by Lin et al.,[166] Mao et al.[202] were able to integrate TiO_2 nanowires with the CPM-121 structure. Comparing the current density of the hybrid material with the TiO_2 nanowires, it was observed that the photocurrent of the hybrid material is about three times higher and presents an elevated activity both in the UV and in the visible light regions than of the isolated nanowires, thus showing the synergistic effect that exists between the semiconductor and metal materials.

Hu et al.[203,204] were able to confine organic molecules into a zeotype chalcogenide material, for the purpose of designing a high efficient light-harvesting antennae. Due to the semiconducting properties of the chalcogenide material, it is responsible to absorb the UV-light and passes the excited energy to the organic dyes molecules. Later, the same team of researchers[205] were able to confine Cu_2S nanoparticles into the cavities of the zeotype material previous obtained by Zheng et. al.[31]

2.4 Alternative Methods of Synthesis

The materials presented so far were obtained through traditional methods of synthesis. The method that stands out is the hydro(solvo)thermal. This methodology, based on the use of polar solvents, organic amines and temperatures below 200°C, is currently the most used to prepare crystalline metal chalcogenides with various structures. Similar to the zeolite synthesis, it is possible to find examples of synthesis of these materials where metal ions instead of organic amines are used as SDA. More recently, two new methodologies, based on the use of ionic liquids and surfactants, have been developed to prepare such materials.[18] The need to look for new methodologies of synthesis arose from the growing interest in obtaining inorganic structures at room temperature or in solvent-free environments, hence taking into account the environmental and economic concerns that affect today's society.[34]

2.4.1 Organic amine free synthesis

The majority of the layered or 3-dimensional materials previously presented were synthesized by hydro(solvo)thermal methods using SDAs, which occupied a position within the pore system. When a typical calcination is used to eliminate the organic component, most of the structures collapse due to the low thermal stability. On some cases, those organic compounds could be exchanged with other inorganic cations, such as Cs^+, without destroying the framework, thus releasing the porous volume of the structure. The synthesis of a system without the use of OSDA's is still subject of research, both for environmental and economic reasons.

The only purely inorganic systems, which are known, consist of In^{3+}, In^{3+}/Cu^+ or In^{3+}/M^{2+} (M^{2+} = Mn, Zn, Cd) and are generally composed by T2, T4, T5 or P2 clusters. All materials were synthesized in the presence of alkali or alkaline earth metal cations under highly alkaline conditions. The synthesis conditions used lead to the crystallization of chalcogenides with encapsulated inorganic cations in their cavities. Seven different 3-dimensional frameworks were synthesized and may present different chemical compositions:

ICF-5, ICF-17, ICF-21, ICF-22, ICF-24, ICF-25, ICF-26, ICF-27 and ICF-29.[102,206,207] A great diversity of clusters can be observed, as well as topologies of the different synthesized structures (see Table 13).

Table 13: Different OSDAs free materials obtained by Zheng et al.[206 102 207] and their chemical composition, final topology and pore size

Material	Composition				Cluster Composition	Structure	Pore Size	Ref.
	M^{3+}	M^{2+}	M^{+}	X^{2-}				
ICF-5-CuInS-Na	In	Cu	Na	S	T4 - $Cu_3In_{17}S_{33}$	3D - DD[1]	-	[206]
ICF-5-CdInS-Na	In	Cd	Na	S	T4 - $Cd_4In_{16}S_{33}$	3D - DD[1]	-	[206]
ICF-5-MnZnInS-Na	In	Mn, Zn	Na	S	T4 - $Mn_{1,8}Zn_{2,2}In_{16}S_{33}$	3D - DD[1]	-	[206]
ICF-5-CdInS-Li	In	Cd	Li	S	T4 - $Cd_4In_{16}S_{33}$	3D - DD[1]	-	[206]
ICF-5-ZnInS-Na	In	Zn	Na	S	T4 - $Zn_4In_{16}S_{33}$	3D - DD[1]	-	[206]
ICF-5-MnInS-Li	In	Mn	Li	S	T4 - $Mn_4In_{16}S_{33}$	3D - DD[1]	-	[206]
ICF-17-InZnS-Na	In	Zn	Na	S	T5 - $In_{22}Zn_{13}S_{54}$	3D - DD[1]	-	[206]
ICF-21-InSe-Na	In	-	Na	Se	T2 - In_4Se_{842}	3D - D[2]	-	[206]
ICF-22-InS-Li	In	-	Li	S	pseudo T4 - $In_{16}S_{32}$	3D - DD[1]	-	[206]
ICF-24-InSSe-Na	In	-	Na	S, Se	T2 - $In_4S_{2,9}Se_{5,1}$	3D - ICF-24[3]	20 T Atoms	[206]
ICF-25-InS-SrCaLi	In	-	Sr, Ca, Li	S	T2 - In_4S_8	3D - ICF-25[4]	16 T Atoms	[206]
ICF-26-InLiS-Ca	In	-	Li, Ca	S	P2 - $Li_4In_{22}S_{44}$	3D - DD[1]	-	[102]
ICF-27-InS-SrLi	In	-	Sr, Li	S	$In_{15}S_{29}$	3D	-	[206]
ICF-29-InS-Na	In	-	Na	S	$SIn_4(InS_4)_{6/2}$	3D - Perovskite	-	[207]

[1]Double Diamond. [2]Diamond (see Figure 1a). [3]ICF-24 topology (see Figure 58a). [4]ICF-25 topology (see Figure 58b)

ICF-5 consists of T4 clusters as building units and presents two interpenetrating diamond-type lattices. ICF-17 presents the biggest cluster as building unit, the T5. Regarding the topology, ICF-17 presents the same as ICF-5. ICF-21 consists of the connection of T2 clusters into a non-interpenetrating diamond-type lattice and it is the first selenium with a 4-connected, 3-dimensional structure. The ICF-22 structure is composed of two interpenetrating lattices, whose building block is a pseudo T4 cluster. Both ICF-24 and ICF-25 present as building unit the T2 cluster and a spiro-5 unit. ICF-24 has a ring size of 20 T atoms, being the first 4-connected, 3-dimensional framework with such ring size. ICF-25 also has a large pore size, having a ring size of 16 T atoms. Like ICF-21, ICF-24 and ICF-25 have a 3-dimensional non-centrosymmetric framework structures (see Figures 58a and 58b respectively). Regarding the last framework, ICF-27 presents a 6-connected network (see Figure 58c) where the $In_{18}S_{41}$ clusters can be consider as the octhaedral unit. Although there is enormous variability in terms of the obtained clusters, no structure was synthesized

that had as a building unit the T3 cluster. According to Feng et al.,[46] it is likely that for sulfur sites exposed to extraframework inorganic cations the coordination with other three M^{3+} becomes unfavorable due to the increase in bond valence sum, thus becoming unstable. As Loewenstein's rule, which states that the M^{4+}/M^{3+} ratio has to be higher than one,[165] is not fulfilled, the concentration of extraframework mobile cations is higher, allowing the increase of ionic conductivity of the materials. As the synthesized structures present the limit situation, i.e. the M^{4+}/M^{3+} ratio is zero, as well as having an open porous system, the synthesized chalcogenides materials present a surprisingly high ionic conductivity.

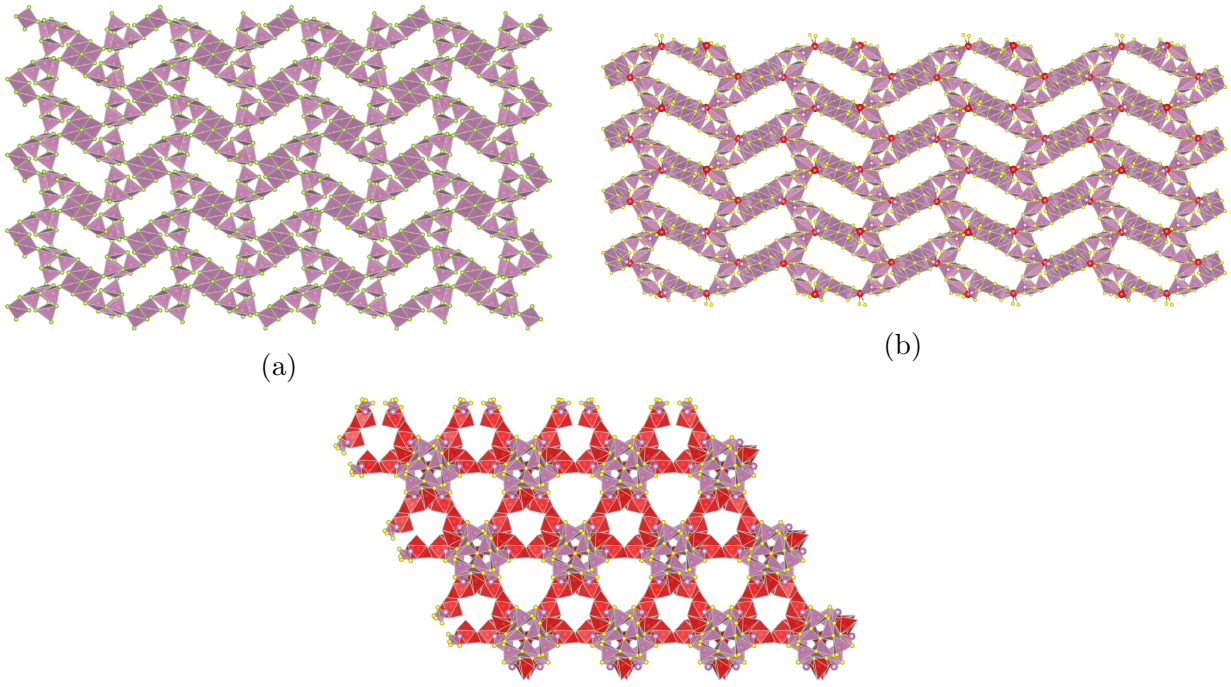

Figure 58: Representation of (58a) ICF-24, (58b) ICF-25 and (58c) ICF-27 (In - pink, S - yellow, Se - green, Sr - red)[206]

Another example of a structure obtained without the use of organic compounds as structural agents is ICF-26.[102] ICF-26 is based on the P2 $Li_4In_{22}S_{44}$ cluster where Ca was used as countercation to stabilize the structure. As for the topology, it presents a double diamond topology. Due to the highly mobile extraframework cations, ICF-26 presents a fast ion condutivity like the structures presented in.[206]

Continuing the research in this subject, Zheng et al.[207] synthesized a sodium indium sulfide hydrate, called ICF-29 (see figure 59). The topology of this material can be derived from the perovskite, $CaTiO_3$. In order to obtain the ICF-29 structure from $CaTiO_3$ a triple substitution is performed: Ti^{4+} by SIn^{4+}, O^{2-} by $InS_4{}^{5-}$ and Ca^{2+} by $Na_5(H_2O)_6{}^{5+}$. This material presents, for the first time, sulfur tetrahedrally bonded to four In ions. The remaining sulfurs have a 2-coordination, none with a 3-coordination. That absence is explained by the presence of the unusual SIn_4 unit. The existence of a tetracoordinated sulfur by four In ions can be explained by Brown's bond valence rule.[56] The In-S bond length is slightly longer than expected (2,55 Å instead of 2,44 Å), so the valence sum is 2,24, close to the theoretical value of two. This lengthening of the bond is explained by the fact that the remaining three In-S bonds involve bicoordenated sulfur, with a higher bond valence value than expected. The cavities of the synthesized material are occupied by $[Na_5(H_2O)_6]^{5+}$ clusters. Since the extraframework species are highly ordered when compared to previously synthesised ICF materials, ICF-29 has a low ion conductivity.

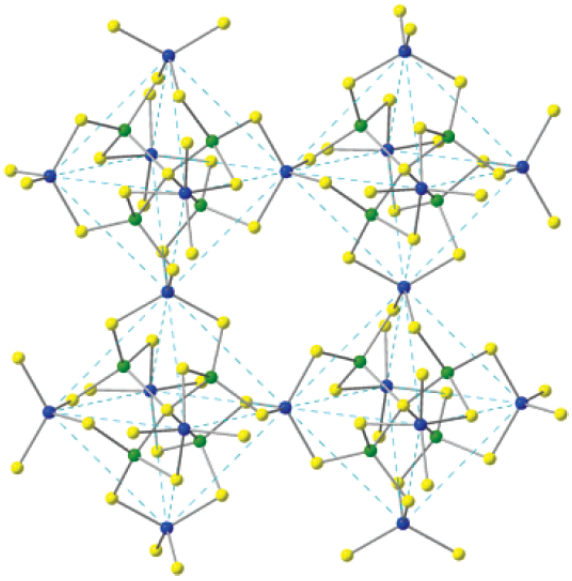

Figure 59: ICF-29 structure (blue: In^{3+}; yellow: S^{2-}; green: In^{3+} around tetrahedral S^{2-})[207]

2.4.2 Ionothermal Synthesis

An ionic liquid is a saltlike compound that melts below 100°C and that presents a preorganized solvent structure. Since its discovery in 1914,[208] more than a thousand ionic liquids have been produced and published and are now commercially available. Due to their unusual properties, quite different from usual solvents, the interest in using ionic liquids for inorganic synthesis has grown lately.[34,209–211]

Cooper et al.[212] published the first example of the use of ionic liquids in the inorganic synthesis, acting at the same time as a solvent and as a SDA, of aluminophosphate zeotype frameworks. Compared to the use of conventional solvents, due to the low vapor pressure of ionic liquids, the synthesis does not need to be performed under high autogenous pressures, thus avoiding the safety concerns and the equipment costs associated with the use of autoclaves. When an ionic liquid is used as solvent and SDA, the competition that exists between the interaction of the solvent and SDA with the solid (nuclei) that is being formed is eliminated. Since the first use of ionic liquids to obtain inorganic structures, the ionothermal synthesis technique has been used to obtain zeolites, metal–organic frameworks and nanomaterials.[210]

The structure of the different ionic liquids used until now in the synthesis of cluster-based chalcogenide materials is represented in Figure 60.

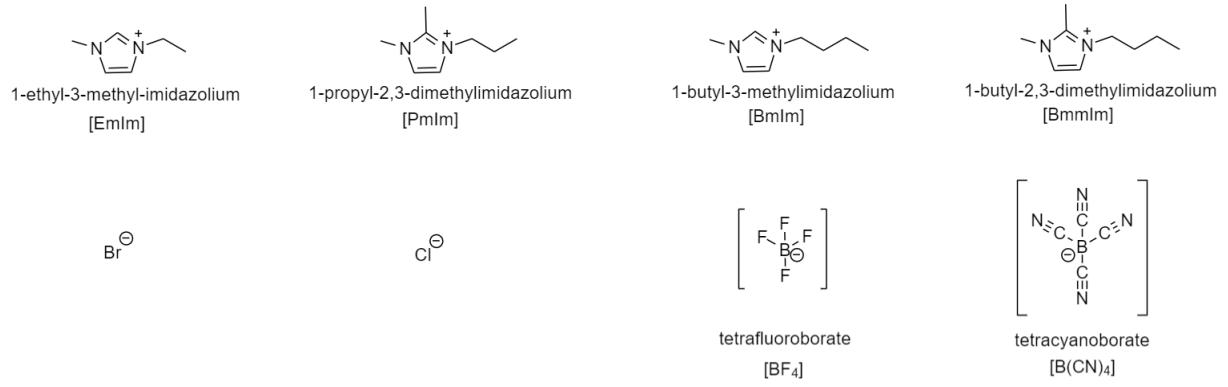

Figure 60: Representation of the different cations and anions used so far in ionotermal synthesis[34]

The synthesis of isolated T5 clusters was one of the first uses of ionothermal synthesis in the field of chalcogenide cluster-based materials.[213] Four distinct clusters were obtained with the Ga-Cu-S or In-Cu-S composition where 1-butyl-2,3-dimethylimidazolium chroride ([BmmIm][Cl]) was used as an ionic liquid. The corners of the clusters have SH^-, Cl^- or BIm^+ groups that allow the stabilization of the negative charge inherent to the cluster, preventing them from polymerization. Continuing research into obtaining large isolated structures, Li et al.[214] obtained two new discrete molecular anions, ZBT-1 and ZBT-2, with a spherical shape. Such anions were obtained using Ge_4Se_{10} as a precursor, $SnCl_4 \cdot 5\ H_2O$ as a Sn source and 1-butyl-3-methylimidazolium tetrafluoroborate ([BmIm][BF_4]) or 1-butyl-2,3-dimethylimidazolium tetrafluoroborate [BmmIm][BF_4] as an ionic liquid. The structures are based on two clusters as building units: Ge_3Se_9, a fragment of the tetrahedral precursor Ge_4Se_{10}, and Sn_6Se_{18}, two semi-cubes clusters that are connected by two Se atoms. Regarding the architecture of the structures, it can be simplified in a truncated dodecahedron with a large spherical cavity, with dimensions similar to the FAU supercage (see Figure 61).

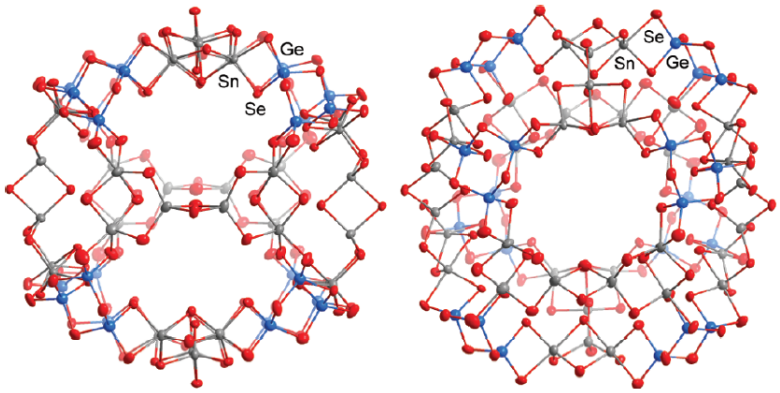

Figure 61: Different orientations of ZBT-1[214]

Due to the growing interest in obtaining isolated clusters, due to their dimensions similar to quantum dots, T3 In-Q (Q = S, Se, S/Se) clusters,[215] T4 In-Cd-Q (Q = S, Se, S/Se, Te/Se) clusters[216] and T5 In-Cu-Q (Q = Se, S/Se) clusters[217] were recently obtained.

Regarding 2-dimensional structures, Santner et al.[218] obtained it using P1 cluster $Mn_4Sn_4Se_{17}$

as a percursor and treating it with 1,2-diaminoethane in [BmIm][BF_4]. The structure obtained can be seen as a honeycomb network with heavily distorted hexagonal rings composed by Sn_3Se_4 clusters.

Moving on to structures with higher dimensions, Li et al.[219] obtained the first 3-dimensional structures using ionothermal synthesis as a synthesis procedure. By adding small amounts of hydrazine to the reaction medium containing imidazolium chlorides as the ionic liquid, different 3-dimensional structures based on Sn-Se were obtained. By changing the relative amount of hydrazine, as well as the length of the carbon chain of the ionic liquid ($[BmIm]^+$, 1-butyl-3-methyl imidazolium, $[BmmIm]^+$, 1-butyl-2,3-dimethyl imidazolium, or $[PmmIm]^+$, 1-pentyl-2,3-dimethyl imidazolium) it was possible to obtain three distinct structures, all of them having Sn_3Se_4 semicubes as building units. The structure of the first compound (see Figure 62a) can be simplified into infinite Sn-Se chains that are connected to each other, resulting in a 3-dimensional structure with multi directional channels filled with $[BmIm]^+$ cations. As for the second structure (see Figure 62b), it also presents multi directional channels filled with $[BmmIm]^+$ cations. However, it presents a different connection mode between the Sn_3Se_4 semicubes clusters. Each Sn_3Se_4 semicube is connected alternately with $SnSe_4$ or $SnSe_3(Se_2)_{0,9}Se_{0,1}$. The third compound has a similar structure to the second compound. In this case, the channels are filled with $[PmmIm]^+$ cations instead of $[BmmIm]^+$. When the relative amount of hydrazine increases in the gel that gives rise to the third compound, a layered compound rather than a 3-dimensional structure is formed.

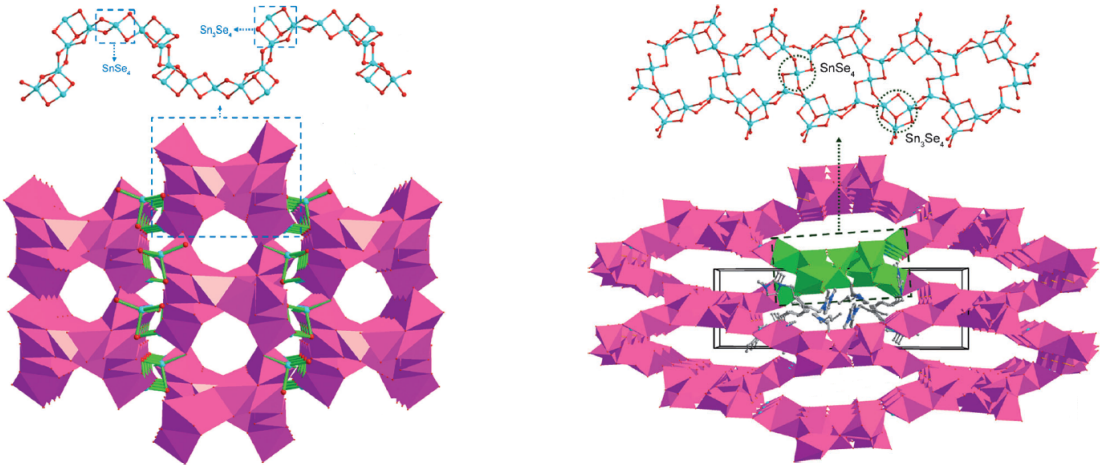

(a) (b)

Figure 62: Representation of the different 3-dimensional structures, (62a) compound 1 and (62b) compounds 2 and 3, obtained by Li et al.[219]

Lin et al.[220] were able to synthesize a 3-dimensional material, also composed by Sn and Se, where [BmIm][BF_4] was used as an ionic liquid, avoiding the use of hydrazine the reaction medium. The building unit of this structure is once again the Sn_3Se_4 semicube, presenting three distinct means of connection between the clusters, originating a 3-dimensional structure with a complex system of channels responsible for the extra-large microporosity of the sample (see Figure 63). When there is the replacement of [BmIm][BF_4] with 1-Ethyl-3-methyl-imidazolium-bromide ([EmIm][Br]) a layered material with the framework previous describe in[123] is obtained.

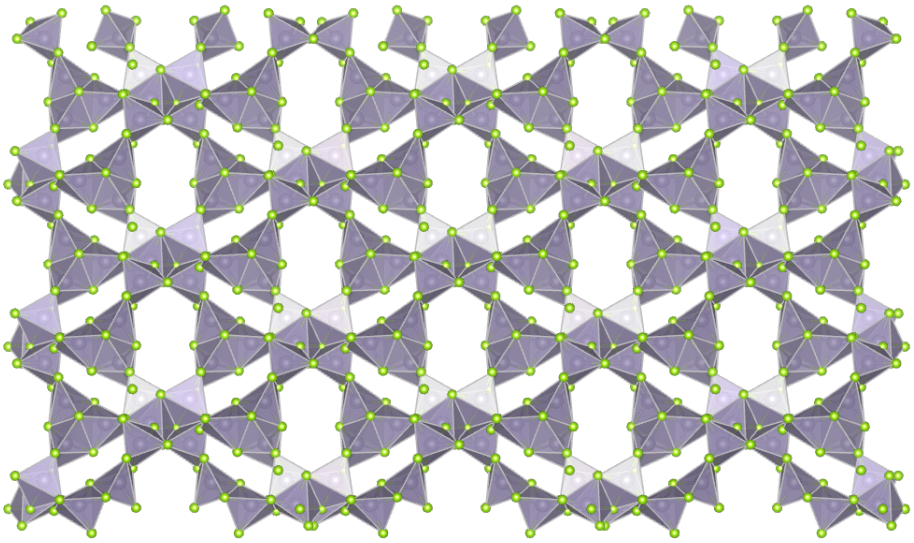

Figure 63: Representation of the 3-dimensional structure obtained by Lin et al.[220] where the organic part was not represented (Sn - gray, Se - green)

It is possible, through ionothermal synthesis, to obtain new structures using 3-dimensional structures as a precursor. Lin et al.[221] observed that when a heat treatment is applied to the 3-dimensional $K_2Sn_2Se_5$ structure (3D-1) it undergoes a deconstruction, reducing to a 1-dimensional structure (1D-1), passing through a layered material (2D-1) (see Figure 64). Although a dramatic change in structure is observed between 3D-1 and 2D-1, 1D-1 and 2D-1 can be considered polymorphic with different dimensions. When cis-2,6-dimethylmorpholine (DMPP) is added to the 2D-1 heat treatment a different 1-dimensional structure, referred to as 1D-1, is obtained. The addition of DMPP leads to the replacement of a $[BmmIm]^+$ cation into the structure. From both 1-dimensional structures it is possible to obtain 2D-1 if a thermal treatment is carried out in the presence of ethylenediamine (en). Although the function of en is not fully known, it seems to stabilize the Sn-Se connections, as the dominant phase at a temperature of 150°C or higher is 2D-1, acting as a transformation agent, since it is not part of the final structure. When a heat treatment is applied again to 1D-1 or to 1D-2 in the presence of DMMP, a 3-dimensional structure, referred as 3D-2 different from $K_2Sn_2Se_5$ is obtained. It is concluded that although temperature is the determining factor in the transformation of the structures, the amines present a secondary role that seems to

influence the cleavage or reconstruction of Sn-Se bonds.

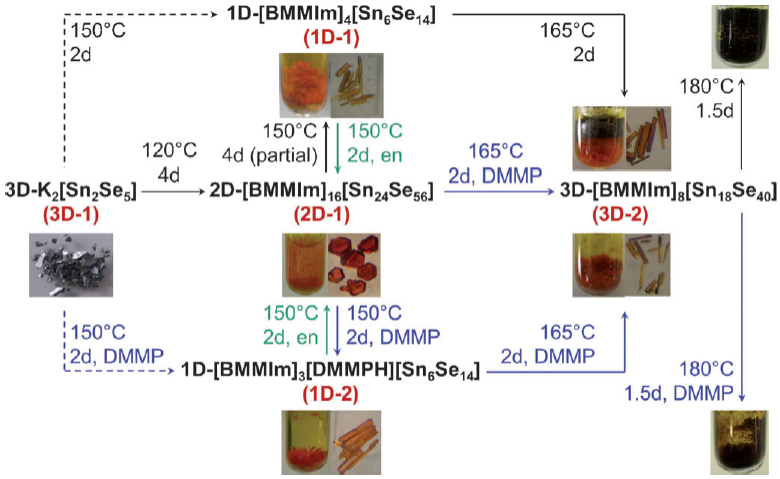

Figure 64: Scheme summarizing the main experimental results obtained by Lin et al.[221]

After the first syntheses of these structures, Lin et al.[222] conducted a more in-depth study of the Sn/Ge/Se system in the presence of ionic liquids. With different experimental conditions, i.e. different amount and nature of amines, it was possible to obtain structures from 0- to 3-dimensional (see Table 14). It was observed that the amount and nature of amines in the reaction medium has a direct influence on the chemical composition and on the dimension of the final structure. The presence of amines, which is directly related to the pH of the reaction medium, seems to influence the initial formation of clusters that will originate the final structure. Comparing the final composition of compounds 2, 5 and 7 (see Table 14), it is concluded that, due to the increased basicity of the medium, there is a greater tendency to incorporate Sn in the final structure.

Table 14: Different compounds obtained by Lin et al.,[222] as well as the reagents which gave rise to it and the chemical composition of the final products

Compound	Ge reactant	Sn reactant	IL	Sn/Ge_{Gel}	Amine (μL)	Product Formula	$Sn/Ge_{Product}$
1	$K_4(H_2O)_3][Ge_4Se_{10}]$	$SnCl_4{\cdot}5H_2O$	$[BmIm][BF_4]$	0,66	DMMP (50)	OD - $[BmIm]_{24}[Ge_{27,5}Sn_{32,5}Se_{132}]$	1,18
2	$K_4(H_2O)_3][Ge_4Se_{10}]$	$SnCl_4{\cdot}5H_2O$	$[BmmIm][BF_4]$	0,66	DMMP (50)	OD - $[BmmIM]_{24}[Ge_{24}Sn_{36}Se_{132}]$	1,50
3	$K_4(H_2O)_3][Ge_4Se_{10}]$	$SnCl_4{\cdot}5H_2O$	$[BmIm][BF_4]$	0,46	DMMP (50)	1D - $[BmIM]_2[Ge_4Se_9]$	0
4	$K_4(H_2O)_3][Ge_4Se_{10}]$	$SnCl_2$	$[BmmIm][BF_4]$	0,92	DMMP (50)	1D - $[BmmIM]_{24}[Ge_4SnSe_{10}]$	0,25
5	$K_4(H_2O)_3][Ge_4Se_{10}]$	$SnCl_4{\cdot}5H_2O$	$[BmmIm][BF_4]$	0,66	DMMP (100)	2D - $[BmmIM]_2[Ge_{0,83}Sn_{3,17}Se_{9,06}]$	3,82
6	$K_4(H_2O)_3][Ge_4Se_{10}]$	$SnCl_4{\cdot}5H_2O$	$[BmIm][BF_4]$	0,66	en (50)	3D - $[BmIM]_4[Sn_9Se_{20}]$	∞
7	$K_4(H_2O)_3][Ge_4Se_{10}]$	$SnCl_4{\cdot}5H_2O$	$[BmmIm][BF_4]$	0,66	en (50)	3D - $[BmIM]_4[Sn_{18}Se_{40}]$	∞

The importance of amines in the reaction was also observed by other authors who were able to obtain heterometallic structures through the insertion of Ag[223] or Mn[224] into the Sn-Se system. Li et al.[223] obtained six different structures by varying the amount of amines, temperature and time of synthesis. Of the structures obtained, the laminar structure composed by Ag, Sn and Se stands out, since heterometallic structures with Ag are not common. The structure of this compound can be simplified into Sn and Se double chains connected by Ag, thus forming a laminar structure with $[BmmIm]^+$ cations acting as charge compensates (see Figure 65).

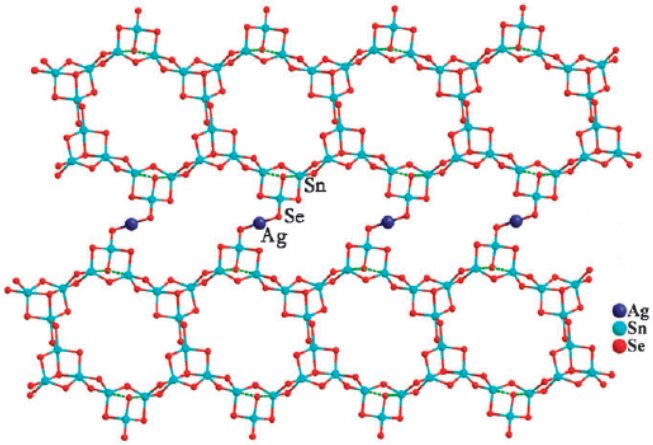

Figure 65: Representation of the Sn-Ag-Se laminar material obtained in[223]

Regarding the structures based on the combination of Sn-Mn-Se, Du et al.[224] were able to obtain such structures by adding $MnCl_2 \cdot 4\ H_2O$ to the reaction medium. Changing the amount of ionic liquid used, as well as the type of amine used, four structures were obtained. All structures obtained are layered, with the Sn_3Se_4 semicube as building units, differing in the ring size and the type of compound that exists in the inter layered space. When only metal-amine complexes are found in the interlayered space, laminar structures with elliptical six-membered rings are obtained (structures 1 and 2 at the Figure 66). When the space between layers is occupied by a mixture of metal-amine complexes and ionic liquid cations, the materials obtained have distorted hexagonal rings. When ethylenediamine (en) is used as the amine, a structure with an eight-membered heart-shaped ring is obtained (structure

3 in Figure 66). When the amine is replaced by diethylenetriamine (dien) the structure obtained consists of both eight-membered heart-shaped rings and compressed six-membered rings (structure 4 in Figure 66). It is thus observed that when the metal-amine complex is the only structuring agent, the amine used does not influence the final structure. When there is competition between the metal-complex and the ionic liquid as structuring agents, the final structure obtained is influenced by the amine used.

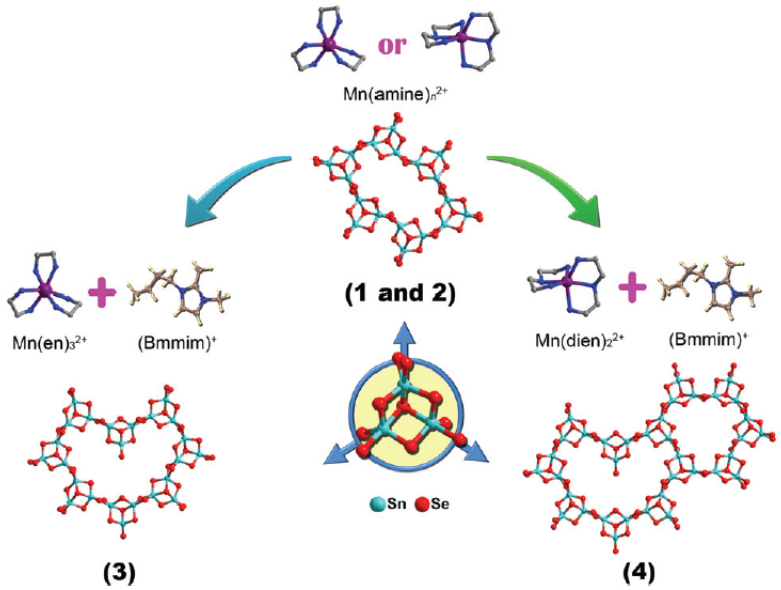

Figure 66: Different 2D materials obtained by,[224] with focus on the components that are in the interlayer space

Continuing the research on this subject, Santner et al.[225] evaluated the influence that the ionic liquid anion has on the final structure as well as the temperature of synthesis. To this end, several structures were synthesized in which ion liquids with different BX_4 anions were used: BF_4 and $B(CN)_4$. When [BmmIm][BF_4] is used as an ionic liquid, it is fully incorporated in the final 3-dimensional structure. However, when [EmIm][$B(CN)_4$] is used as ionic liquid at low temperatures, there is no presence of the ionic liquid in the structure, obtaining a 2-dimensional structure with a low distance between layers.

2.4.3 Surfactant-thermal Method

Surfactants are organic compounds containing hydrophilic groups, which tend to be soluble in water, and hydrophobic groups, usually composed of hydrocarbon chains that are typically insoluble in water. This type of compounds has been widely used in the preparation of nanocrystals and ordered mesoporous materials. In the case of nanocrystals it is possible to tailor the size, shape and surface properties of the nanoparticles. In the case of mesoporous frameworks, it allows to control the pore size and phase of porous materials.[18,226,227]

Since surfactants can control the morphology of materials at micro scale, studies are currently being carried out to investigate the possibility of using surfactants as structuring direct agents or solvents. Compared to traditional solvents, surfactants have low vapour pressure and high thermal stability. With respect to ionic liquids, another class of materials that has been the target of studies for presenting excellent properties as a solvent in the synthesis of inorganic crystalline materials, surfactants present numerous advantages, namely low cost, great commercial availability and different properties (cationic, anionic, neutral, basic or acidic).[226,227]

One of the first examples of chalcogenide materials prepared using surfactant is a lamellar tin sulfide compound.[228,229] Later, some crystalline lamellar materials based on Sn_2S_6 dimer,[230] $Ge_4S_{10}^{4-}$ T2 cluster,[231–233] $Ge_4Se_{10}^{4-}$ T2 cluster[234] or $Cd_8Se(SePh)_{12}Cl_4^{2-}$ P1 cluster[235] were also obtained.

Wacchold et al.[234] also evaluated how the surfactant alkyl chain length and the presence of N-H groups on the surfactant influence the final structure, after having obtained laminar materials based on $Ge_4Se_{10}^{4-}$. Regarding the alkyl chain length, it was observed that there is a change on the spatial arrangement of the material when using a surfactant with an alkyl chain composed by more than nine carbons. When a surfactant with a N-H is used, isolated adamantane clusters are obtained instead of a lamellar material.

All the materials presented so far use surfactants as reagent. Xiong et al.[236] used for the first time surfactants as a reaction medium to obtain chalcogenic materials. Using chalco-

genidoarsenates as a model system, 0-, 1-, 2- and 3-dimensional structures were obtained. When no surfactant was used on the reaction medium, no type of structure was obtained, thus showing the fundamental role of surfactants in obtaining such structures. Now using mercury selenidostannates instead of chalcogenidoarsenates as a model system, the same team of researchers observed that the use of PEG-400 in such a chemical system allows to kinetically transform between two thermodynamically stable 1-dimensional phases.[237]

Continuing the research in this area, a 2-dimensional antimony oxosulfide was synthesized.[238] Zhang et al.[239] made several syntheses where they evaluated the consequences in the final material of placing surfactants and amines, compounds used as SDAs, in the reaction medium. Different amines were used and, depending on the amine, different structures were obtained. Using PEG-400 as a reaction medium, a 2-dimensional material based on the $MnGe_2S_8N_2$ trimer was obtained when using hydrazine as amine. By replacing hydrazine with ethylenediamine a quasi-layered material consisting of T2 $MnGe_3Se_{10}$ clusters is obtained. When 1,2-propanediamine or 1,3-propanediamine is used, a 1-dimensional chain composed of Ge_2Se_7 or $MnGeSe_6$ dimers is obtained, respectively. When the surfactant is replaced by another solvent no structure is obtained. Shen et al.,[240] using the A-Cu-Sb-S (A = Rb, Cs) chemical system and PEG-400 as a reaction medium, obtained for the first time two new 3-dimensional structures.

The use of surfactants also makes it possible to obtain nanocomposites with unique characteristics. Xiong et al.[241] obtained a nanocomposite that consists of Sn_3Se_7 layers with PEG chains into its nanochanels (see Figure 67). Usually, in this type of materials, the polymers are located between the layers of the inorganic material, and not in the channels of the structure (see Figure 67b).

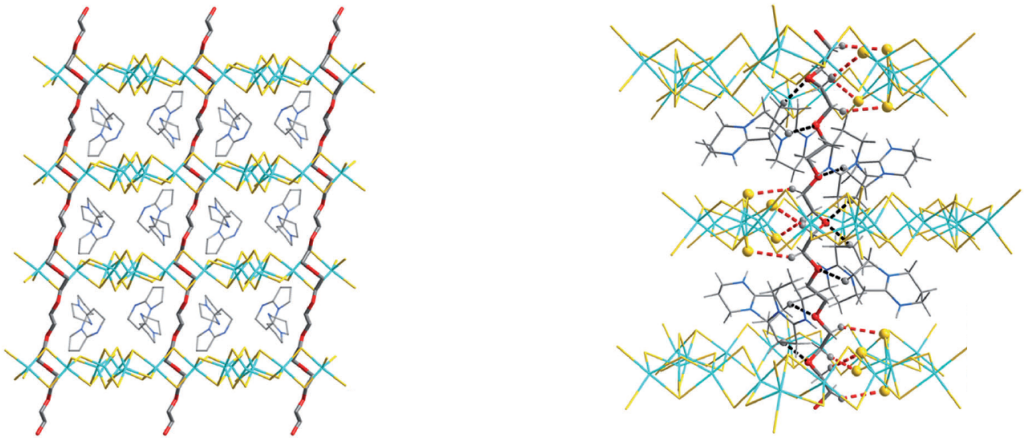

(a) (b)

Figure 67: Representation of of the 2-dimensional structures obtained by Xiong et al.[241] (Sn - blue; Se - yellow; C - black; O - red)

3 Photocatalysis Applications

3.1 Introduction

Although it is used worldwide, the term photocatalysis is misleading, since it suggests that light is the catalyst for the reaction. By definition, a catalyst should be recovered after the chemical reaction without, theoretically, being modified in the process and can be used several times. In a photochemical reaction, it is observed that light is absorbed and cannot be recovered at the end of the chemical reaction. Thus, photocatalysis refers to the acceleration of a photoreaction through the presence of a catalyst, and not a reaction catalyzed by light.[242]

A photocatalytic process becomes interesting for environmentally friendly applications when the photocatalyst used is cheap and stable and it is possible to use sunlight as an energy source.[243] Due to the challenges that today's society is facing, research in this area, particularly in the application of photocatalysis for the production of solar fuels (such as H_2 or high added value chemicals like methanol), from the H_2O photodecomposition or CO_2 photoreduction, and the degradation of organic pollutants, has been the subject of high interest.[2,39]

Given the ecological problems associated with CO_2, the main gas responsible for the greenhouse effect, its reduction for the production of useful chemical compounds has been one of the current priorities in green catalysis. The use of CO_2 for the production of hydrocarbon fuel using solar energy has currently been the subject of great interest, as the final product obtained is compatible with existing infrastructure. However, H_2 is still seen by many as the fuel of the future due to its high energy content per mass and clean transformation, although it does present a number of safety concerns when it is handled, stored and distributed, as well as low volumetric energy density.[2,243–245] It is also important to note that by photochemical converting sunpower directly to fuel, the problems of storage and distribution associated with the production of electricity from photovoltaic cells could be overcome.[246] The combination of H_2 and fuel cells allows the regulation of the energy flow between the production and the consumers. Currently, the regulation of energy flow has grown in importance due to the increased use of renewable energy sources. Renewable energy sources are naturally intermittent, so the use of storage is necessary to compensate the gap between production and consumption of electricity.[39,247] In addition to becoming an energy carrier, hydrogen can also participate in the formation of other organic compounds (such as alcohols and hydrocarbons), which are easier to store and transport.[39,248]

3.2 Photocatalytic process

The process begins when the photocatalyst is irradiated by sunlight. When the photons from the solar radiation have a higher energy than the band gap of the photocatalyst, electrons and holes are produced. Subsequently, the charge carriers are partly transported to the surface of the photocatalyst, where the electrons may participate in a reduction reaction (see path A in Figure 68) and the holes in an oxidation process (see path B in Figure 68).[17,249–252]

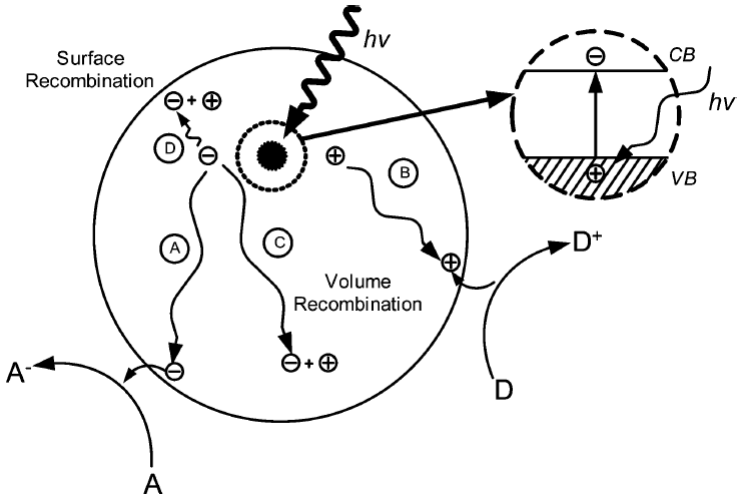

Figure 68: Schematic of a redox process through photocatalysis, where A is an electron acceptor species and D is an electron donor[252]

In addition to participating in redox reactions, charge carriers can also undergo recombination (see paths C and D in Figure 68). Charge recombination competes directly with the redox reactions that occur at the surface of the photocatalyst, becoming one of the main factors responsible for the low yield of the process.[251]

To ensure that the desired reaction process takes place as efficiently as possible, charge separation has to be maximized and redox reactions to the surface have to occur within the average lifetime of the charges.[17] In order to decrease charge recombination rate, a semiconductor with high crystallinity should be used, since the defects and the boundaries in the crystalline framework act as traps, thus facilitating the electron-hole recombination.[251]

For a semiconductor to be used as a photocatalyst, it is required that it presents a set of properties that make it suitable for such application. It is necessary that the base of the semiconductor conduction band is located at a more negative potential than the reduction potential of the acceptor species and that the top of the valence band is located at a more positive potential than the oxidation potential of the donor species.[247,249,252,253] Therefore, in order to attain high photocatalytic performance, the photocatalyst should have excellent light harvesting, generation and charge separation properties.

There are two configurations of photocatalytic systems generally used. The first con-

figuration consists of suspending the photocatalyst in a solvent that is exposed directly to the solar radiation. It is a simple and an easy system to use and study. However, the oxidation and reduction reactions occur at different points of the photocatalyst surface, thus having a mixture of the final products. The second system is entitled photoelectrochemical (PEC) cell system. It consists of three main components: a semiconducting photoelectrode (working electrode), a counter electrode and usually a reference electrode. The photoelectrode is responsible for collecting the solar radiation, where charge generation occurs. The photoelectrode is generally the photoanode, where the oxidation reaction occurs. At the counter electrode, the photocatode, the reduction reaction takes place. Since the reduction and oxidation reactions take place in different locations, it is possible to separate the final products and avoid a possible back oxidation. By comparing the two systems, it is possible to achieve higher efficiencies in PEC systems.[254] However, PEC cells integrate complex multilayer systems and have stability problems when used.[253]

3.2.1 Band gap

The band gap of a material corresponds to the energy difference between the top of the valence band and the bottom of the conduction band. This parameter corresponds to the minimum energy that must be supplied to the material to promote an electron from the valence band to the conduction band. Thus, the band gap is closely related to the electrical conductivity. A material with a high band gap corresponds to an insulator and when the band gap is very small or the valence and conduction bands overlap the material is called a conductor. A semiconductor has an intermediate band gap value and, as such, has an electrical conductivity between that of a conductor and that of an insulator.[255]

This property of semiconductors gains special attention when it comes to using such materials as photocatalysts. The performance of a photocatalyst depends strongly on the band structure and the value of the band gap. To use solar radiation efficiently as a source of radiation in a photocatalytic process, the band gap should be less than 3 eV in order to

absorb light into the visible region.[256]

The class of materials covered in this review allows the combination of the characteristics of condensed-phase semiconductors with an open architecture. Due to the small dimensions of the clusters that constitute these materials, quantum confinement effects can be observed. Quantum confinement begins to show when the particle dimensions are similar to the wavelength of the incident radiation. When this occurs, the optoelectronic properties of the material, namely the value of the band gap, become a function of the shape and size of the particles.[257]

The value of the band gap is highly influenced by clusters chemical composition and dimensions and the component present on the extra framework volume. The connection mode between clusters and consequent final topology of the material do not influence the band gap value very strongly.[100,130] Taking into account the materials synthesized so far, it is possible to obtain materials with band gap values ranging from 0,69 eV[79] to 4,10 eV[76] and it is currently possible to modulate the value of this parameter as needed.

3.2.1.1 Chemical composition

The chemical composition of clusters is one of the main factors that influence the band gap value and it is through its variation that it is possible to customize the electronic properties of the structure. The two materials synthesized by Wu et al.[168] are two examples that show the importance of chemical composition in the value of band gap. SOF-20 and SOF-21 are two 3-dimensional materials composed of T2 clusters which, although are both composed by In, Sn and S, have different Sn/In ratios. SOF-20 has a band gap value equal to 3,25 eV and SOF-21 to 3,07 eV and, according to the authors, this difference is directly related to the distinct Sn/In ratios in the materials.

Comparing the Ga-Se and Ga-S systems[75] (see Figure 69 and Table 3 for more information about this materials), it can be seen that the Ga-Se system band gap varies between 1,4 eV

and 1,7 eV. Turning to the Ga-S system, the values of the band gap almost double, varying between 2,6 eV and 2,8 eV. Even with the insertion of Zn in the Ga-S system, the band gap still presents values higher than 2 eV. Thus, in this system, the framework anions have a greater impact on the value of the band gap than the framework cations.

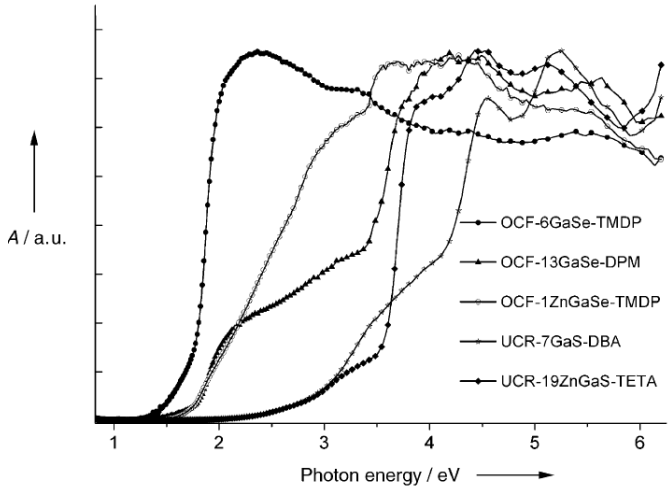

Figure 69: Optical absorption spectra of OCF-6GaSe-TMDP (E_g = 1,43 eV), OCF-13GaSe-DPM (E_g = 1,76 eV), OCF-1ZnGaSe-TMDP (E_g = 1,71 eV), UCR-7GaS-DBA (E_g = 2,84 eV) and UCF-19ZnGaS-TETA (E_g = 2,60 eV)[75]

The doping of a certain chemical system allows the customization of the electronic properties of the final material. The Cu-doping of ISC-10-CdInS, which consists of the isolated T5 clusters obtained in Ref.,[94] results in a band gap reduction from 3,01 eV to 2,11 eV. It is also observed that when clusters are composed only by In-Cu-S, the value of the band gap is 2,29 eV. Thus, the combination of Cu and Cd allows for the obtention of the lowest band gap value. Although a reduction in the band gap value is observed when doping ISC-10-CdInS with Mn, from 3,01 eV to 2,87 eV, this reduction is not as significant as when doping with Cu.[95]

As previously mentioned, icosahedral clusters permits the obtention of structures rich in copper, an element known to reduce the value of the band gap. Luo et al.[149] synthesized different structures based on this cluster, which all have a band gap below 2,1 eV. The low value of the band gap is due, according to the authors, to the high copper content in the

structures. Of the combinations tested, Cu-Sn-Se is the one with the smallest band gap (see Figure 70).

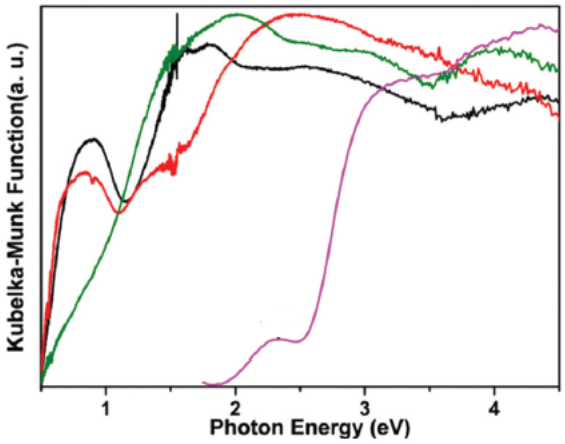

Figure 70: Optical absorption spectra of Cu-Ge-Se (black line - E_g = 1,42 eV), Cu-Sn-Se (red line - E_g = 1,19 eV), Cu-Ge-S (purple line - E_g = 2,08 eV) and Cu-Ge-Se (green line - E_g = 1,40 eV) [149]

It was possible to synthesize different isolated T4 clusters[83] and to compare the effect of Zn, Cu, S and Se in the band gap value. Looking at Figure 71a it is easy to conclude that when Cu and Se are present, a lower value for the band gap is guaranteed. The type of amine present on the surface of the cluster also influences the final electronic properties (see Figure 71b).

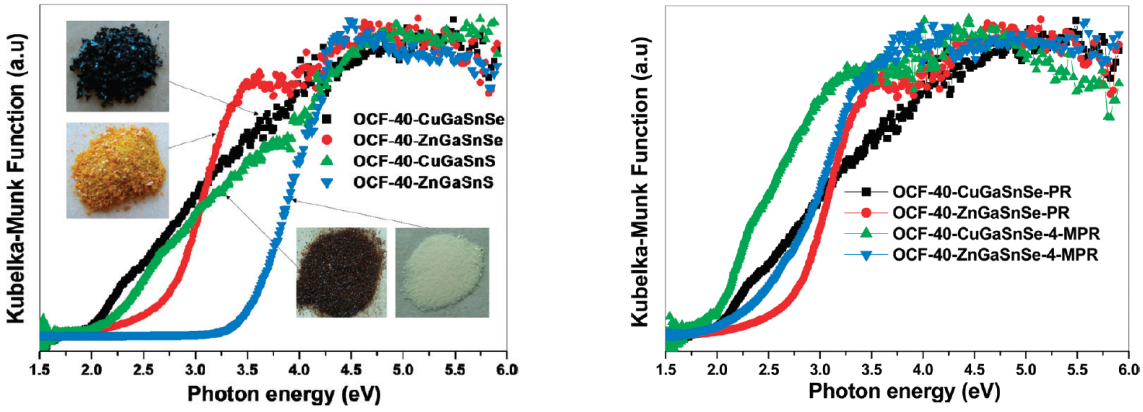

(a) (b)

Figure 71: Optical absorption spectra of (71a) OCF-40-CuGaSnSe-PR (E_g = 1,91 eV), OCF-40-ZnGaSnSe-PR (E_g = 2,71 eV), OCF-40-CuGaSnS-PR (E_g = 2,11 eV), OCF-40-ZnGaSnS-PR (E_g = 3,59 eV), (71b) OCF-40-CuGaSnSe-4-MPR (E_g = 1,80 eV) and OCF-40-ZnGaSnSe-4-MPR (E_g = 2,60 eV)[83]

Since metal selenides and tellurides tend to have a lower band gap than sulfides, multi-chalcogen doping has been seen as a technique to customize electronic properties. Shen et al.[215] synthesized a set of isolated T3 clusters with different contents of chalcogen and observed that there is a systematic reduction of the band gap value along with the change from S, S/Se to Se/Te (see Figure 72).

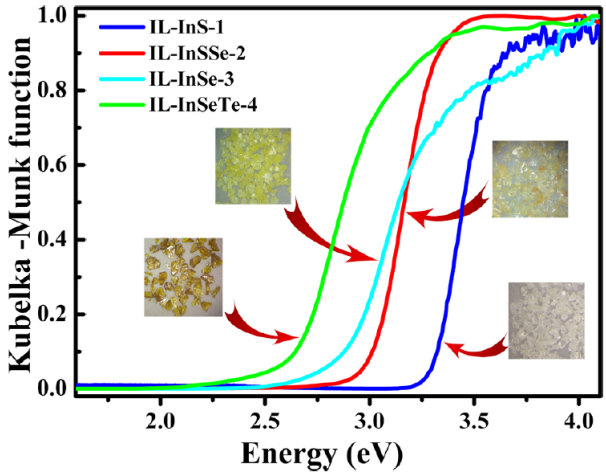

Figure 72: Optical absorption spectra of IL-InS-1 (E_g = 3,31 eV), IL-InSSe-2 (E_g = 3,00 eV), IL-InSe-3 (E_g = 2,89 eV) and IL-InSeTe-4 (E_g = 2,65 eV)[215]

Wu et al.[86] synthesized a series of materials with the same topology but with different

chemical composition, in order to evaluate the impact that the chemical composition has on band structure. Thus, the Zn-Ga-Se was doped with Sn, S or both elements. When the system is doped with Sn, a red shift in the band gap is observed, evidenced by the reduction of OCF-5 band gap from 3,23 eV to 2,49 eV (see Figure 73a). However, when doping with S takes place, a blue shift of the band gap occurs, since OCF-1 band gap goes from 1,71 eV to 3,37 eV. Since doping has opposite effects on the value of the bang gap, it becomes interesting to evaluate the consequences of dual-doping. It is concluded that the direction of the shift depends on which of the elements is dominant. However, when comparing the undoped OCF-5-ZnGaSe-AEP (E_g = 3,23 eV) and OCF-5-ZnGaSnSeS-ECHA (E_g = 2,54 eV) it seems that Sn plays a dominant role against S. The influence of the extra framework amine on the electronic properties was also evaluated. For the same topology, the nature of the amine on the band gap value has less influence than doping (see Figure 73b).

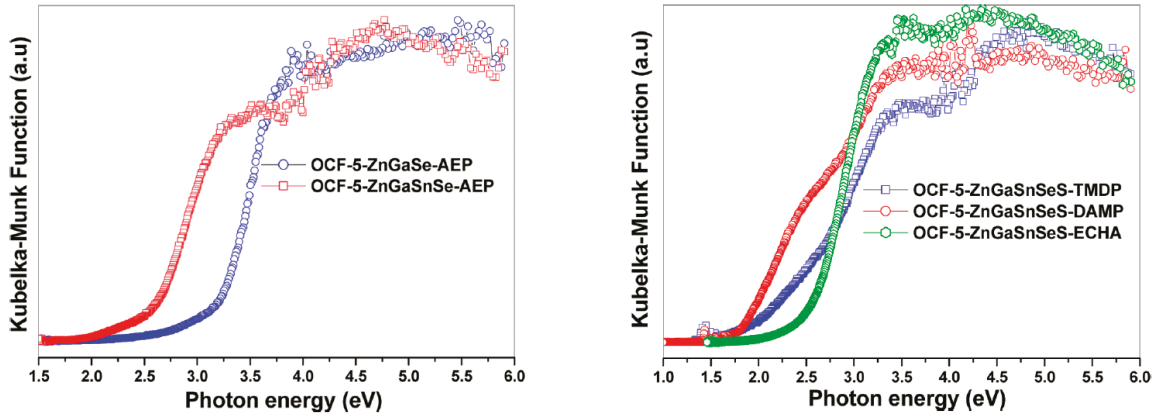

(a) (b)

Figure 73: Optical absorption spectra of (73a) OCF-5-ZnGaSe-AEP (E_g = 3,23 eV), OCF-5-ZnGaSnSeS-ECHA (E_g = 2,54 eV) and (73b) OCF-5-ZnGaSnSeS-TMDP and OCF-5-ZnGaSnSeS-DAMP and OCF-5-ZnGaSnSeS-ECHA (E_g = 2,54 eV)[86]

Although the clusters's chemical composition is one of the main characteristics that influence the band gap value, Chen. et al[169] showed that the position of the dopant in the clusters influences the direction of the band gap shift. When CPM-120-Zn-Ge-S-AEM is doped with Ga, which will substitute Ge, an increase in the band gap is observed. CPM-

120-Zn-GeS-AEM has a band gap equal to 1,90 eV, and when doped with Ga, this value increases to 2,30 eV. However, when Ga replaces Zn, a red shift of the band gap is observed. The band gap shift will depend on the amount of Ga added (see Figure 74).

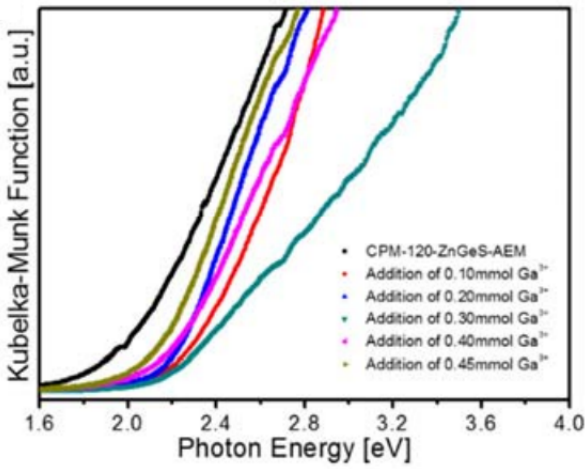

Figure 74: Optical absorption spectra of CPM-120-ZnGeS-AEM (E_g = 1,87 eV) and Ga-doped analogues (for an addition of 0,10 mmol Ga^{3+} - E_g = 2,30 eV, 0,20 mmol Ga^{3+} - E_g = 2,20 eV, 0,30 mmol Ga^{3+} - E_g = 2,12 eV, 0,40 mmol Ga^{3+} - E_g = 2,13 eV, 0,45 mmol Ga^{3+} - E_g = 2,16 eV)[169]

The influence that the species present in the extra framework space has on the final electronic properties was also studied by other authors.

When the laminar structure obtained by Manos et al.[194] was exchanged with H^+, that is, when the $[Zn(H_2O)_4]^{2+}$ complex was exchanged with H^+, a reduction of the band gap value from 2,08 eV to 1,76 eV was observed.

Qi et al.,[146] when studying the SnS-1 laminar structure, observed that there is a decrease in the value of the band gap when the structure is exchanged with Cs^+ or Sr^{2+}. The value of the band gap, when it presents the organic compound in the interlaminar space, is 2,92 eV. After ionic exchange with Cs^+ the value decreases to 2,82 eV or after ionic exchange with Sr^{2+} to 2,60 eV. Filso et al.[145] compared the presence of two distinct organic species in the interlaminar space. They observed that when tris(2-aminoethyl)amine is located in the interlaminar space the band gap of the structure is 2,96 eV. When this species is exchanged with 1-(2-aminoethyl)piperidine the band gap increases to 3,21 eV.

3.2.1.2 Cluster dimensions

Due to the size of the clusters, the quantum confinement is an effect that has to be taken into account. It is observed that clusters with smaller dimensions present an increase in the value of the band gap due to quantum confinement.

The importance of the cluster dimensions is evident when comparing the band gaps of SCIF-3, SCIF-7, SCIF-8 and SCIF-9. SCIF-3 and SCIF-7 are composed by T3 clusters and have as band gap values 3,35 eV and 3,43 eV, respectively. SCIF-8 and SCIF-9, composed by T4 clusters, have as band gap values 3,12 eV and 3,22 eV, respectively.[195]

The laminar structures obtained by Xu et al.[74] also highlight the consequences of cluster dimensions. OCF-99 is a laminar structure composed by T4 clusters and OCF-100 is also a laminar structure but composed by T6 clusters. Evaluating Figure 75 it can be concluded that the materials composed by the larger clusters have again lower band gap values, even when these are doped with Mn.

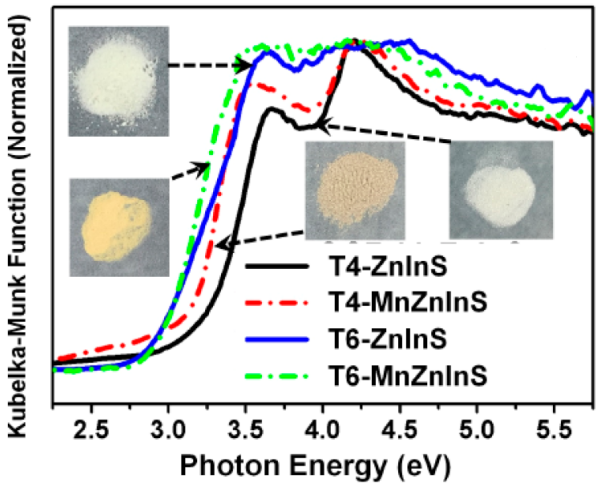

Figure 75: Optical absorption spectra of OCF-99-ZnInS (black; E_g = 3,36 eV), OCF-99-MnZnInS (red; E_g = 3,23 eV), OCF-100-ZnInS (blue; E_g = 3,25 eV) and OCF-100-MnZnInS (green; E_g = 2,99 eV)[74]

3.2.1.3 Connection between clusters

There are different examples that show that the way clusters are connected does not have a great importance in the value of the final band gap.[118]

From the materials with different structures but with similar band gap values, it is worth highlighting SOF-23 vs. SOF-24 vs. SOF-27, MCOF-1 vs. MCOF-2, SOF-25 vs. SOF-28, SCIF-1 vs. SCIF-11 and IL-InS-1 vs. SCIF-7 (see Table 15).

However, when comparing isolated clusters with clusters that form a covalent network, differences in band gap values may arise due to quantum confinement effects. There is a decrease in the value of the band gap when moving from isolated clusters to clusters that form a 3-dimensional framework - OCF-40-CuGaSnSe-PR vs. OCF-5-CuGaSnSeDPM[83] or $(Me_4N)_2M[Sn_4Se_{10}]$ (M = Mn, Fe, Co, Zn) vs $(Me_4N)_4[Sn_4Se_{10}]$[79] (see Table 15).

Table 15: Main characteristics, highlighting the band gap, of some selected materials[70,71,79,83,104,128,196,215]

Compound	Chemical Composition	SBU[1]	Material Dimension	Band gap (eV)	Ref.
SOF-23	$[In_{35}Sn_5S_{74}]^{23-}$	T3	2D	3,2	[70]
SOF-24	$[In_{19}SnS_{37}]^{13-}$	T3	2D	3,2	[70]
SOF-27	$[In_{8,5}Sn_{1,5}S_{18}]^{4,5-}$	T3	3D	3,2	[71]
MCOF-1	$[Cu_{6,2}In_{10,6}Sn_{9,2}S_{42,5}]^{11,2-}$	P2	3D	1,8	[104]
MCOF-2	$[Cu_6In_{12,5}Sn_{7,5}S_{42}]^{11,9-}$	P2	3D	1,8	[104]
SOF-25	$[In_{34,5}Sn_{3,5}S_{65}]^{12,5-}$	TO2	3D	3,1	[128]
SOF-28	$[In_{35,4}Sn_{2,6}S_{65}(H_2O)_6]^{13,4-}$	TO2	3D	3,1	[128]
SCIF-1	$[(In_{10}S_{16})(Im)_2]^{4-}$	T3	n/a[2]	3,2	[196]
SCIF-11	$[(In_{10}S_{17})(Im)]^{5-}$	T3	3D	3,2	[196]
IL-InS-1	$[BmmIm]_5[In_{10}S_{16}Cl_3(BIm)]$	T3	0D	3,3	[215]
SCIF-7	$[(In_{10}S_{16})(DmBIm^3)_2]^{4-}$	T3	3D	3,4	[195]
OCF-40-CuGaSnSe-PR	$Cu_2Ga_{16}Sn_2Se_{35}{\cdot}12\ C_5NH_{12}$	T4	0D	1,9	[83]
OCF-5-CuGaSnSe-DPM	$Cu_2Ga_{16}Sn_2Se_{33}{\cdot}\ C_{11}N_2H_{22}$	T4	3D	1,5	[83]
-	$(Me_4N)_2Mn[Sn_4Se_{10}]$	T2	3D	2,1	[79]
-	$(Me_4N)_2Fe[Sn_4Se_{10}]$	T2	3D	1,3	[79]
-	$(Me_4N)_2Co[Sn_4Se_{10}]$	T2	3D	1,9	[79]
-	$(Me_4N)_2Zn[Sn_4Se_{10}]$	T2	3D	2,2	[79]
-	$(Me_4N)[Sn_4Se_{10}]$	T2	n/a[2]	2,4	[79]

[1]Secondary Building Unit. [2]Not available. [3]DmBIm: 5,6-Dimethyl-benzimidazole - $C_9H_{10}N_2$

3.3 Solar Fuels

3.3.1 H_2 Generation

3.3.1.1 Introduction

The use of H_2 as an energy vector has been the subject of growing interest, as its oxidation produces only water and releases large amounts of energy (see Equation 1).[243,258]

$$^1/_2\,O_2\,(g)\;+\;H_2\,(g)\;\rightarrow\;H_2O\,(l)\quad \Delta G^0 = -237\ \text{kJ mol}^{-1}\qquad \Delta H^0 = -286\ \text{kJ mol}^{-1}\quad (1)$$

Currently, the production of H_2 is done through natural gas reforming. Besides having a non-renewable origin and requiring high temperatures, CO_2 and traces of CO are co-obtained. Consequently, in order to obtain H_2 without the need of non-renewable sources as well as avoiding the production of greenhouse gases, the dissociation of water has been seen as a viable alternative.[243]

The sustainable production of hydrogen can be divided into two groups, depending on the source of electrons. It is possible to produce H_2 through electrochemical water splitting (see Figure 76a) using electricity from renewable resources, by collecting energy directly from sunlight via photoelectrocatalytic (PEC) (see Figure 76b) or photocatalytic powder solution (see Figure 76c) water splitting.

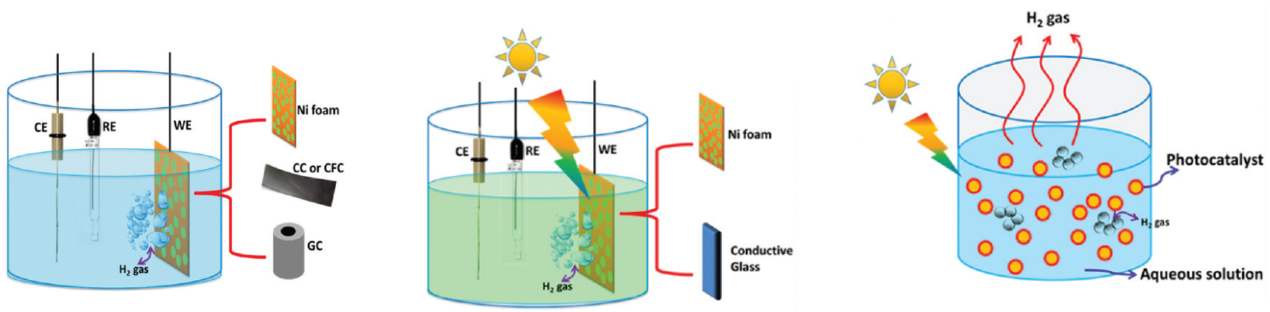

(a) Electrochemical

(b) PEC

(c) Photocatalytic powder solution

Figure 76: Schematic representation of the experimental arrangement of the different forms of sustainable production of H_2 [17]

In the first process mentioned, the source of electrons comes from an applied current. In the other configurations the electrons come from the interaction between the semiconductor and the incident radiation. Although the first process is already available, the other two still present a low efficiency which does not justify its commercialization.[247] Recently, the process of producing H_2 from a dispersed semiconductor in an aqueous solution has attracted a lot of interest, as it allows direct use of sunlight without the need to use solar cells and electrolysis units.[247] According to Maeda et al.[253] it is necessary to produce a photocatalyst with a quantum efficiency [2] of about 30% at 600 nm that justifies a photocatalytic powder solution. When it is possible to build such a system, it will have a solar-to-hydrogen energy conversion efficiency [3] of about 5%, still below what can be achieved by a PEC system. However, it is a good starting point to start practical applications.

Whether the energy source comes from electricity or sunlight, the decomposition of water to form H_2 starts with the adsorption of H^* on the surface of the catalyst, which can be described by Volmer's reaction for an acidic (see Equation 2) or a basic medium (see Equation 3). In the Equations 2 and 3, $*$ represents an empty active site and H^* a hydrogen atom connected to an active site.[247]

[2]Quantum efficiency can be defined by the ratio of the number of reacted electrons to the number of absorbed photons[249]

[3]Solar-to-hydrogen energy conversion efficiency can be defined as the ratio of the total energy produced to the input energy from standard sunlight irradiation[17]

$$H_3O^+\,(aq) + e^- + * \rightleftharpoons H^* + H_2O\,(l) \qquad \text{(Volmer reaction - acidic)} \qquad (2)$$

$$H_2O\,(l) + e^- + * \rightleftharpoons H^* + OH^-\,(aq) \qquad \text{(Volmer reaction - basic)} \qquad (3)$$

Depending on the nature of the catalyst, the reaction may be between two adsorbed hydrogen, i.e. it may be described by the Tafel equation (see Equation 4), or it may be between an adsorbed hydrogen atom and a H^+ from the electrolyte, which can be described by the Heyrovsky equations (see Equations 5 and 6 for acidic and basic medium, respectively).[247]

$$H^* + H^* \rightleftharpoons H_2\,(g) + 2* \qquad \text{(Tafel reaction - acidic and basic)} \qquad (4)$$

$$H^* + H_3O^+\,(aq) + e^- \rightleftharpoons H_2\,(g) + H_2O\,(l) + * \qquad \text{(Heyrovsky reaction - acidic)} \qquad (5)$$

$$H^* + H_2O\,(l) + e^- \rightleftharpoons H_2\,(g) + OH^-\,(aq) + * \qquad \text{(Heyrovsky reaction - basic)} \qquad (6)$$

The decomposition of water is a non-spontaneous reaction, that is, it presents a $\Delta G^0 > 0$ (see Equation 1). A catalyst allows the alteration of the kinetics of a reaction, but not its thermodynamics. Thus, it only promotes spontaneous reactions, i.e., reactions with negative ΔG^0. Photocatalysis, by converting light into chemical energy, makes the process of water decomposition feasible. In this way, it is possible to produce a clean fuel, H_2, from an abundant and cheap source, H_2O.[259] Equations 7 and 8 illustrate the two reactions that occur during the photodegration of water.

$$2H^+ + 2e^- \rightarrow H_2 \quad (7)$$

$$2\,H_2O + 4\,h^+ \rightarrow O_2 + 4\,H^+ \quad (8)$$

Considering the reduction potential of H^+ to H_2 (E^0 = -0,41 V vs. NHE at pH 7,00) and the oxidation potential of H_2O in O_2 (E^0 = 0,82 V vs. NHE at pH 7,00), the photon's minimum theoretical energy is 1,23 V. However, it is observed that there is an activation barrier when transferring the charges from the photocatalyst to the water molecules. Taking into account the overpotential associated with the oxidation and reduction reactions, a band gap between 1,7 eV and 2,2 eV is required to decompose the water.[247,249,253]

When only pure water is used in the reaction system the process is generally inefficient, because in the water oxidation process four holes are needed (see Equation 8).[243] As such, in order to increase the production of H_2, sacrificial molecules are usually used as electron donors, since they allow the scavenged of holes and the electron-hole recombination is reduced. Moreover, no O_2 is produced, since the water oxidation reaction does not occur, so there is no need to purify the final gas. Electron donors have to react faster with the holes than water in order to avoid water oxidation. Usually, CH_3OH or a mixture of NaS/Na_2SO_3 is added to the aqueous system for that purpose. However, it produces waste products, thereby reducing the sustainability of the process.[249,259]

3.3.1.2 Cluster-based chalcogenide materials

Table 16 presents several chalcogenide cluster-based materials that were used as photocatalysts in the generation of H_2. Different authors use this reaction to show that the material they synthesized can be used as a photocatalyst.[63,127,151,166]

3.3.1.2.1 Impact of the sacrificial agent used

Zheng et al.[30,63] used for the first time cluster-based materials as photocatalysts for H_2 production.

Of the different structures previously obtained in Refs.[31] and,[206] the one that stands out most is the ICF-5InCuS-Na structure, since it has a chemical composition similar to $CuInS_2$, a material with important photovoltaic applications.[39] ICF-5CuInS-Na is capable of producing up to 18 µmol h^{-1} g^{-1} of H_2 when irradiated with visible light and while using Na_2S (0,5 M) as a sacrificial agent (see Figure 77a). This catalyst has a quantum efficiency of 3,7% at 420 nm. Although it has a lower quantum efficiency than the Pt/CdS photocatalyst ($\sim$ 28%),[260] the quantum efficiency is much higher when compared with the dense phases of $CuIn_5S_8$ ($\sim$ 0,02% while using AgS_2 as a co-catalysts) or $CuInS_2$ (lower than the one presented by $CuIn_5S_8$).[20] When the sacrificial agent is replaced by Na_2SO_3, the amount of H_2 produced is reduced to about one tenth (see Figure 77b). These results suggest that the SO_3^{2-} ion is a less efficient sacrificial agent than the S^{2-} ion.

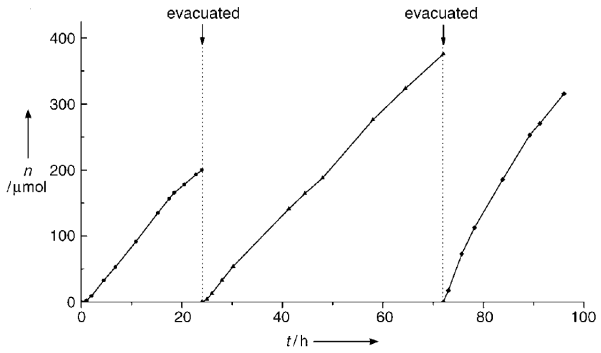

(a) Photocatalytic H_2 evolution from an aqueous solution of Na_2S (0,5 M)

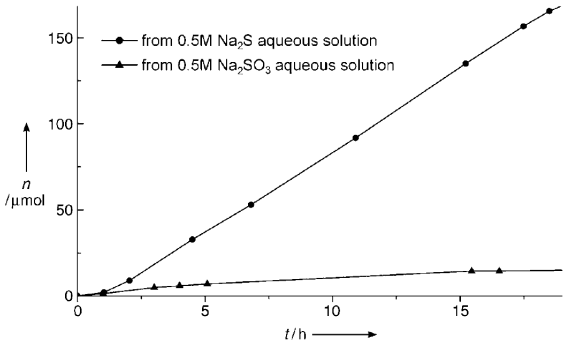

(b) Comparison of photocatalytic H_2 evolution from an aqueous solution of Na_2S (0,5 M) and and aqueous solution of Na_2SO_3 (0,5 M)

Figure 77: Photocatalytic H_2 evolution of ICF-5CuInS-Na (0,5 g) using as sacrificial agents aqueous solutions of Na_2S (O,5 M) or Na_2SO_3 (0,5 M) and using as light source 300 W Xe lamp, λ>420 nm[30]

3.3.1.2.2 Effect of open architecture

It can be observed that, by shifting from a dense structure to an open architecture structure, it is possible to obtain materials with a band structure suitable for water splitting.

For example, it is not possible to observe the generation of H_2 in In_2S_3, a 3-dimensional dense structure, even using UV irradiation.[261] However, UCR-7InS-AEP, a semiconductor material with an open architecture obtained by Zheng et al.[30] shows photocatalytic activity when irradiated with UV radiation (see Figure 78). In addition, when compared to the photocatalytic activity of ZnS, a material usually used as a photocatalyst, UCR-7InS-AEP

presents a higher activity, without the need to use any co-catalyst.

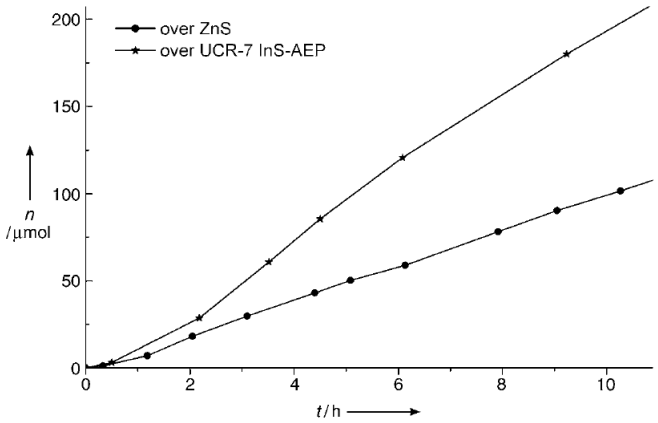

Figure 78: Comparison of photocatalytic H_2 evolution from an aqueous solution of Na_2SO_3 (0,5 M) over UCR-7InS-AEP or ZnS (0,5 g) using 300-W Xe lamp as a light source[30]

The open architecture also allows the incorporation of optically active organic molecules or metal complexes that improve visible-light absorption. The $[Fe(2,2'\text{-bipyridine})_2]^{3+}$ complex was incorporated into UCR-20GaGeS-TAEA by means of an ion exchange. After the ion exchange, the hybrid material obtained has an absorption that extends from the UV to the visible-light region (see Figure 79). When irradiating UCR-20 GaGeS-TAEA with UV light it presents catalytic activity, and no activity occurs when irradiating the structure with visible light. However, the hybrid material already shows photocatalytic activity with visible light for at least 24 hours.

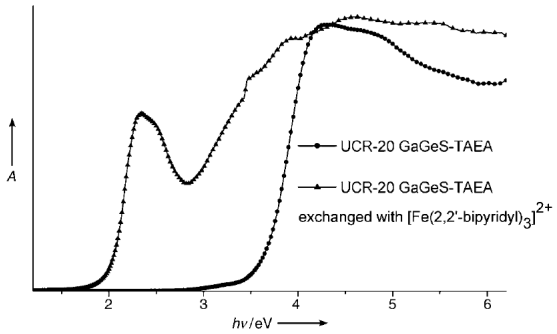

Figure 79: UV/Vis diffuse reflectance spectra of UCR-20 GaGeS-TAEA before and after an ionic exchange with the $[Fe(2,2'\text{-bipyridine})_2]^{3+}$ complex[30]

3.3.1.2.3 Impact of the chemical composition and cluster size

Chen. et al[169] used the materials CPM-120 and CPM-121 as photocatalysts for H_2 generation. The structures CPM-121-ZnCdGeS, CPM-120-ZnGaGeS and CPM-121-ZnGeSnS were evaluated (see Figure 80). CPM-121-ZnCdGeS presents the highest activity, showing that the presence of Cd^{2+} in the T2 cluster presents a positive effect on the photocatalytic performance.

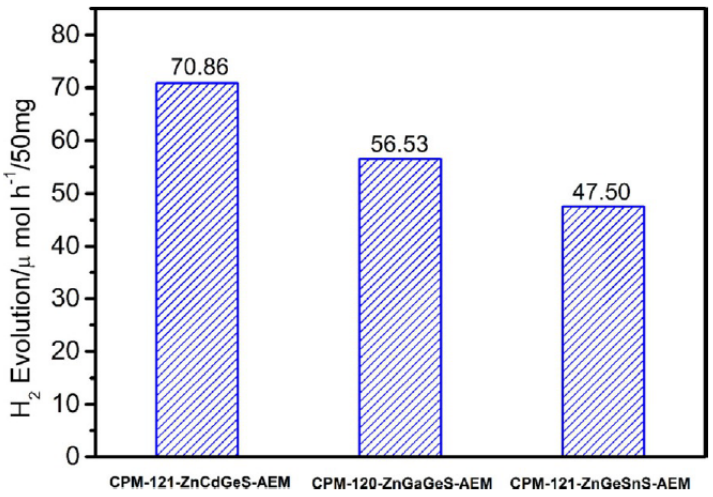

Figure 80: Photocatalytic H_2 evolution of CPM-121-ZnCdGeS, CPM-120-ZnGaGeS and CPM-121-ZnGeSnS (50 mg) in the presence of Na_2S (0,25 M) and Na_2SO_3 (0,10 M) as sacrificial agents and using 300 W Xe lamp as light source[169]

Hao et al.[216] synthesized three distinct 3-dimensional structures, named T4-1 ($[BMMIm]_9[Cd_3In_{17}S_{31}Cl_4]$), T4-2 ($[BMMIm]_9[Cd_3In_{17}S_{13}Se_{18}Cl_4]$) and T4-3 ($[BMMIm]_9[Cd_3In_{17}Se_{31}Cl_4]$ [4,4'-bpy]), and these structures were treated with ultrasounds in DMSO in order to obtain isolated and highly dispersed T4 clusters in solution. Figure 81a shows the results of the photocatalytic tests of the samples, before and after the ultrasonic treatment. Before this process the samples show low photocatalytic, which gradually increases during the 5 hours of the test. After the ultrasonic treatment, it was observed that T4-2 and T4-3 present a photocatalytic activity about five times higher than the solid samples. However, the T4-1 sample does not present such an increase in photocatalytic activity since this sample pre-

sented difficulties of dispersion in most common solvents.

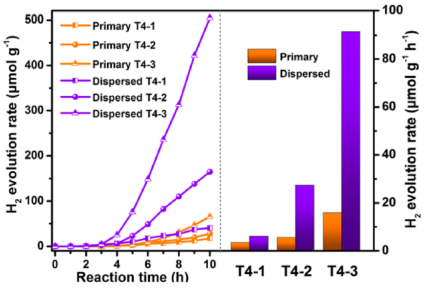

(a)

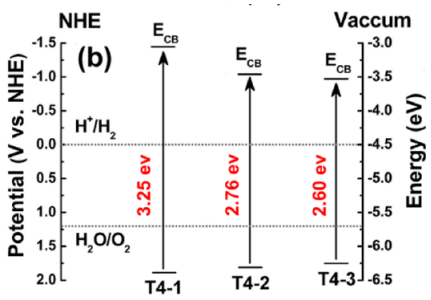

(b)

Figure 81: (81a) Photocatalytic H_2 evolution of T4-1, T4-2 and T4-3 (25 mg) in the presence of TEOA as sacrificial agent, Pt as co-catalyst and using 300 W Xe lamp with a cutoff filter (λ>420 nm) as light source. (81b) Band structures of T4-1, T4-2 and T4-3 obtained by impedance-potential measurements[216]

The differences in photocatalytic activities can be explained due to different factors. Different chemical compositions and cluster sizes lead to changes in the position of the bands (see Figure 81b), directly affecting the photocatalytic generation of H_2. As seen before, selenides usually have a lower band gap than sulfides. Thus, through the insertion of Se in the clusters it is expected that the band gap of the structures decreases, a phenomenom that occurs in the three structures studied. Isolated T4 clusters allow a larger number of surface sites to be exposed and the average mean-path of the electrons is reduced, so the probability of charges recombination is reduced and the electrons reach the surface with more energy.

It is also possible, by analyzing the transient photocurrent response of a structure, to make observations regarding its capacity to create and separate charges. This analysis was

performed on the isolated clusters T4-2 and T4-3 (see Figure 82) and it was observed that, since T4-3 presents an induced photocurrent higher than T4-2, T4-3 presents a higher production capacity and charge separation, thus explaining why it exhibits a higher photocatalytic activity.

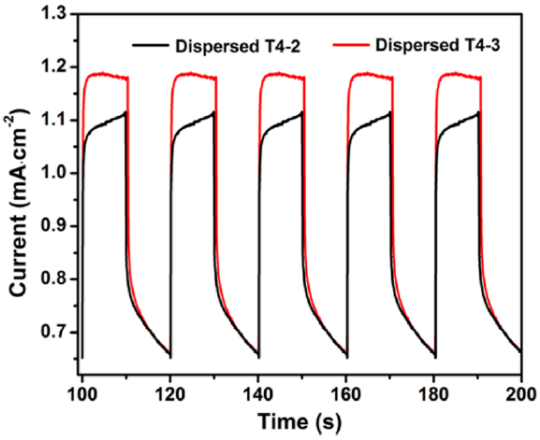

Figure 82: Current vs. time curves of T4−2 and T4−3 isolated clusters[216]

Regarding the stability of photocatalysts, it was observed that there were no changes in the UV−vis spectra after 10 hours of photocatalytic reaction, and the production rate of H_2 remained practically constant after five cycles.

Wang et al.[217] also using ionic liquids, obtained six structures based on T5 clusters: T5-1 ($[BMMIm]_{12}[Cu_5In_{30}Se_{52}Cl_3(Im)]$), T5-2 ($[BMMIm]_{12}[Cu_5In_{30}Se_{48} \cdot 5\,S_3 \cdot 5\,Cl_3(Im)]$), T5-3 ($[BMMIm]_{11}[Cd_6In_{28}Se_{52}Cl_3(MIm)]$), T5-4 ($[BMMIm]_{11}[Cd_6In_{28}Se_{28} \cdot 5\,S_{23} \cdot 5\,Cl_3(MIm)]$), T5-5 ($[BMMIm]_{11}[Cd_6In_{28}Se_{16}S_{36}Cl_3(MIm)]$) and T5-6 ($[BMMIm]_9[Cd_6In_{28}Se_8S_{44}Cl_3(MIm)_3]$).

By analyzing the structure of the bands of the synthesized materials (see Figure 83b), T5-1 and T5-2 cannot be used in the photodegradation of water, since the valence band does not present an adequate potential. It is observed again that the higher the sulfur content in the structure, the higher the band gap. However, the higher the sulfur content, the greater the photocatalytic activity of the structure (see Figure 83a). One of the possible explanations presented by the authors is that the higher the sulfur content, the more negative

the conduction band, so the driving force of the photogenerated electrons to reduce H^+ is higher. Hence, there is a balance between the band gap value and the conduction band position.[262] Again, in order to evaluate the capacity of charge generation and separation, the photocurrent densities were measured (see Figure 83c) and the results are in accordance with the photocatalytic activity shown by the samples.

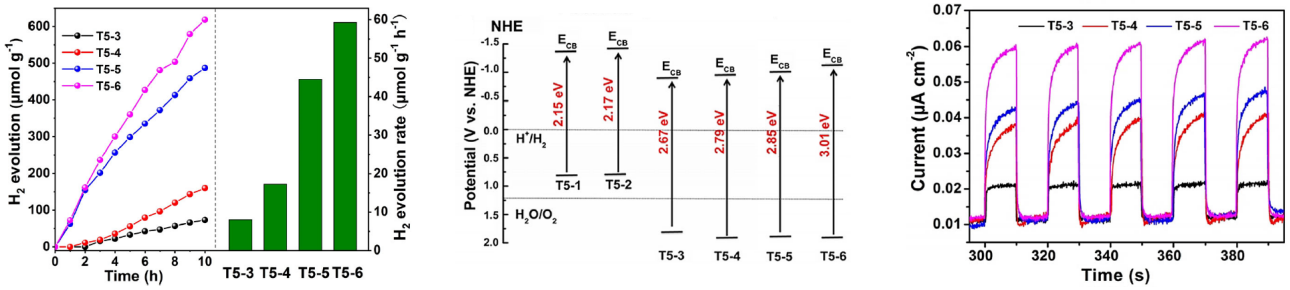

(a) (b) (c)

Figure 83: (83a) Photocatalytic H_2 evolution of T5−3, T5−4, T5−5 and T5−6 (10 mg) in the presence of TEOA as sacrifical agent, Pt as co-catalyst and using 300 W Xe lamp with a cutoff filter (λ>420 nm) as light source. (83b) Band structures of T5−1 to T5−6 obtained by impedance-potential measurements. (83c) Current vs. time curves of T5−3 to T5−6[217]

3.3.1.2.4 Hybrid architectures

Hybrid structures made of metals and semiconductors have been the subject of intense research, since the presence of metal-semiconductor heterojunction improves the charge separation of the material. Liu et al.[200] have developed hybrid materials consisting of silver nanowires (Ag-NWs) whose surface is evenly coated by T4 Mn-Zn-Ga-Sn-S clusters. In this way, a 0D/1D/1D material, referred as T4/Ag_2S/Ag-NW, was obtained consisting of silver nanowires covered with T4 clusters with an ultra thin layer of Ag_2S between them, which serves as an adhesive between the two materials. Besides testing the photocatalytic activity of T4/Ag_2S/Ag-NW, other clusters, such as T2, T3 and T4, and the Ag-NWs and Ag_2S nano particles without any cluster were also tested. Regardless of the type of cluster used, there is always an increase in activity when these are deposited in Ag-NWs (see Figure 84a). The structure with the highest photocatalytic activity is T4/Ag_2S/Ag-NW. Different Zn :

Mn mass ratios were also evaluated in the clusters and how they affects the photocatalytic activity of the final material. A 7:8 ratio leads to maximum photocatalytic activity (see Figure 84b). A material containing T4 Zn-Ga-Sn-S and Mn-Ga-Sn-S clusters was also synthesized in order to find out what the impact of having Zn and Mn in different clusters is. It was observed that the photocatalytic activity of the sample containing the Zn and Mn in separate clusters is much lower than the sample containing the Zn and Mn in the same cluster (see Figure 84b). It was thus concluded that the synergistic effect between the different metals plays a fundamental role in the photocatalytic activity of the material. However, the mechanism of this synergistic effect is not yet known. In order to evaluate the importance that the thickness of the cluster layer has in the photocatalytic activity, materials with different amount of clusters were produced. It was observed that the photocatalytic activity is dependent on the amount of clusters present in the material, presenting a maximum activity for a loading amount equal to 9,13 % wt (see Figure 84c).

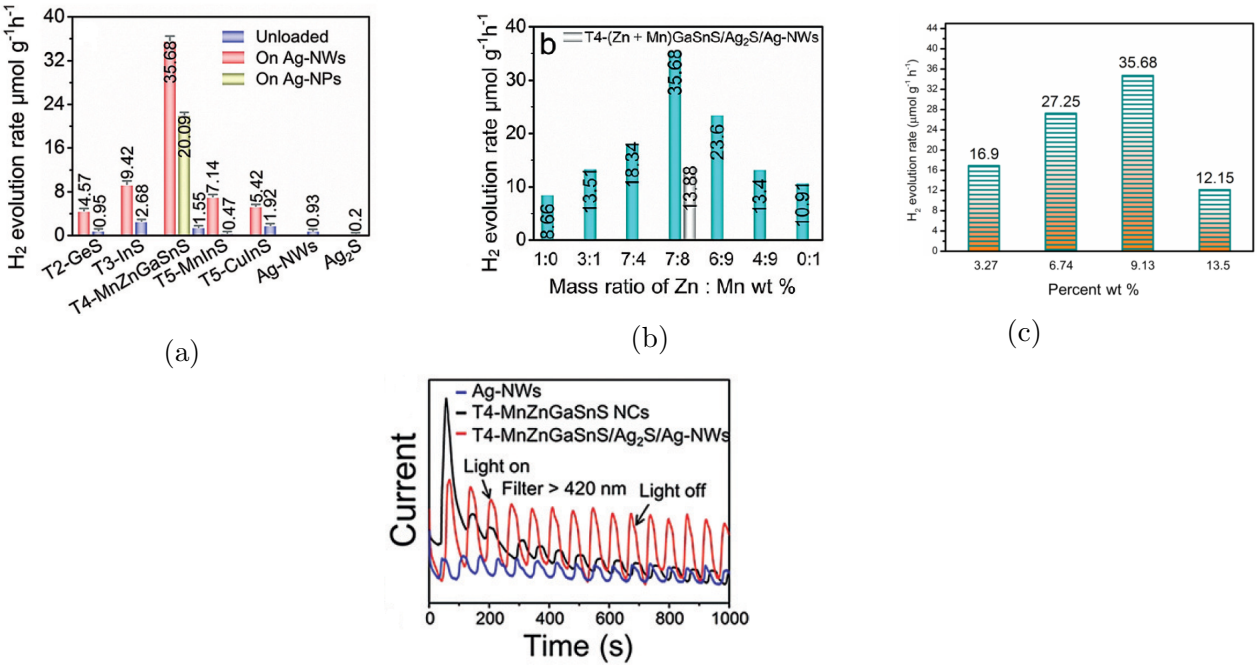

Figure 84: Photocatalytic H_2 evolution of (84a) materials with different clusters and their corresponding heterojuntions (5 mg), (84b) T4/Ag_2S/Ag-NW with different Zn:Mn mass ratios (5 mg) and (84c) T4/Ag_2S/Ag-NW with different loading amounts (5 mg) in the presence of Na_2S (0,1 M) and Na_2SO_3 (0,1M) as sacrifical agent and using 5 W Xe lamp with a cutoff filter (λ>420 nm) as light source. (84d) Current vs. time curves of silver nano wires, discrete T4 clusters and T4/Ag_2S/Ag-NW[200]

The photocurrent response properties of Ag-NWs, discrete T4 clusters and T4/Ag_2S/Ag-NW were measured in order to assess the charge production capacity and charge separation of the materials, as well as their stability. For the discrete T4 clusters, a rapid increase of the photocurrent is observed at first, followed by a rapid decrease (see Figure 84d). This rapid decrease can be explained by the photocorrosion that occurs. T4/Ag_2S/Ag-NW presents an increase in photocurrent regarding Ag-NWs, managing to keep the photocurrent more or less constant (see Figure 84d), thus overcoming the stability problems associated with photocorrosion of the discrete T4 clusters.

Table 16: Summary of cluster-based chalcogenide materials for H_2 photogeneration

Photocatalysts	Cluster	Chemical Composition	Band gap (eV)	Dimension	Light Source	Co-catalyst	Reactant solution	Activity (µmol h^{-1} g^{-1})	Ref.
ICF-5CuInS-Na	T4	In-Cu-S	2	3D	Xe 300W (>420 nm)	-	Na_2S (0,5 M) Na2SO3 (O,5 M)	18 1,8	[30]
UCR-28	T2, T1	Ge-Zn-S	3,4	2D	Xe 300 W	-	Na_2SO_3 (O,5 M)	6,5	[63]
GeCuS-1	Icosahedral	Ge-Cu-S	2,5	3D	Xe 300 W Xe 300 W (λ>400 nm)	- -	Na_2SO_3 (1 M)	20,6 2,64	[151]
OCF-41	TO2	In-S	2,95	3D	Xe 300 W Xe 300 W (λ>400 nm)	- -	Na_2S (0,5 M)	440 0,97	[127]
CPM-120-ZnGeS	T2	Ge-Zn-S	1,87	3D	Xe 300 W	-	Na_2S (0,25 M), Na_2SO_3 (0,1M) CH_3OH	2000 300	[166]
CPM-121-ZnCdGeS	T2	Ge-Cd-Zn-S	1,95	3D	Xe 300 W	-	Na_2S (0,25 M), Na_2SO_3 (0,1M)	1417,2	[169]
CPM-120-ZnGaGeS	T2	Ge-Ga-Zn-S	2,13	3D	Xe 300 W	-	Na_2S (0,25 M) & Na_2SO_3 (0,1M)	1130,6	[169]
CPM-121-ZnGeSnS	T2	Ge-Sn-Zn-S	2,18	3D	Xe 300 W	-	Na_2S (0,25 M) & Na_2SO_3 (0,1M)	950	[169]
-	T2	Ge-S	-	0D	Xe 5 W (λ>420 nm)	Ag	Na_2S (0,1 M), Na_2SO_3 (0,1M)	0,95	[200]
Cluster + Ag NWs	T2	Ge-S	-	0D/1D/1D	Xe 5 W (λ>420 nm)	Ag	Na_2S (0,1 M), Na_2SO_3 (0,1M)	4,57	[200]
-	T3	In-S	-	0D	Xe 5 W (λ>420 nm)	Ag	Na_2S (0,1 M) & Na_2SO_3 (0,1M)	2,68	[200]
Cluster + Ag NWs	T3	In-S	-	0D/1D/1D	Xe 5 W (λ>420 nm)	Ag	Na_2S (0,1 M), Na_2SO_3 (0,1M)	9,42	[200]
-	T4	Sn-Ga-Zn-Mn	-	0D	Xe 5 W (λ>420 nm)	Ag	Na_2S (0,1 M), Na_2SO_3 (0,1M)	1,55	[200]
Cluster + Ag NPs	T4	Sn-Ga-Zn-Mn	-	0D/0D/0D	Xe 5 W (λ>420 nm)	Ag	Na_2S (0,1 M), Na_2SO_3 (0,1M)	20,09	[200]
Cluster + Ag NWs	T4	Sn-Ga-Zn-Mn	-	0D/1D/1D	Xe 5 W (λ>420 nm)	Ag	Na_2S (0,1 M), Na_2SO_3 (0,1M)	35,68	[200]
-	T5	In-Mn-S	-	0D	Xe 5 W (λ>420 nm)	Ag	Na_2S (0,1 M), Na_2SO_3 (0,1M)	0,47	[200]
Cluster + Ag NWs	T5	In-Mn-S	-	0D/1D/1D	Xe 5 W (λ>420 nm)	Ag	Na_2S (0,1 M), Na_2SO_3 (0,1M)	7,14	[200]
-	T5	In-Cu-S	-	0D	Xe 5 W (λ>420 nm)	Ag	Na_2S (0,1 M), Na_2SO_3 (0,1M)	1,92	[200]
Cluster + Ag NWs	T5	In-Cu-S	-	0D/1D/1D	Xe 5 W (λ>420 nm)	Ag	Na_2S (0,1 M), Na_2SO_3 (0,1M)	5,42	[200]
T4-1	T4	In-Cd-S	3,25	3D	Xe 300 W (λ>420 nm)	Pt	Triethanolamine	3,5	[216]
T4-2	T4	In-Cd-S-Se	2,76	3D	Xe 300 W (λ>420 nm)	Pt	Triethanolamine	5,6	[216]
T4-3	T4	In-Cd-Se	2,6	3D	Xe 300 W (λ>420 nm)	Pt	Triethanolamine	15,9	[216]
T4-1	T4	In-Cd-S	Pt	OD	Xe 300 W (λ>420 nm)	Pt	Triethanolamine	6,1	[216]
T4-2	T4	In-Cd-S-Se	Pt	OD	Xe 300 W (λ>420 nm)	Pt	Triethanolamine	27,5	[216]
T4-3	T4	In-Cd-Se	Pt	OD	Xe 300 W (λ>420 nm)	Pt	Triethanolamine	91,5	[216]
T5-3	T5	In-Cd-Se	2,67	0D	Xe 300 W (λ>420 nm)	Pt	Triethanolamine	8,1	[217]
T5-4	T5	In-Cd-S-Se	2,79	0D	Xe 300 W (λ>420 nm)	Pt	Triethanolamine	17,3	[217]
T5-5	T5	In-Cd-S-Se	2,85	0D	Xe 300 W (λ>420 nm)	Pt	Triethanolamine	44,5	[217]

3.3.2 CO_2 Photoreduction

3.3.2.1 Introduction

It is widely known that the CO_2 anthropic emissions need to be suppress in order to limit climate change. In the last 200 years there has been an approximate increase in atmospheric CO_2 from 270 ppm to 412 ppm. This increase is thought to be responsible for the heating of the atmosphere due to the impossibility of re-emitting infrared radiation, thus causing global changes in the climate.[263] Since the main source of CO_2 emissions is fossil fuel consumption (burning 1 t of carbon in fossil fuels releases approximately 3,5 t of CO_2[264]), a reduction in its consumption is necessary, although it is estimated that energy demand will increase. Several strategies to reduce the concentration of CO_2 in the atmosphere have been studied, such as the efficient use of carbon-based energy sources, the use of carbon-free energy sources and the use of CO_2 capture techniques. As fossil fuels are still relatively abundant today and alternatives to them are not yet economically viable, CO_2 capture has been seen as a potential solution to reduce emissions of this gas.[265] The storage of the captured CO_2 is seen only as a temporary solution, since it only displaces the CO_2 from the atmosphere to another location. In addition, there are long-term ecological consequences of using the Earth as CO_2 storage and the technologies available today are expensive and require a high energy input.[245,266,267] Instead of sequestering CO_2, the use of captured CO_2 as a raw material for the production of value-added chemicals has been seen as an attractive alternative.[244] It is now possible to find processes where CO_2 is used as feedstock, for example in the production of urea, salicyclic acid and polycarbonates. However, only about 0,5% of the CO_2 emitted by human sources is used in industry.[263] Therefore, the use of CO_2 as a raw material will only have a significant influence on the reduction of emissions when it is used in the production of fuel, as the consumption of fuel is about two orders of magnitude higher than the consumption of chemical products.[268]

Since CO_2 is a relatively stable and inert compound, most reduction procedures involve

high pressures or temperatures.[252] Photocatalysis has been seen as an alternative to these processes. The conversion of CO_2 into hydrocarbons or alcohols at room temperature and atmospheric pressure using sunlight has been seen as a very feasible option to close the carbon cycle.

Inoue et al.,[269] using several photocatalysts such as WO_3, TiO_2, ZnO, CdS, GaP and SiC, photoreduced CO_2 for the first time in aqueous phase, obtaining formaldehyde, formic acid, methyl alcohol and traces of methane.

Most publications suggest that the first step towards the CO_2 photoreduction is the formation of the species $H^{\bullet}$ (Equation 9) and $CO_2{}^{\bullet-}$ (Equation 10).[270] The most energetic stage, and often the limiting step, is the formation of the species $CO_2{}^{\bullet-}$, which has a reduction potential equal to E^0 = - 1,90 V vs NHE at a pH = 7,00.[271] Since this potential is quite high and never reached by any semiconductor, it is suggested by some researchers that $CO_2{}^{\bullet-}$ is not an intermediate of this reaction, thus passing through a bi-electronic mechanism that does not need such high activation potential.[272,273]

$$H^+ + e^- \rightarrow H^{\bullet} \tag{9}$$

$$CO_2 + e^- \rightarrow CO_2{}^{\bullet-} \tag{10}$$

Although the formation of $CO_2{}^{\bullet-}$ presents a high reduction potential, the transfer of multiple electrons (see Equations 11 to 16)[4] with the assistance of H^+ presents reduction potentials comparable to its own reduction potential (see Equation 17).[270,273,274] Looking at Equations 11 to 16, it is easy to infer that there are kinetic challenges regarding the reduction of CO_2 to obtain more complex products. It is possible to find proof of concept that allows the obtention of carbon monoxide and formate from CO_2. However, more complex products, such as methane and methanol, require multiple transfers of both electrons and protons.

[4]The redox potentials presented in Equations 11 to 17 are vs. NHE at pH 7,00

Currently, it is possible to obtain such products but with a low efficiency.[271,275] Besides obtaining the desired products, it is also possible to observe some inverse reactions. For example, due to the strong oxidative potential of the holes and the presence of O_2, it is possible to oxidize the desired hydrocarbons formed to CO_2 again.[267]

$$CO_2 + 2H^+ + 2e^- \rightarrow CO + H_2O \qquad E^0 = -0,53\ V \tag{11}$$

$$CO_2 + 2H^+ + 2e^- \rightarrow HCOOH \qquad E^0 = -0,61\ V \tag{12}$$

$$CO_2 + 4H^+ + 4e^- \rightarrow HCHO + H_2O \qquad E^0 = -0,48\ V \tag{13}$$

$$CO_2 + 6H^+ + 6e^- \rightarrow CH_3OH + H_2O \qquad E^0 = -0,38\ V \tag{14}$$

$$CO_2 + 8H^+ + 8e^- \rightarrow CH_4 + 2H_2O \qquad E^0 = -0,24\ V \tag{15}$$

$$2CO_2 + 12H^+ + 12e^- \rightarrow CH_3CH_2OH + 3H_2O \qquad E^0 = 0,08\ V \tag{16}$$

$$2H^+ + 2e^- \rightarrow H_2 \qquad E^0 = -0,41\ V \tag{17}$$

When the photoreduction of CO_2 is performed in water, liquid or gas phase, it is in direct competition with H_2 (see Equation 7) and H_2O_2 formation by O_2 reduction (see Equation 18). Although thermodynamically the reduction of CO_2 is favored over H_2 formation, in kinetic terms the formation of H_2 is favored. CO_2 photoreduction is about two to three orders of magnitude slower than H_2 production.[276] Thus, the evolution of H_2 predominates when thermodynamic conditions are met. The competition between these two reactions is

partly responsible for the low efficiency and selectivity of the CO_2 photoreduction process.[254]

$$O_2 + 2H^+ + 2e^- \rightarrow H_2O_2 \quad (18)$$

3.3.2.2 Materials for CO_2 photoreduction

Since the first use of photocatalysis to reduce CO_2, several studies on various photocatalysts, such as TiO_2 with or without doping,[12,277–282] Bi_2WO_6,[283] Zn_2GeO_4[284] or CeO_2[285] have been carried out. However, most of these materials only have a response in the ultraviolet region or present low stability when irradiated. In addition, bulk materials have a high electron-hole recombination.[286] In order to obtain materials that are more efficient in the CO_2 photoreduction process, the use of quantum dots,[71,287] hierarchical nanostructures or laminar materials[37,288] as alternatives to traditional photocatalysts have been investigated.

Quantum dots have been seen recently as promising photocatalysts candidates. Compared to other commonly used photocatalysts, such as organic donor–acceptor molecules or transition metal complexes, quantum dots have greater stability and photoactivity. Due to the quantum confinement effect, it is possible to extend the absorption range to near-infrared, thus improving the radiation absorption properties. The phenomenon of multi-exciton generation was also observed in some quantum dots, namely on PbS, PbSe and PbTe. Normally, a photon generates an electron and a hole. However, it was observed that in some materials, when the energy of the incident photon has at least twice the bandgap energy, multiple charges are generated.[289] This phenomenon can therefore increase the efficiency of photocatalytic systems based on quantum dots. However, most of the quantum dots studied so far have heavy metals in their composition, such as Cd and Pb, not being candidates for practical applications, namely green applications.[287] It is therefore imperative to develop this class of materials without the presence of heavy metals. Previously, several examples of isolated Tn clusters without heavy metals were presented, as well as their use as photocatalysts in H_2

production. These structures can be seen as a special type of quantum dots, as they have a high surface/volume ratio, exact chemical composition, precise structure, uniform size and a light response over a broad spectrum range.[216] Although these structures have already been used for the production of H_2,[216,217] it is not possible to find substantial literature on their use for CO_2 photoreduction.

Another class of materials that presents high potentialities in CO_2 photoreduction is the hierarchical nanostructures one. These structures have a high CO_2 adsorption capability, a high surface area, improved molecular diffusion and enhanced light harvesting due to scattering effect.[288] Such characteristics make it possible to obtain a photocatalyst for the CO_2 photoreduction with superior activities. From this class of materials there are several examples that contain sulfur in their composition such as CdS multicavity hollow particles,[290] CdS nanoparticles dispersed on WO_3 hollow spheres,[291] $CuInS_2$[292] or MoS_2[293] dispersed into TiO_2 nanofibers, In_2S_3-$CdIn_2S_4$[286] or $ZnIn_2S_4$-In_2O_3[294] nanotubes and the combination of mesoporous TiO_2 and layers of MoS_2 into 3D graphene.[295]

Layered materials have also been seen as potential candidates, as they have high surface areas compared to their bulk structures and, therefore, present a high number of active sites on the surface. 2-dimensional composites resulting from the combination of two laminar materials may also present an enhanced photocatalytic activity due to possibility of band gap tunnig and heterojunction formation.[296] The synthesis of thin films allows the reduction of the average mean path of charge carriers, reducing or even eliminating it recombination.[297] It is possible to find examples in the literature of the use of thin films made of $CuInS_2$,[298] $ZnIn_2S_4$[297,299] and $CuIn_5S_8$[300] in CO_2 photoreduction.

3.3.2.2.1 Cluster-based chalcogenide materials

As seen before, cluster-based chalcogenide materials are marked by an enormous diversity of both chemical composition and types of structure. Since it is possible to obtain mate-

rials with characteristics similar to quantum dots, nanostructured and layered materials, structures that have been reviewed recently for presenting promising results in CO_2 photoreduction, it makes sense to investigate them as active photocatalysts. However, it was only possible to find one example of the use of cluster based materials as photocatalyst in CO_2 photoreduction.

Using the CPM-120-ZnGeS structure previously obtained by Lin et al.,[166] Sasan et al.[301] tested it in the CO_2 photoreduction reaction. Through ionic exchange, the SDA was exchanged with Au^{3+} or Pd^{2+} in order to evaluate the impact that the extraframework cations have on the band gap of the materials and its consequence on the photocatalytic performance of the material. The structure with the SDA, designated as AEM@GeZnS, has a bandgap of 2,8 eV. After ion exchange with Au^{3+} (sample entitled Au@GeZnS) or with Pd^{2+} (sample entitled Pd@GeZnS), a reduction of the bandgap to 2,6 eV and 2,5 eV is observed, respectively. In order to evaluate the photogeneration and charge separation properties, PEC measurements were carried out (see Figure 85a). It is noted that the sample with the highest photocurrent density is the Au@GeZnS sample, with a density about five times higher that of AEM@GeZnS and about twice to that of Pd@GeZnS.

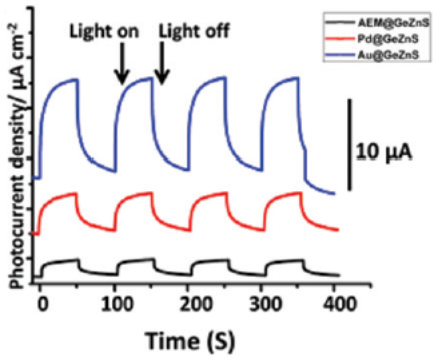

(a)

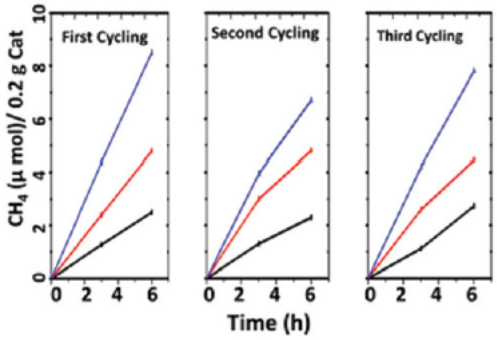

(b)

Figure 85: (85a) Current vs. time curves of AEM@GeZnS, Pd@GeZnS and Au@GeZnS. (85b) Photocatalytic CH_4 evolution of AEM@GeZnS, Pd@GeZnS and Au@GeZnS (0,2 g) in a gas-solid system and using 300 W Xe lamp as light source[301]

In order to assess the photocatalytic performance of the samples AEM@GeZnS, Pd@GeZnS and Au@GeZnS, CO_2 photoreduction to produce CH_4 in the presence of H_2O vapor over a gas-solid system was performed (see Figure 85b). The samples with metal incorporation present a higher photocatalytic activity. Under the same experimental conditions, the Au@GeZnS sample exhibits a superior photocatalytic activity. It was also observed that any of the materials is capable of keeping photocatalytic activity after three cycles without appreciable degradation. According to the authors, the samples with incorporated metals present a superior photocatalytic performance due to two reasons. First, it is observed that the ion exchange with metals leads to a reduction of the bandgap of the materials. Secondly, with the incorporation of metals, an increase in photocurrent density is observed. Such phenomenon is associated with a better charge generation and separation properties, thus

contributing to a better photocatalytic performance.

3.4 Degradation of Organic Dyes

3.4.1 Introduction

Due to the increase of organic pollutants in the air and in waste water streams, it has become imperative to develop green technologies that allow the degradation of these compounds. To this end, advanced oxidation processes have been developed which allow the destruction of a wide variety of organic pollutants due to the presence of highly potent and strongly oxidizing radicals. Of the different processes available, heterogeneous photocatalysis is highlighted, since it allows the effective treatment of liquid and gas streams.[302,303] This process facilitates, at room temperature, the degradation of a wide variety of organic compounds into CO_2 and H_2O without requiring a high energy input.[304]

The photocatalytic process of degradation of organic components starts in the same way as any photocatalytic process: the absorption of radiation with energy suitable for the semiconductor bandgap leads to the excitation of an electron to the conduction band and the formation of a hole in the valence band. When the charge carriers reach the surface, they can participate in redox reactions. In aqueous gassed suspensions, the electrons can reduce the oxygen, originating superoxide ions $O_2^{\bullet -}$ and their protonated form $HO_2^{\bullet}$ (see Equations 19 and 20), and the holes oxidize the molecules of adsorbed water, forming hydroxyl radicals $HO^{\bullet}$ (see Equation 23). $HO_2^{\bullet}$ can be further reduced by obtaining H_2O_2 (see Equations 21 and 22). The reduction of oxygen is an important step, since it consumes the electrons that are formed, avoiding the recombination of charges with consequent increase of hole lifetimes.[303]

$$O_2 + e^- \rightarrow O_2^{\bullet -} \tag{19}$$

$$O_2^{\bullet -} + H^+ \rightarrow HO_2^{\bullet} \quad (20)$$

$$HO_2^{\bullet} + e^- \rightarrow HO_2^- \quad (21)$$

$$HO_2^- + H^+ \rightarrow H_2O_2 \quad (22)$$

$$H_2O + h^+ \rightarrow HO^{\bullet} + H^+ \quad (23)$$

There are still some issues concerning the main oxidative species. Although the generated holes have the potential to oxidize organics directly (see Equation 24), in aqueous solution it is more likely that the hydroxyl radical acts as the main oxidative species (see Equation 25).[302,304]

$$R + h^+ \rightarrow R^{\bullet +} \rightarrow \text{Degradation Products} \quad (24)$$

$$R + HO^{\bullet} + O_2 \rightarrow \text{Degradation Products} \quad (25)$$

3.4.2 Cluster-based chalcogenide materials

Table 17 shows several examples of the use of cluster based materials as photocatalysts in the degradation of organic components. On a laboratory scale, rhodamine B (see Figure 86a), metyl orange (see Figure 86b) and methylene blue (see Figure 86c) are used as organic compounds to be degraded.

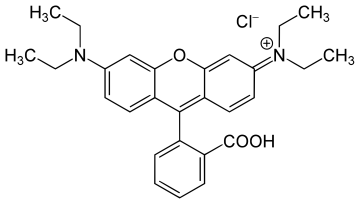

(a) Rhodamine B (RhB)

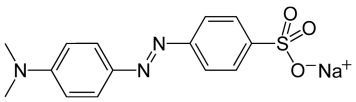

(b) Metyl Orange (MO)

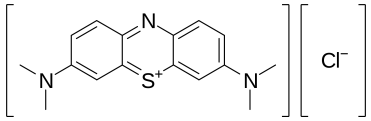

(c) Methylene Blue (MB)

Figure 86: Different organic compounds used as model molecules in the photodegradation of organic compounds

3.4.2.1 Impact of porosity and framework properties

Chen et al.[167] used the CPM-120-ZnGeS-AEM structure previously obtained by Lin et al.[166] as a photocatalyst in the photodegradation of RhB and MB. To evaluate the impact of the porosity on the photocatalytic activity, an ionic exchange with Cs^+ was performed in order to eliminate the SDA. Two structures were tested: 1-AEM, material before ionic exchange and therefore structure with negligible porosity, and 1-Cs, material after ionic exchange with an unobstructed porous system. When 1-AEM is used as photocatalysts, after 6 hours of irradiation with visible light, a degradation of about 80% of RhB was observed (see Figure 87a). When 1-Cs is used as a photocatalysts instead of 1-AEM, after 1,5 hours the organic compound has been fully degraded. RhB photodegradation rates under the two catalysts can be fitted by a pseudo-first order reaction (see Figure 87b). The photodegradation reaction under 1-Cs presents a rate constant equal to 2,39 h^{-1} and under 1-AEM to 0,27 h^{-1}, about nine times less than the rate constant of 1-Cs. The differences in activity between the two photocatalysts can be explained from the different porosity of the samples. 1-AEM has a BET area of 7,28 m^2 g^{-1} and 1-Cs of 467,19 m^2 g^{-1}, about 64 times the BET area of 1-AEM. Other factors such as the stability of the photocatalyst, the type of the counter-ion or band structure cannot explain such a difference in activity. The diffraction pattern of both photocatalysts before and after the reaction remains similar. A control experiment was performed where only Cs^+ was placed in the reaction medium to

find out if this compound was capable of degrading the RhB and, observing Figure 87a, it is concluded that the presence of this compound is not capable of degrading the organic dye. In terms of band structure, both materials have a similar band gap.

The activity of 1-Cs was also compared with the activity of TiO_2 doped with Ti^{3+}, a normal doping technique used to increase the visible light photoactivity of TiO_2. As can be seen in Figure 87c, after 1,5 hours TiO_2 can only degrade about 10% of the RhB present. Thus, it can be concluded that 1-Cs presents a photocatalytic activity much higher than TiO_2 doped with Ti^{3+}.

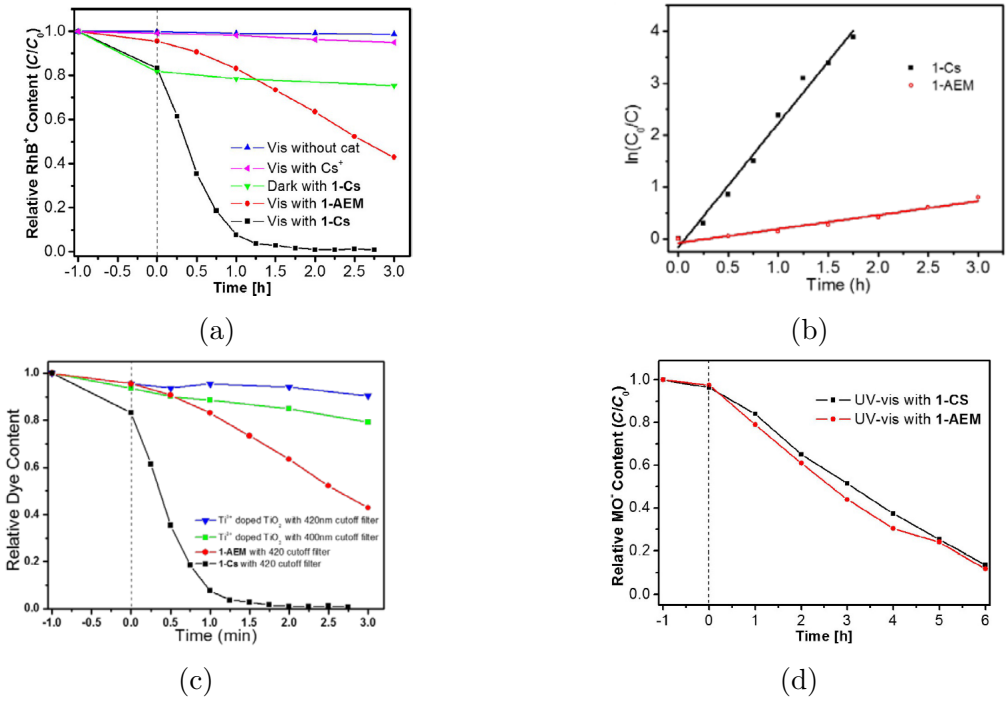

Figure 87: (87a) Photodegradation of RhB over 50 mg of 1-AEM or 1-Cs using a 300 W Xe with a cutoff filter (λ>420 nm) as a light source. (87b) Psuedo-first order plots for the photodegradation of RhB over 1-AEM and 1-Cs. (87c) Photodegradation of RhB over 50 mg of 1-AEM, 1-Cs or TiO_2 doped with Ti^{3+} using a 300 W Xe with a cutoff filter (λ>420 nm) as a light source. (87d) Photodegradation of MO over 50 mg of 1-AEM or 1-Cs using a 300 W Xe as a light source.[167]

Regarding MO degradation (see Figure 87d), after 6 hours of irradiation with UV/Vis light there was a degradation of 88% of such organic compound when 1-AEM is used. When 1-Cs is utilized for the MO photodegradation, its behavior is similar to that shown by 1-AEM.

The difference in the degradation rates of RhB and MO can be explained by the inherent properties of the framework. Both photocatalysts have a negatively charged framework. Thus, the RhB can diffuse freely through the porous system of the photocatalyst, by cation exchange with AEM or Cs and therefore access the active sites of the photocatalysts of the porous system. As the ion exchange in 1-AEM is slower than in 1-Cs, due to the large size of AEM, fewer active sites are available in 1-AEM, which explains the difference in activity between the two photocatalysts. Regarding the degradation of MO, this organic dye has a negative charge, so due to the electrostatic repulsion, its diffusion in the porous system of the photocatalyst used is not possible. Thus, only the active sites at the external surface of the photocatalyst are available.[167]

Xue et al.[163] synthesized two structures, CSZ-9 and CSZ-10, based on the connection between T2 and P1 clusters composed by In and Se. What differentiates the two structures is the way the clusters are connected, thus originating distinct topologies with different pore openings. CSZ-9 presents a minimum pore opening of 9,30 Å and CSZ-10 has two types of pores with different dimensions, 7,82 Å× 8,16 Å and 10,13 Å× 16,77 Å. Because both structures showed absorption in the visible region and a band gap equal to 2,1 eV, they were used in RhB photodegradation. As can be seen in Figure 88 both structures are photoactive, maintaining their crystallinity after the photocatalytic reaction. After 50 minutes, CSZ-9 is capable of degrading about 46,4% of the RhB present and CSZ-10 about 65,8%. The different degradation rates are related to the different window aperture of the two materials, as they have similar chemical composition, same type of clusters and same band gap value. CSZ-9 has a smaller pore opening than CSZ-10, which limits the diffusion of the organic dye, thus justifying the lower degradation rate.

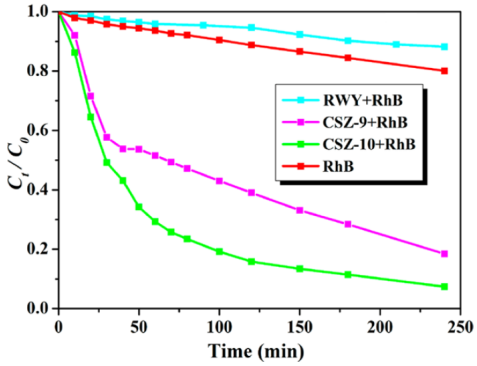

Figure 88: Photodegradation of RhB over 10 mg of photocatalysts using a 300 W Xe as a light source[163]

Wu et al.[168] obtained two layered interrupted materials, SOF-23 and SOF-24, whose building unit is the T3-InSnS cluster. What differs between the two materials is the way the clusters are connected, giving rise to two different topologies. MB photodegradation was used to evaluate the photocatalytic capabilities of the synthesized materials.

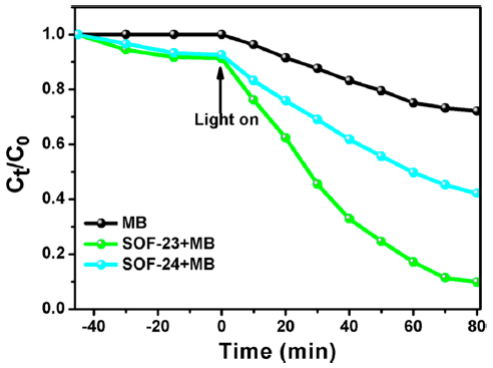

(a)

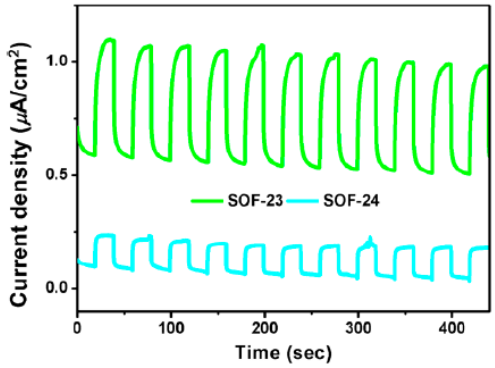

(b)

Figure 89: (89a) Photodegradation of MB over 1 mg of photocatalysts using a 300 W Xe as a light source. (89b) Current vs. time curves of SOF-23 and SOF-24[168]

Looking at Figure 89a, it is easy conclude that both materials can photodegrade MB efficiently. Of the two synthesized materials, SOF-23 degrades a larger amount of MB in the same time interval as SOF-24. Since both materials have the same chemical composition, and they are composed by the same type of clusters and have the same band gap value, a photoelectric response was analyzed to evaluate the separation properties of photogenerated charges. Figure 89b easily shows that SOF-23 has a higher photocurrent density than SOF-24, thus presenting better separation properties of photogenerated charges than SOF-23. The authors conclude that the differences in photocatalytic performance can be explained by the different charge separation properties of the materials, that may be related to the different forms of connection between the clusters.

3.4.2.2 Impact of chemical composition

Shen et al.[215] obtained isolated T3 clusters composed of $[In_{10}Q_{16}Cl_3(BIm)]^{5-}$ (Q = S (IL-InS-1), $S_{7,12}Se_{8,88}$ (IL-InSSe-2), Se (IL-InSe-3), $Se_{13,80}Te_{2,20}$ (IL-InSeTe-4)) that are stabilized by $[BmmIm]^+$ cations. The photodegradation reaction of the MO was used to evaluate the photoactivity of the synthesized samples. The capacity of the samples to photodegrade MO under ultraviolet (see Figure 90a) and visible-light (see Figure 90b) radiation was considered.

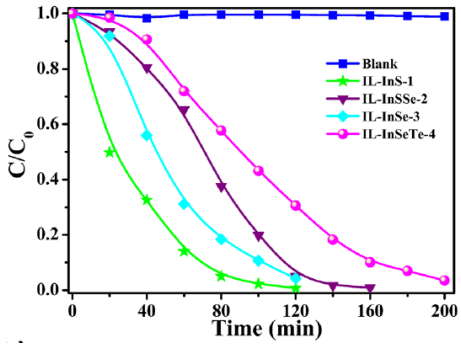

(a)

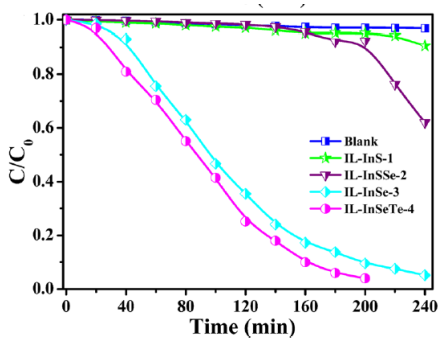

(b)

Figure 90: Photodegradation of MO over 30 mg of photocatalysts using a (90a) 300 W Xe as a UV light source or a (90b) 300 W Xe with a cutoff filter (λ>420 nm) as a visible-light source[215]

Looking at Figure 90a, it can be observed that the sample with the highest degradation rate is IL-InS-1. Changing the incident radiation to visible changes the outcome drastically. Although IL-InSeTe-4 has the worst performance with UV, it is the sample with the best performance with visible radiation (see Figure 90b). Such differences in reaction rates can be explained through the band structure of the materials. It is observed that with the different

contents of chalcogens in the clusters, from S, S/Se, Se to Se/Te, the absorption limits suffer a red shift, thus promoting responses from the ultraviolet region to the visible region.

Huan et al.[147] synthesized a series of materials composed by Sn and Se. From the different materials obtained, the photocatalytic activity of compounds 1, 2, 5 and 6 was evaluated (see Figure 91). Compounds 1 and 2 are isostructural, presenting a laminar structure which has as primary building unit the semicube cluster. What distinguishes these two materials is the complex counter cation present. Compound 1 has as counter-ion the $[Mn(en)_3]^{2+}$ complex and compound 2 $[Fe(en)_3]^{2+}$. Whereas compounds 5 and 6 can be seen as 0-dimensional non-clusters structures composed of $[Sn(Se_4)_3]^{2-}$ and as counter anion the complex $[Mn(en)_3]^{2+}$ or $[Fe(en)_3]^{2+}$, respectively.

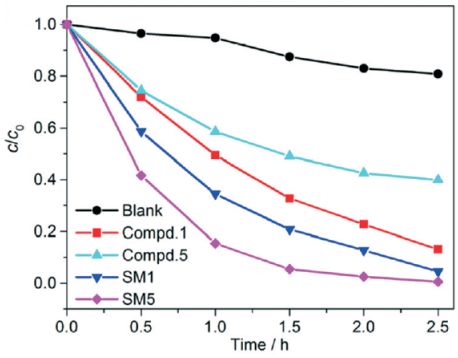

(a)

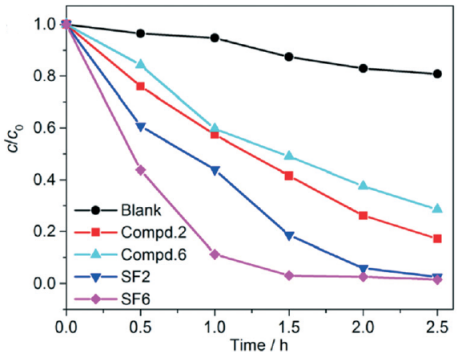

(b)

Figure 91: Photodegradation of MB over 30 mg of photocatalysts ((91a) photocatalysts with Mn and (91b) photocatalysts with Fe) using a 275 W Hg with a cutoff filter (λ>420 nm) as a visible-light source[147]

Comparing the photocatalytic activities of the four compounds, it can be seen that

compounds 1 and 2 can degrade a larger amount of MB in the same time interval than compounds 5 and 6 under visible light radiation (see Figure 91a for 1 vs 5 and Figure 91b for 2 vs 6). This difference in photoactivity can be explained through the different dimensions of the materials. Materials 1 and 2 have a 2-dimensional structure that seems to minimize the electron-hole recombination, with consequent better photocatalytic performance. In addition, the photoactivity of the residues $SnSe_2$/MnSe of 1 and 2, respectably listed SM1 and SM5, $SnSe_2$/FeSe of 2, named SF2, and $SnSe_2/Fe_3Se_4$, named SF6, was studied. As can be seen in Figure 91, the residues present a higher photoactivity than their precursors. The composition at the surface of SM1 and SF2 was evaluated and, besides the Sn, Se, Mn or Fe elements, it was possible to find small amounts of C and N. The presence of carbon is responsible for increasing charge mobility, thus promoting reactions that involve the transfer of electrons. Therefore, according to the authors, the presence of residual amount of carbon at the surface of the photocatalysts is responsible for the increase of photocatalytic activity.

3.4.2.3 Hybrid architectures

Liu et al.[199] doped TiO_2 nanochips with In-Cd-S T5 clusters in order to reduced TiO_2 bandgap value. In order to produce these nanochips, the T5 clusters were first synthesized. Then, the clusters were dissolved with a Ti precursor and, finally, a pyrolysis was performed at different temperatures (400°C, 500°C, 600°C, 700°C, 800°C) to obtain the nanochips. With the increase in pyrolysis temperature an increase in the crystallinity of the sample is observed. When the pyrolysis temperature is equal to 800°C, small holes are formed in the nanochip with the dimensions of the clusters. In addition, XPS signals associated with Cd 3d and In 3d disappear, supporting the idea that when a pyrolysis at 800°C is performed, the clusters are eliminated from the nanochip. With respect to the bandgap values, this value decreases with the increase in pyrolysis temperature until it reaches 800°C. Of the different photocatalysts tested (see Figure 92), the one that presents a greater capacity of

degradation (and greater reaction rate constant K_a) is the sample that suffered a pyrolysis at 700°C. When K_a is normalized with the BET area, the photocatalyst with the highest normalized K_a value is the one that underwent pyrolysis at 500°C. Thus, the photocatalyst degradation efficiency is not only related to the sample porosity, but is strongly related, and perhaps more importantly, to the band structure and radiation absorption capacity of the sample.

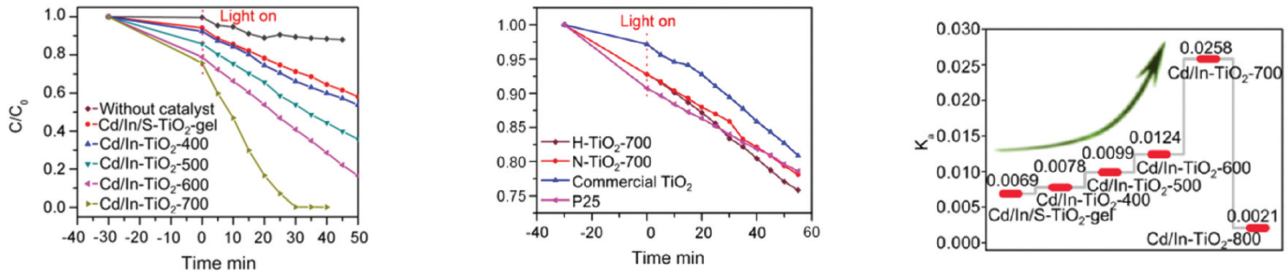

(a) (b) (c)

Figure 92: (92a and 92b) Photodegradation of MB over 5 mg of photocatalysts using a 125 W Xe with a cutoff filter (λ>420 nm) as a visible-light source. (92c) Degradation reaction rate constant K_a [199]

Table 17: Summary of cluster-based chalcogenide materials for organic dyes degradation

Photocatalysts	Cluster	Chemical Composition	Band gap (eV)	Dimension	Light Source	Organic Dye	Decompostion Rate (%)	Ref.
CPM-120-ZnGaGeS-AEM	T2	Ge-Ga-Zn-S	2,13	3D	Xe 300 W (>420 nm) Xe 300 W	RhB MO	80% (6 hours) 88% (6 hours)	[167] (2017)
CPM-120-ZnGaGeS-Cs	T2	Ge-Ga-Zn-S	2,18	3D	Xe 300 W (>420 nm) Xe 300 W	RhB MO	100% (1,5 hours) 88% (6 hours)	[167] (2017)
SOF-2	T3 - T3,2	Sn-In-S	3	3D	Hg 300 W	MB	95% (1 hour)	[98] (2017)
CSZ-9	T2 - P1	In-Se	2,1	3D	Xe 300 W	RhB	46,4 % (50 min)	[163] (2017)
CSZ-10	T2 - P1	In-Se	2,1	3D	Xe 300 W	RhB	65,8% (50 min)	[163] (2017)
Cd/In-TiO2-700	T5	In-Cd-S	2,32	-	Xe 125 W (>420 nm)	MB	99% (30 min)	[199] (2018)
IL-InS-1	T3	In-S	3,31	0D	Xe 300 W Xe 300 W (>420 nm)	MO	95,4% (80 min) 4,36% (180 min)	[215] (2018)
IL-InSSe-2	T3	In-S-Se	3	0D	Xe 300 W Xe 300 W (>420 nm)	MO	95,7% (120 min) 7,72% (180 min)	[215] (2018)
IL-InSe-3	T3	In-Se	2,89	0D	Xe 300 W Xe 300 W (>420 nm)	MO	95,7% (120 min) 86,4% (180 min)	[215] (2018)
IL-InSeTe-4	T3	In-Se-Te	2,65	0D	Xe 300 W Xe 300 W (>420 nm)	MO	69,4% (120 min) 94,1% (180 min)	[215] (2018)
-	Icosahedral	Cu-S	2,45	3D	Xe 300 W (>420 nm)	MB	93% (120 min)	[154] (2018)
-	Semicubic	Sn-Se	2,04	2D	Hg 275 W (>400 nm)	MB	86,5% (150 min)	[147] (2019)
-	Semicubic	Sn-Se	2,1	2D	Hg 275 W (>400 nm)	MB	82,8% (150 min)	[147] (2019)
-	Semicubic	Sn-Se	1,55	1D	Hg 275 W (>400 nm)	MB	60,1% (150 min)	[147] (2019)
-	Semicubic	Sn-Se	1,56	1D	Hg 275 W (>400 nm)	MB	71,5% (150 min)	[147] (2019)
SOF-23	T3	Sn-In-S	3,2	2D	Xe 300 W	MB	60% (80 min)	[168] (2019)
SOF-24	T3	Sn-In-S	3,2	2D	Xe 300 W	MB	90% (80 min)	[168] (2019)

3.5 Final Considerations

Cluster-based chalcogenide materials are suitable to be used as photocatalysts for the production of H_2, from water decomposition and for the degradation of organic compounds. Regarding CO_2 photoreduction, although it is possible to find one example of the use of these materials, further research is still needed.

For H_2 production, it has been observed that these materials have a quantum yield higher than dense phases composed by the same chemical elements. Although structures with an open architecture present a band gap superior to their dense phase, such increase is not necessarily a negative consequence. For example, In_2S_3 does not present photocatalytic activity even when irradiated with UV radiation. On the other hand, even though UCR-7InS-AEP exhibits a band gap superior to In_2S_3, it can produce H_2 even when irradiated with visible radiation. The presence of a porous system also allows the insertion of dyes or metal complexes, thus increasing its light absorption properties.

Looking at Table 16 it can be seen that even though the structures are capable of producing H_2, the production rate is low. This may be due to the fact that in 3-dimensional structures, the porous volume is partially occupied by the SDA, thus reducing the active sites available for participation in the reaction. By evaluating the results obtained from the photodegradation of organic compounds, the importance of porous volume and shape is confirmed. When the SDA is replaced by Cs, thus increasing the BET surface area, there is a nine-fold increase in the reaction constant.

One solution found to circumvent the problem of eliminating the SDA was the use of isolated clusters instead of structures with higher dimensions. These clusters have characteristics similar to quantum dots and might be stabilized by the ionic liquids used during the synthesis process. However, the used technique implied their dispersion in solvents. Thus, although this solution works in gas-liquid approaches, it may not be the best methodology when it comes to synthesizing photocatalysts to be used in gas-solid systems. In systems where the pore obstruction does not arise, materials with superior dimensions can present

higher photocatalytic performances, as observed in the experimental results obtained in.[147]

As can be seen, the value of the band gap as well as the position of the valence and conduction bands have a huge impact on photocatalytic performance. The chemical composition of the material seems to be one of the parameters that most influences the band gap. Copper is one of the metals that seems to lead to a red shift in the band gap. It was also possible to establish a relationship between the chalcogen composition and the band gap value. Higher sulfur contents lead to a larger band gap, with the conduction band becoming more negative. On the contrary, a higher selenium content in the clusters leads to a lower band gap. The content of these two elements allows the customization of the band structure of the final material, taking into account two factors: the position of the bands and the band gap value. A more negative conduction band will produce charge carries with more reductive potential. However, higher band gaps mean that more energetic photons are needed to generate charges and losses in energetic yields. Thus, there is a balance between the two phenomena that must be taken into account when synthesizing a material to be used as a photocatalyst for a specific reaction. Although the connection mode between the clusters does not seem to have much influence on the value of the band gap, it does seem to influence the charge separation properties of the material, as shown in.[168]

Hence, there are two factors that influence the photocatalytic performance of a material: the characteristics associated with the band structure and light absorption capacity together with the porosity of the samples. Although both factors are important, according to the conclusions drawn in,[199] the characteristics associated with the structure of the material bands have a greater impact on the photocatalytic performance of the material.

The synthesis of hybrid materials is a great way to improve photocatalytic performance. The existence of a synergy between the multimetalic clusters dispersed in a metallic substrate was observed. This effect contributes to the increase in photocatalytic activity and has yet to be scientifically explained. It was also noted that the presence of small amounts of carbon or nitrogen at the surface of the materials resulting from the degradation of the SDA is

sufficient to improve the photocatalytic performance.

4 Conclusion and Future Perspectives

Intensive research is being done on the synthesis of new materials that could present superior photocatalytic performance. Recently, quantum dots, nanostructured or laminar materials have been investigated as photocatalysts, as they present optimal properties for applications in this field of science. Nevertheless, the use of new oxide-based materials remains the most common. Materials based on less conventional species, such as sulfur and selenium, are increasingly being seen as possible alternatives to oxides. It is observed that chalcogenide-based materials have electronic properties, namely band structure and band gap value, more suitable to be used in solar-power driven processes than oxide-base materials. There are already several studies regarding the usage of chalcogenide-based materials as photocatalysts for the production of H_2 through water splitting and degradation of organic compounds. Although it is possible to find in the literature examples of the use of sulfur-based materials in CO_2 photoreduction, the use of cluster-based materials in this reaction is still at a very early stage. Since it is possible to find materials consisting of clusters with characteristics similar to quantum dots, nanostructured and laminar materials, it is imperative to study their use as photocatalysts in CO_2 reduction, both in gas-liquid and gas-solid photocatalytic systems.

Nowadays it is possible to obtain materials based on chalcogenide clusters with an enormous diversity, both in terms of chemical composition, that leads to a wide range of band gap values, but also structures with uncommon topologies. However, there are some problems associated with these cluster-based materials. These materials generally have low thermal stability, i.e. they tend to collapse at temperatures above 300°C. The difficult elimination of the SDA used during the synthesis, which occupies an extra framework position, is another problem, since it does not allow to take full advantage of the structure's open architecture.

Large parts of these materials have in their composition toxic or non-abundant metals, which makes their use in a green process ethically questionable. Taking into account the limitations of the use of these materials, it is suggested a set of possible improvements is suggested, that could result in increased photocatalytic performance, since the current performance does not justify their marketing on a large scale.

The presence of SDA in the porous system is one of the main problems, since it obstructs the porous volume, with a consequent decrease in active sites available. The most used technique is an ionic exchange with a cesium salt. However, such a technique does not always guarantee success. The use of non-conventional SDAs, namely compounds that can be used in sulfides or selenides systems and are not suitable for oxides, which are easier to degrade can be seen as a solution. More recently, there has been a special interest in nanocasting. This method, which has already been used to obtain porous materials from CdS, could be an alternative to the more conventional hydrothermal synthesis.

One of the challenges in obtaining a photocatalyst adapted to a given reaction, using a specific radiation, is to have a band structure suitable for the reaction under study and a band gap fitted for incident radiation. Taking into account the enormous diversity of known cluster-based materials, it would be interesting to perform a band structure engineering by manipulating the cluster chemical composition or composite formation, in order to obtain a band gap value more suitable to a specific reaction. The fast electron-hole recombination in another physical phenomenon that contributes to the low performance of the current known photocatalyts. In order to improve the properties of charge separation, the study and development of heterojunctions, such as Z schemes or Schottky juntion, that involve this type of materials is something to consider, since it is a widely used methodology but still in its initial phase regarding cluster-based materials.[305,306]

The radiation absorption properties, in addition to band structure features, is another characteristic to take into account when someone engineers a photocatalyst. The use of organic dyes, which act as antennas, is commonly used to increase the photocatalyts absorption

capability. There is a lack of exploration of the inherent characteristics of laminar materials and how these same characteristics could be used to increase photocatalytic performance, namely the possibility of inserting organic dyes in the interlaminar space.

Having said that, the production of solar fuels is still at a very early stage, and there has to be a coordinated effort from all areas of science so that, one day, this technology can be made a reality.

References

(1) Armaroli, N.; Balzani, V. The future of energy supply: Challenges and opportunities. *Angewandte Chemie (International ed. in English)* **2007**, *46*, 52–66.

(2) Olah, G. A. Beyond oil and gas: the methanol economy. *Angewandte Chemie (International ed. in English)* **2005**, *44*, 2636–2639.

(3) Song, C. Global challenges and strategies for control, conversion and utilization of CO_2 for sustainable development involving energy, catalysis, adsorption and chemical processing. *Catalysis Today* **2006**, *115*, 2 – 32.

(4) Fujishima, A.; Honda, K. Electrochemical Photolysis of Water at a Semiconductor Electrode. *Nature* **1972**, *238*, 37–38.

(5) Acar, C.; Dincer, I.; Naterer, G. F. Review of photocatalytic water-splitting methods for sustainable hydrogen production. *International Journal of Energy Research* **2016**, *40*, 1449–1473.

(6) Tan, J. Z. Y.; Maroto-Valer, M. M. A review of nanostructured non-titania photocatalysts and hole scavenging agents for CO2 photoreduction processes. *J. Mater. Chem. A* **2019**, *7*, 9368–9385.

(7) Guo, S.-H.; Zhou, J.; Zhao, X.; Sun, C.-Y.; You, S.-Q.; Wang, X.-L.; Su, Z.-M. Enhanced CO2 photoreduction via tuning halides in perovskites. *Journal of Catalysis* **2019**, *369*, 201–208.

(8) Jamesh, M.-I.; Kuang, Y.; Sun, X. Constructing Earth-abundant 3D Nanoarrays for Efficient Overall Water Splitting – A Review. *ChemCatChem* **2019**, *11*, 1550–1575.

(9) Mishra, A.; Mehta, A.; Basu, S.; Shetti, N. P.; Reddy, K. R.; Aminabhavi, T. M. Graphitic carbon nitride (g–C3N4)–based metal-free photocatalysts for water splitting: A review. *Carbon* **2019**, *149*, 693–721.

(10) Zhang, Y.; Liu, J.; Li, S.-L.; Su, Z.-M.; Lan, Y.-Q. Polyoxometalate-based materials for sustainable and clean energy conversion and storage. *EnergyChem* **2019**, *1*, 100021.

(11) Reddy, C. V.; Reddy, K. R.; Shetti, N. P.; Shim, J.; Aminabhavi, T. M.; Dionysiou, D. D. Hetero-nanostructured metal oxide-based hybrid photocatalysts for enhanced photoelectrochemical water splitting – A review. *International Journal of Hydrogen Energy* **2020**, *45*, 18331–18347, Waste and Biomass-derived Hydrogen Synthesis and Implementation.

(12) Kreft, S.; Wei, D.; Junge, H.; Beller, M. Recent advances on TiO2-based photocatalytic CO2 reduction. *EnergyChem* **2020**, *2*, 100044.

(13) Wang, J.; Yue, X.; Yang, Y.; Sirisomboonchai, S.; Wang, P.; Ma, X.; Abudula, A.; Guan, G. Earth-abundant transition-metal-based bifunctional catalysts for overall electrochemical water splitting: A review. *Journal of Alloys and Compounds* **2020**, *819*, 153346.

(14) Liu, D.-C.; Zhong, D.-C.; Lu, T.-B. Non-noble metal-based molecular complexes for CO2 reduction: From the ligand design perspective. *EnergyChem* **2020**, *2*, 100034.

(15) Li, X.; Zhu, Q.-L. MOF-based materials for photo- and electrocatalytic CO2 reduction. *EnergyChem* **2020**, *2*, 100033.

(16) Cedeño Morales, E. M.; Kharisov, B. I.; Méndez-Rojas, M. A. CO2 photoreduction by MOF-derived carbon nanomaterials: A review. *Materials Today: Proceedings* **2021**, *46*, 2982–2997, International Conference on Advances in Material Science and Chemistry – 2020 (ICAMSC-2020).

(17) Chandrasekaran, S.; Yao, L.; Deng, L.; Bowen, C.; Zhang, Y.; Chen, S.; Lin, Z.; Peng, F.; Zhang, P. Recent advances in metal sulfides: from controlled fabrication to electrocatalytic, photocatalytic and photoelectrochemical water splitting and beyond. *Chemical Society Reviews* **2019**, *48*, 4178–4280.

(18) Nie, L.; Zhang, Q. Recent progress in crystalline metal chalcogenides as efficient photocatalysts for organic pollutant degradation. *Inorganic Chemistry Frontiers* **2017**, *4*, 1953–1962.

(19) Yong Xu, M. A. A. S. The absolute energy positions of conduction and valence bands of selected semiconducting minerals. *American Mineralogist* **2000**, *85*, 543–556.

(20) Kobayakawa, K.; Teranishi, A.; Tsurumaki, T.; Sato, Y.; Fujishima, A. Photocatalytic Activity of $CuInS_2$ and $CuIn_5S_8$. *Electrochimica Acta* **1992**, *37*, 465–467.

(21) Lei, Z.; You, W.; Liu, M.; Zhou, G.; Takata, T.; Hara, M.; Domen, K.; Li, C. Photocatalytic water reduction under visible light on a novel $ZnIn_2S_4$ catalyst synthesized by hydrothermal method. *Chemical Communications* **2003**, 2142–2143.

(22) Di Chen,; Ye, J. Photocatalytic H_2 evolution under visible light irradiation on $AgIn_5S_8$ photocatalyst. *Journal of Physics and Chemistry of Solids* **2007**, *68*, 2317–2320.

(23) Chen, Z.; Li, D.; Zhang, W.; Chen, C.; Li, W.; Sun, M.; He, Y.; Fu, X. Low-

temperature and template-free synthesis of $ZnIn_2S_4$ microspheres. *Inorganic Chemistry* **2008**, *47*, 9766–9772.

(24) Li, W.; Li, D.; Chen, Z.; Huang, H.; Sun, M.; He, Y.; Fu, X. High-efficient Degradation of Dyes by $Zn_xCd_{1-x}S$ Solid Solutions under Visible Light Irradiation. *The Journal of Physical Chemistry C* **2008**, *112*, 14943–14947.

(25) Li, Y.; He, X.; Cao, M. Micro-emulsion-assisted synthesis of ZnS nanospheres and their photocatalytic activity. *Materials Research Bulletin* **2008**, *43*, 3100–3110.

(26) Sun, M.; Li, D.; Li, W.; Chen, Y.; Chen, Z.; He, Y.; Fu, X. New Photocatalyst, Sb_2S_3, for Degradation of Methyl Orange under Visible-Light Irradiation. *The Journal of Physical Chemistry C* **2008**, *112*, 18076–18081.

(27) He, Y.; Li, D.; Xiao, G.; Chen, W.; Chen, Y.; Sun, M.; Huang, H.; Fu, X. A New Application of Nanocrystal In_2S_3 in Efficient Degradation of Organic Pollutants under Visible Light Irradiation. *The Journal of Physical Chemistry C* **2009**, *113*, 5254–5262.

(28) Zhang, W.; Li, D.; Sun, M.; Shao, Y.; Chen, Z.; Xiao, G.; Fu, X. Microwave hydrothermal synthesis and photocatalytic activity of $AgIn_5S_8$ for the degradation of dye. *Journal of Solid State Chemistry* **2010**, *183*, 2466–2474.

(29) Davis, M. E. Ordered porous materials for emerging applications. *Nature* **2002**, *417*, 813–821.

(30) Zheng, N.; Bu, X.; Wang, B.; Feng, P. Open-Framework Chalcogenides as Visible-Light Photocatalysts for Hydrogen Generation from Water. *Angewandte Chemie (International ed. in English)* **2005**, *44*, 5299–5303.

(31) Zheng, N.; Bu, X.; Wang, B.; Feng, P. Microporous and Photoluminescent Chalcogenide Zeolite Analogs. *Science* **2002**, *298*, 2366–2369.

(32) Shuey, R. T. *Semiconducting ore minerals*, 1st ed.; Elsevier scientific Publishing Company, 1975.

(33) Vaughan, D. J.; Craig, J. R. *Mineral chemistry of metal sulfides*; Cambridge University, 1978.

(34) Santner, S.; Heine, J.; Dehnen, S. Synthesis of Crystalline Chalcogenides in Ionic Liquids. *Angewandte Chemie (International ed. in English)* **2016**, *55*, 876–893.

(35) Lai, C.-H.; Lu, M.-Y.; Chen, L.-J. Metal sulfide nanostructures: synthesis, properties and applications in energy conversion and storage. *Journal of Materials Chemistry* **2012**, *22*, 19–30.

(36) Zhao, Y.; Burda, C. Development of plasmonic semiconductor nanomaterials with copper chalcogenides for a future with sustainable energy materials. *Energy & Environmental Science* **2012**, *5*, 5564–5576.

(37) Wang, J.; Lin, S.; Tian, N.; Ma, T.; Zhang, Y.; Huang, H. Nanostructured Metal Sulfides: Classification, Modification Strategy, and Solar-Driven CO_2 Reduction Application. *Advanced Functional Materials* **2020**, 2008008.

(38) Yu, X.-Y.; Le Yu,; Lou, X. W. D. Metal Sulfide Hollow Nanostructures for Electrochemical Energy Storage. *Advanced Energy Materials* **2016**, *6*, 1501333.

(39) Coughlan, C.; Ibáñez, M.; Dobrozhan, O.; Singh, A.; Cabot, A.; Ryan, K. M. Compound Copper Chalcogenide Nanocrystals. *Chemical Reviews* **2017**, *117*, 5865–6109.

(40) Geng, P.; Zheng, S.; Tang, H.; Zhu, R.; Zhang, L.; Cao, S.; Xue, H.; Pang, H. Transition Metal Sulfides Based on Graphene for Electrochemical Energy Storage. *Advanced Energy Materials* **2018**, *8*, 1703259.

(41) Vaqueiro, P. Hybrid materials through linkage of chalcogenide tetrahedral clusters. *Dalton Transactions* **2010**, *39*, 5965–5972.

(42) Brant, J.; Brunetta, C.; Aitken, J. In *Comprehensive Inorganic Chemistry II*, second edition ed.; Reedijk, J., Poeppelmeier, K., Eds.; Elsevier: Amsterdam, 2013; pp 213 – 283.

(43) Jensen, W. B. A Note on the Term "Chalcogen". *Journal of Chemical Education* **1997**, *74*, 1063.

(44) Bouroushian, M. *Electrochemistry of Metal Chalcogenides*; Springer: Berlin, Heidelberg, 2010; pp 1–56.

(45) Zakai, U. I. Design, Synthesis, and Evaluation of Chalcogen Interactions. Ph.D. thesis, The University of Arizona, 2007.

(46) Feng, P.; Bu, X.; Zheng, N. The Interface Chemistry between Chalcogenide Clusters and Open Framework Chalcogenides. *Accounts of Chemical Research* **2005**, *38*, 293–303.

(47) Cahill, C. L.; Parise, J. B. On the formation of framework indium sulfides. *Journal of the Chemical Society, Dalton Transactions* **2000**, 1475–1482.

(48) Dance, I.; Fisher, K. In *Progress in Inorganic Chemistry*; Karlin, K. D., Ed.; John Wiley, 1994; Vol. 41; p 637–803.

(49) Bedard, R. L.; Vail, L. D.; Wilson, S. T.; Flanigen, E. M. Crystalline microporous metal sulfide compositions. December 6, 1988, US 4,880,761.

(50) Bedard, R.; Wilson, S.; Vail, L.; Bennett, J.; Flanigen, E. In *Zeolites: Facts, Figures, Future Part A - Proceedings of the 8th International Zeolite Conference*; Jacobs, P., van Santen, R., Eds.; Studies in Surface Science and Catalysis; Elsevier, 1989; Vol. 49; pp 375 – 387.

(51) Scott, R. W.; MacLachlan, M. J.; Ozin, G. A. Synthesis of metal sulfide materials with

controlled architecture. *Current Opinion in Solid State and Materials Science* **1999**, *4*, 113 – 121.

(52) Férey, G. Supertetrahedra in sulfides: matter against mathematical series? *Angewandte Chemie (International ed. in English)* **2003**, *42*, 2576–2579.

(53) O'Keeffe, M.; Eddaoudi, M.; Li, H.; Reineke, T.; Yaghi, O. Frameworks for Extended Solids: Geometrical Design Principles. *Journal of Solid State Chemistry* **2000**, *152*, 3 – 20.

(54) Gong, Y.-N.; Zhong, D.-C.; Lu, T.-B. Interpenetrating metal–organic frameworks. *CrystEngComm* **2016**, *18*, 2596–2606.

(55) Li, H.; Laine, A.; O'Keeffe, M.; Yaghi, O. M. Supertetrahedral Sulfide Crystals with Giant Cavities and Channels. *Science* **1999**, *283*, 1145–1147.

(56) Slupecki, O.; Brown, I. D. Bond-valence–bond-length parameters for bonds between cations and sulfur. *Acta Crystallographica Section B* **1982**, *38*, 1078–1079.

(57) Li, H.; Kim, J.; Groy, T. L.; O'Keeffe, M.; Yaghi, O. M. 20 Å $Cd_4In_{16}S_{3514}$- Supertetrahedral T4 Clusters as Building Units in Decorated Cristobalite Frameworks. *Journal of the American Chemical Society* **2001**, *123*, 4867–4868.

(58) Yaghi, O. M.; Sun, Z.; Richardson, D. A.; Groy, T. L. Directed Transformation of Molecules to Solids: Synthesis of a Microporous Sulfide from Molecular Germanium Sulfide Cages. *Journal of the American Chemical Society* **1994**, *116*, 807–808.

(59) Tan, K.; Darovsky, A.; Parise, J. B. Synthesis of a novel open-framework sulfide, $CuGe_2S_5(C_2H_5)_4N$, and its structure solution using synchrotron imaging plate data. *Journal of the American Chemical Society* **1995**, *117*, 7039–7040.

(60) Tan, K.; Ko, Y.; Parise, J. B.; Darovsky, A. Hydrothermal Growth of Single Crystals

of TMA-CuGS-2, $[C_4H_{12}N]_6[(Cu_{044}Ge_{056}S_{223})_4(Ge_4S_8)_3]$ and Their Characterization Using Synchrotron/Imaging Plate Data. *Chemistry of Materials* **1996**, *8*, 448–453.

(61) Bowes, C. L.; Huynh, W. U.; Kirkby, S. J.; Malek, A.; Ozin, G. A.; Petrov, S.; Twardowski, M.; Young, D.; Bedard, R. L.; Broach, R. Dimetal Linked Open Frameworks: $[(CH_3)_4N]_2(Ag_{2C}u_2)Ge_4S_{10}$. *Chemistry of Materials* **1996**, *8*, 2147–2152.

(62) Cahill, C. L.; Ko, Y.; Hanson, J. C.; Tan, K.; Parise, J. B. Structure of Microporous QUI-MnGS-1 and in Situ Studies of Its Formation Using Time-Resolved Synchrotron X-ray Powder Diffraction. *Chemistry of Materials* **1998**, *10*, 1453–1458.

(63) Zheng, N.; Bu, X.; Feng, P. Two-dimensional organization of $[ZnGe_3S_9(H_2O)]_4$ supertetrahedral clusters templated by a metal complex. *Chemical Communications* **2005**, 2805–2807.

(64) Bu, X.; Zheng, N.; Feng, P. Tetrahedral Chalcogenide Clusters and Open Frameworks. *Chemistry – A European Journal* **2004**, *10*, 3356–3362.

(65) Cahill, C. L.; Ko, Y.; Parise, J. B. A Novel 3-Dimensional Open Framework Sulfide Based upon the $[In_{10}S_{20}]^{10-}$ Supertetrahedron: DMA-InS-SB1. *Chemistry of Materials* **1998**, *10*, 19–21.

(66) Li, H.; Eddaoudi, M.; Laine, A.; O'Keeffe, M.; Yaghi, O. M. Noninterpenetrating Indium Sulfide Supertetrahedral Cristobalite Framework. *Journal of the American Chemical Society* **1999**, *121*, 6096–6097.

(67) Wu, J.; Jin, B.; Wang, X.; Ding, Y.; Wang, X.-L.; Tang, D.; Li, X.; Shu, J.; Li, D.-S.; Lin, Q.; Wu, Y.-B.; Wu, T. Breakdown of Valence Shell Electron Pair Repulsion Theory in an H-Bond-Stabilized Linear sp-Hybridized Sulfur. *CCS Chemistry 0*.

(68) Zheng, N.; Bu, X.; Feng, P. Nonaqueous Synthesis and Selective Crystallization of Gal-

lium Sulfide Clusters into Three-Dimensional Photoluminescent Superlattices. *Journal of the American Chemical Society* **2003**, *125*, 1138–1139.

(69) Wang, W.; Yang, H.; Luo, M.; Zhong, Y.; Xu, D.; Wu, T.; Lin, Z. A 36-Membered Ring Metal Chalcogenide with a Very Low Framework Density. *Inorganic Chemistry* **2017**, *56*, 14730–14733.

(70) Wu, Z.; Luo, M.; Xue, C.; Zhang, J.; Lv, J.; Wang, X.; Wu, T. New 2D Assemblage of Supertetrahedral Chalcogenide Clusters with Tetravalent-Metal-Induced Interrupted Sites. *Crystal Growth & Design* **2019**, *19*, 4151–4156.

(71) Wang, W.; Wang, X.; Hu, D.; Yang, H.; Xue, C.; Lin, Z.; Wu, T. An Unusual Metal Chalcogenide Zeolitic Framework Built from the Extended Spiro-5 Units with Supertetrahedral Clusters as Nodes. *Inorganic Chemistry* **2018**, *57*, 921–925.

(72) Ahari, H.; Garcia, A.; Kirkby, S.; A. Ozin, G.; Young, D.; J. Lough, A. Self-assembling iron and manganese metal–germanium–selenide frameworks: $[NMe_4]_2MGe_4Se_{10}$, where M = Fe or Mn. *Journal of the Chemical Society, Dalton Transactions* **1998**, 2023–2028.

(73) Wang, C.; Bu, X.; Zheng, N.; Feng, P. Indium selenide superlattices from $(In_{10}Se_{18})^6$ supertetrahedral clusters. *Chemical Communications* **2002**, 1344–1345.

(74) Xue, C.; Lin, J.; Yang, H.; Wang, W.; Wang, X.; Hu, D.; Wu, T. Supertetrahedral Cluster-Based In–Se Open Frameworks with Unique Polyselenide Ion as Linker. *Crystal Growth & Design* **2018**, *18*, 2690–2693.

(75) Bu, X.; Zheng, N.; Wang, X.; Wang, B.; Feng, P. Three-dimensional frameworks of gallium selenide supertetrahedral clusters. *Angewandte Chemie (International ed. in English)* **2004**, *43*, 1502–1505.

(76) Vaqueiro, P.; Romero, M. L. Three-dimensional gallium sulphide open frameworks. *Journal of Physics and Chemistry of Solids* **2007**, *68*, 1239 – 1243, 7th International Conference of Solids State Chemistry 2006 (SSC 2006).

(77) Ding, Y.; Zhang, J.; Liu, C.; Wang, X.-L.; Wu, Z.; Wang, X.; Zhou, R.; Li, D.-S.; Wu, T. Antimony-Assisted Assembly of Basic Supertetrahedral Clusters into Heterometallic Chalcogenide Supraclusters. *Inorganic Chemistry* **2020**, *59*, 13000–13004, PMID: 32886495.

(78) Wang, C.; Bu, X.; Zheng, N.; Feng, P. A 3D Open-Framework Indium Telluride and Its Selenide and Sulfide Analogues. *Angewandte Chemie (International ed. in English)* **2002**, *41*, 1959–1961.

(79) Tsamourtzi, K.; Song, J.-H.; Bakas, T.; Freeman, A. J.; Trikalitis, P. N.; Kanatzidis, M. G. Straightforward Route to the Adamantane Clusters $[Sn_4Q_{10}]^4$ (Q = S, Se, Te) and Use in the Assembly of Open-Framework Chalcogenides $(Me_4N)_2M[Sn_4Se_{10}]$ (M = MnII, FeII, CoII, ZnII) Including the First Telluride Member $(Me_4N)_2Mn[Ge_4Te_{10}]$. *Inorganic Chemistry* **2008**, *47*, 11920–11929.

(80) Zhang, Q.; Chung, I.; Jang, J. I.; Ketterson, J. B.; Kanatzidis, M. G. A Polar and Chiral Indium Telluride Featuring Supertetrahedral T2 Clusters and Nonlinear Optical Second Harmonic Generation. *Chemistry of Materials* **2009**, *21*, 12–14.

(81) Bu, X.; Zheng, N.; Li, Y.; Feng, P. Templated Assembly of Sulfide Nanoclusters into Cubic-C_3N_4 Type Framework. *Journal of the American Chemical Society* **2003**, *125*, 6024–6025.

(82) Xue, C.; Zhang, L.; Wang, X.; Wang, X.; Zhang, J.; Wu, T. Highly open chalcogenide frameworks built from unusual defective supertetrahedral clusters. *Dalton Transactions* **2019**, *48*, 10799–10803.

(83) Wu, T.; Wang, L.; Bu, X.; Chau, V.; Feng, P. Largest Molecular Clusters in the Supertetrahedral Tn Series. *Journal of the American Chemical Society* **2010**, *132*, 10823–10831.

(84) Wang, C.; Li, Y.; Bu, X.; Zheng, N.; Zivkovic, O.; Yang, C.-S.; Feng, P. Three-Dimensional Superlattices Built from $(M_4In_{16}S_{33})^{10-}$ (M = Mn, Co, Zn, Cd) Supertetrahedral Clusters. *Journal of the American Chemical Society* **2001**, *123*, 11506–11507.

(85) Wang, Y.-H.; Zhang, M.-H.; Yan, Y.-M.; Bian, G.-Q.; Zhu, Q.-Y.; Dai, J. Transition Metal Complexes as Linkages for Assembly of Supertetrahedral T4 Clusters. *Inorganic Chemistry* **2010**, *49*, 9731–9733.

(86) Wu, T.; Bu, X.; Zhao, X.; Khazhakyan, R.; Feng, P. Phase Selection and Site-Selective Distribution by Tin and Sulfur in Supertetrahedral Zinc Gallium Selenides. *Journal of the American Chemical Society* **2011**, *133*, 9616–9625.

(87) Pauling, L. The principles determining the structure of complex ionic crystals. *Journal of the American Chemical Society* **1929**, *51*, 1010–1026.

(88) Pearson, R. G. Hard and Soft Acids and Bases. *Journal of the American Chemical Society* **1963**, *85*, 3533–3539.

(89) Wu, T.; Wang, X.; Bu, X.; Zhao, X.; Le Wang,; Feng, P. Synthetic control of selenide supertetrahedral clusters and three-dimensional co-assembly by charge-complementary metal cations. *Angewandte Chemie (International ed. in English)* **2009**, *48*, 7204–7207.

(90) Zhang, J.; Wang, X.; Lv, J.; Li, D.-S.; Wu, T. A multivalent mixed-metal strategy for single-Cu+-ion-bridged cluster-based chalcogenide open frameworks for sensitive nonenzymatic detection of glucose. *Chem. Commun.* **2019**, *55*, 6357–6360.

(91) Wang, C.; Bu, X.; Zheng, N.; Feng, P. Nanocluster with One Missing Core Atom: A Three-Dimensional Hybrid Superlattice Built from Dual-Sized Supertetrahedral Clusters. *Journal of the American Chemical Society* **2002**, *124*, 10268–10269.

(92) Su, W.; Huang, X.; Li, J.; Fu, H. Crystal of Semiconducting Quantum Dots Built on Covalently Bonded T5 $[In_{28}Cd_6S_{54}]^{12-}$: The Largest Supertetrahedral Cluster in Solid State. *Journal of the American Chemical Society* **2002**, *124*, 12944–12945.

(93) Bu, X.; Zheng, N.; Li, Y.; Feng, P. Pushing Up the Size Limit of Chalcogenide Supertetrahedral Clusters: Two- and Three-Dimensional Photoluminescent Open Frameworks from $(Cu_5In_{30}S_{54})^{13-}$ Clusters. *Journal of the American Chemical Society* **2002**, *124*, 12646–12647.

(94) Wu, T.; Zhang, Q.; Hou, Y.; Wang, L.; Mao, C.; Zheng, S.-T.; Bu, X.; Feng, P. Monocopper Doping in Cd-In-S Supertetrahedral Nanocluster via Two-Step Strategy and Enhanced Photoelectric Response. *Journal of the American Chemical Society* **2013**, *135*, 10250–10253.

(95) Lin, J.; Zhang, Q.; Wang, L.; Liu, X.; Yan, W.; Wu, T.; Bu, X.; Feng, P. Atomically Precise Doping of Monomanganese Ion into Coreless Supertetrahedral Chalcogenide Nanocluster Inducing Unusual Red Shift in Mn^{2+} Emission. *Journal of the American Chemical Society* **2014**, *136*, 4769–4779.

(96) Xu, X.; Wang, W.; Liu, D.; Hu, D.; Wu, T.; Bu, X.; Feng, P. Pushing up the Size Limit of Metal Chalcogenide Supertetrahedral Nanocluster. *Journal of the American Chemical Society* **2018**, *140*, 888–891.

(97) Wang, L.; Wu, T.; Zuo, F.; Zhao, X.; Bu, X.; Wu, J.; Feng, P. Assembly of Supertetrahedral T5 CopperIndium Sulfide Clusters into a Super-Supertetrahedron of Infinite Order. *Journal of the American Chemical Society* **2010**, *132*, 3283–3285.

(98) Wang, W.; Yang, H.; Xue, C.; Luo, M.; Lin, J.; Hu, D.; Wang, X.; Lin, Z.; Wu, T. The First Observation on Dual Self-Closed and Extended Assembly Modes in Supertetrahedral T3 Cluster Based Open-Framework Chalcogenide. *Crystal Growth & Design* **2017**, *17*, 2936–2940.

(99) Li, H.; Kim, J.; O'Keeffe, M.; Yaghi, O. M. $Cd_{16}In_{64}S_{134}^{44-}$: 31-A tetrahedron with a large cavity. *Angewandte Chemie (International ed. in English)* **2003**, *42*, 1819–1821.

(100) Wang, H.; Yang, H.; Wang, W.; Xue, C.; Zhang, Y.; Luo, M.; Hu, D.; Lin, J.; Li, D.; Wu, T. Assembly of supertetrahedral clusters into a Cu–In–S superlattice via an unprecedented vertex–edge connection mode. *CrystEngComm* **2017**, *19*, 4709–4712.

(101) Zhang, L.; Xue, C.; Wang, W.; Hu, D.; Lv, J.; Li, D.; Wu, T. Stable Supersupertetrahedron with Infinite Order via the Assembly of Supertetrahedral T4 Zinc–Indium Sulfide Clusters. *Inorganic Chemistry* **2018**, *57*, 10485–10488.

(102) Zheng, N.; Bu, X.; Feng, P. Pentasupertetrahedral clusters as building blocks for a three-dimensional sulfide superlattice. *Angewandte Chemie (International ed. in English)* **2004**, *43*, 4753–4755.

(103) Dehnen, S.; Brandmayer, M. K. Reactivity of Chalcogenostannate Compounds: Syntheses, Crystal Structures, and Electronic Properties of Novel Compounds Containing Discrete Ternary Anions $[M_4(\mu_4\text{-Se})(SnSe_4)_4]^{10-}$ (M = Zn, Mn). *Journal of the American Chemical Society* **2003**, *125*, 6618–6619.

(104) Lv, J.; Zhang, J.; Xue, C.; Hu, D.; Wang, X.; Li, D.-S.; Wu, T. Two Penta-Supertetrahedral Cluster-Based Chalcogenide Open Frameworks: Effect of the Cluster Spatial Connectivity on the Electron-Transport Efficiency. *Inorganic Chemistry* **2019**, *58*, 3582–3585.

(105) Zimmermann, C.; Melullis, M.; Dehnen, S. Reactivity of Chalcogenostannate Salts: Unusual Synthesis and Structure of a Compound Containing Ternary Cluster Anions

$[Co_4(\mu_4\text{-Se})(SnSe_4)_4]^{10-}$. *Angewandte Chemie (International ed. in English)* **2002**, *41*, 4269–4272.

(106) Ding, N.; Chung, D.-Y.; Kanatzidis, M. G. $K_6Cd_4Sn_3Se_{13}$: A polar open-framework compound based on the partially destroyed supertetrahedral $[Cd_4Sn_4Se_{17}]^{10}$ cluster. *Chemical Communications* **2004**, 1170–1171.

(107) Palchik, O.; Iyer, R. G.; Liao, J. H.; Kanatzidis, M. G. $K_{10}M_4Sn_4S_{17}$ (M = Mn, Fe, Co, Zn): Soluble Quaternary Sulfides with the Discrete $[M_4Sn_4S_{17}]^{10-}$ Supertetrahedral Clusters. *Inorganic Chemistry* **2003**, *42*, 5052–5054.

(108) Manos, M. J.; Iyer, R. G.; Quarez, E.; Liao, J. H.; Kanatzidis, M. G. $SnZn_4Sn_4S_{17}{}^{6-}$: a robust open framework based on metal-linked penta-supertetrahedral $Zn_4Sn_4S_{17}{}^{10-}$ clusters with ion-exchange properties. *Angewandte Chemie (International ed. in English)* **2005**, *44*, 3552–3555.

(109) Manos, M. J.; Chrissafis, K.; Kanatzidis, M. G. Unique Pore Selectivity for Cs^+ and Exceptionally High NH^{4+} Exchange Capacity of the Chalcogenide Material $K_6Sn[Zn_4Sn_4S_{17}]$. *Journal of the American Chemical Society* **2006**, *128*, 8875–8883.

(110) Vossmeyer, T.; Reck, G.; Katsikas, L.; Haupt, E. T. K.; Schulz, B.; Weller, H. A "Double-Diamond Superlattice" Built Up of $Cd_{17}S_4(SCH_2CH_2OH)_{26}$ Clusters. *Science* **1995**, *267*, 1476–1479.

(111) Eichhöfer, A.; Wood, P. T.; Viswanath, R. N.; Mole, R. A. Synthesis, structure and physical properties of the manganese(ii) selenide/selenolate cluster complexes $[Mn_{32}Se_{14}(SePh)_{36}(PnPr_3)_4]$ and $[Na(benzene-15-crown-5)\,(C_4H_8O)_2]_2[Mn_8Se(SePh)_{16}]$. *Chemical Communications* **2008**, 1596–1598.

(112) Lee, G. S. H.; Craig, D. C.; Ma, I.; Scudder, M. L.; Bailey, T. D.; Dance, I. G.

$[S_4Cd_{17}(SPh)_{28}]^{2-}$, the first member of a third series of tetrahedral [SWMX(SR)y]z-clusters. *Journal of the American Chemical Society* **1988**, *110*, 4863–4864.

(113) Jin, X.; Tang, K.; Jia, S.; Tang, Y. Synthesis and crystal structure of a polymeric complex $[S_4Cd_{17}(SPh)_{24}(CH_3OCS_2)_{4/2}]n[S_4Cd_{17}(SPh)_{24}(CH_3OCS_2)_{4/2}]n$. *Polyhedron* **1996**, *15*, 2617 – 2622.

(114) Herron, N.; Calabrese, J. C.; Farneth, W. E.; Wang, Y. Crystal Structure and Optical Properties of $Cd_{32}S_{14}(SC_6H_5)_{36} \cdot DMF_4$, a Cluster with a 15 Angstrom CdS Core. *Science* **1993**, *259*, 1426–1428.

(115) Vossmeyer, T.; Reck, G.; Schulz, B.; Katsikas, L.; Weller, H. Double-Layer Superlattice Structure Built Up of $Cd_{32}S_{14}(SCH_2CH(OH)CH_3)_{36}4\,H_2O$ Clusters. *Journal of the American Chemical Society* **1995**, *117*, 12881–12882.

(116) Behrens, S.; Bettenhausen, M.; Deveson, A. C.; Eichhöfer, A.; Fenske, D.; Lohde, A.; Woggon, U. Synthesis and Structure of the Nanoclusters $[Hg_{32}Se_{14}(SePh)_{36}]$, $[Cd_{32}Se_{14}(SePh)_{36}[Cd_{32}Se_{14}(SePh)_{36},[P(Et)_2(Ph)C_4H_8OSiMe_3]_5[P(Et)_2(Ph)C_4H_8OSiMe_3]_5$, and $[N(Et)_3C_4H_8OSiMe_3]_5[Cd_{18}I_{17}(PSiMe_3)_{12}]$. *Angewandte Chemie International Edition in English* **1996**, *35*, 2215–2218.

(117) Zheng, N.; Bu, X.; Lu, H.; Zhang, Q.; Feng, P. Crystalline Superlattices from Single-Sized Quantum Dots. *Journal of the American Chemical Society* **2005**, *127*, 11963–11965.

(118) Huang, S.-L.; He, L.; Chen, E.-X.; Lai, H.-D.; Zhang, J.; Lin, Q. A wide pH-range stable crystalline framework based on the largest tin-oxysulfide cluster $[Sn_{20}O_{10}S_{34}]$. *Chemical Communications* **2019**, *55*, 11083–11086.

(119) Lin, Q.; Bu, X.; Feng, P. An infinite square lattice of super-supertetrahedral T6-like tin oxyselenide clusters. *Chemical Communications* **2014**, *50*, 4044–4046.

(120) Schiwy, W.; Krebs, B. $Sn_{10}O_4S_{20}^{8-}$: A New Type of Polyanion. *Angewandte Chemie (International ed. in English)* **1975**, *14*, 436.

(121) Kaib, T.; Kapitein, M.; Dehnen, S. Synthesis and Crystal Structure of $[Li_8(H_2O)_{29}]\cdot[Sn_{10}O_4S_{20}]\cdot 2\,H_2O$. *Zeitschrift für anorganische und allgemeine Chemie* **2011**, *637*, 1683–1686.

(122) Parise, J. B.; Ko, Y. Material Consisting of Two Interwoven 4-Connected Networks: Hydrothermal Synthesis and Structure of $[Sn_5S_9O_2][HN(CH_3)_3]_2$. *Chemistry of Materials* **1994**, *6*, 718–720.

(123) Parise, J. B.; Ko, Y.; Tan, K.; Nellis, D. M.; Koch, S. Structural evolution from Tin Sulfide (selenide) layered structures to nove 3- and 4- connected Tin Oxy sulfides. *Journal of Solid State Chemistry* **1995**, *117*, 219–228.

(124) Zhang, X.-M.; Sarma, D.; Wu, Y.-Q.; Wang, L.; Ning, Z.-X.; Zhang, F.-Q.; Kanatzidis, M. G. Open-Framework Oxysulfide Based on the Supertetrahedral $[In_4Sn_{16}O_{10}S_{34}]^{12-}$ Cluster and Efficient Sequestration of Heavy Metals. *Journal of the American Chemical Society* **2016**, *138*, 5543–5546.

(125) Zhang, Y.; Wang, X.; Hu, D.; Xue, C.; Wang, W.; Yang, H.; Li, D.; Wu, T. Monodisperse Ultrasmall Manganese-Doped Multimetallic Oxysulfide Nanoparticles as Highly Efficient Oxygen Reduction Electrocatalyst. *ACS Applied Materials & Interfaces* **2018**, *10*, 13413–13424.

(126) Ahari, H.; Lough, A.; Petrov, S.; A. Ozin, G.; L. Bedard, R. Modular assembly and phase study of two- and three-dimensional porous tin(IV) selenides. *Journal of Materials Chemistry* **1999**, *9*, 1263–1274.

(127) Wu, T.; Zuo, F.; Wang, L.; Bu, X.; Zheng, S.-T.; Ma, R.; Feng, P. A Large Indium Sulfide Supertetrahedral Cluster Built from Integration of ZnS-like Tetrahedral Shell

with NaCl-like Octahedral Core. *Journal of the American Chemical Society* **2011**, *133*, 15886–15889.

(128) Wang, W.; Wang, X.; Zhang, J.; Yang, H.; Luo, M.; Xue, C.; Lin, Z.; Wu, T. Three-Dimensional Superlattices Based on Unusual Chalcogenide Supertetrahedral In–Sn–S Nanoclusters. *Inorganic Chemistry* **2019**, *58*, 31–34.

(129) Han, X.; Wang, Z.; Liu, D.; Xu, J.; Liu, Y.; Wang, C. Co-assembly of a three-dimensional open framework sulfide with a novel linkage between an oxygen-encapsulated T3 cluster and a supertetrahedral T2 cluster. *Chemical Communications* **2014**, *50*, 796–798.

(130) Wang, L.; Wu, T.; Bu, X.; Zhao, X.; Zuo, F.; Feng, P. Coassembly between the Largest and Smallest Metal Chalcogenide Supertetrahedral Clusters. *Inorganic Chemistry* **2013**, *52*, 2259–2261.

(131) Zhang, J.; Liu, X.; Ding, Y.; Xue, C.; Wu, T. Three new metal chalcogenide open frameworks built through co-assembly and/or hybrid assembly from supertetrahedral T5-InOS and T3-InS nanoclusters. *Dalton Transactions* **2019**, *48*, 7537–7540.

(132) Wang, H.; Wang, W.; Hu, D.; Luo, M.; Xue, C.; Li, D.; Wu, T. Hybrid Assembly of Different-Sized Supertetrahedral Clusters into a Unique Non-Interpenetrated Mn–In–S Open Framework with Large Cavity. *Inorganic Chemistry* **2018**, *57*, 6710–6715.

(133) Zhang, Q.; Bu, X.; Han, L.; Feng, P. Two-Dimensional Indium Sulfide Framework Constructed from Pentasupertetrahedral P1 and Supertetrahedral T2 Clusters. *Inorganic Chemistry* **2006**, *45*, 6684–6687.

(134) Parise, J. B.; Ko, Y. Novel antimony sulfides: synthesis and x-ray structural characterization of $Sb_3S_5 \cdot N(C_3H_7)_4$ and $Sb_4S_7 \cdot N_2C_4H_8$. *Chemistry of Materials* **1992**, *4*, 1446–1450.

(135) Jiang, T.; Ozin, G. A.; Bedard, R. L. Nanoporous tin(IV) sulfides: Mode of formation. *Advanced Materials* **1994**, *6*, 860–865.

(136) Parise, J. B. Novel sulphide frameworks: synthesis and X-ray structural characterization of $Cs_6Sb_{10}S_{18}{\cdot}1.2H_2O$. *Journal of the Chemical Society, Chemical Communications* **1990**, 1553–1554.

(137) Parise, J. B. An Antimony Sulfide with a Two-Dimensional, Intersecting System of Channels. *Science* **1991**, *251*, 293–294.

(138) Jiang, T.; Ozin, G. A.; Bedard, R. L. Nanoporous tin(IV) sulfides: Thermochemical properties. *Advanced Materials* **1995**, *7*, 166–170.

(139) Jiang, T.; Lough, A. J.; Ozin, G. A.; Young, D.; Bedard, R. L. Synthesis and Structure of the Novel Nanoporous Tin(IV) Sulfide Material TPA-SnS-3. *Chemistry of Materials* **1995**, *7*, 245–248.

(140) Jiang, T.; Lough, A.; A. Ozin, G.; L. Bedard, R.; Broach, R. Synthesis and structure of microporous layered tin(IV) sulfide materials. *Journal of Materials Chemistry* **1998**, *8*, 721–732.

(141) Jiang, T.; Ozin, G. A. New directions in tin sulfide materials chemistry. *Journal of Materials Chemistry* **1998**, *8*, 1099–1108.

(142) Parise, J. B.; Ko, Y.; Rijssenbeek, J.; Nellis, D. M.; Tan, K.; Koch, S. Novel layered sulfides of tin: synthesis, structural characterization and ion exchange properties of TMA-SnS-1, $Sn_3S_7{\cdot}(NMe_4)_2{\cdot}H_2O$. *Journal of the Chemical Society, Chemical Communications* **1994**, 527–527.

(143) L. Bowes, C.; Petrov, S.; Vovk, G.; Young, D.; A. Ozin, G.; L. Bedard, R. Microporous layered tin sulfide, SnS-1: molecular sieve or intercalant? *Journal of Materials Chemistry* **1998**, *8*, 711–720.

(144) Pienack, N.; Schinkel, D.; Puls, A.; Ordolff, M.-E.; Lühmann, H.; Näther, C.; Bensch, W. New Thiostannates Synthesized Under Solvothermal Conditions: Crystal Structures of $(trenH)_2Sn_3S_7$ and $[Mn(tren)]2Sn2S6$. *Zeitschrift für Naturforschung B* **2012**, *67*, 1098–1106.

(145) Filsø, M. Ø.; Chaaban, I.; Al Shehabi, A.; Skibsted, J.; Lock, N. The structure-directing amine changes everything: structures and optical properties of two-dimensional thiostannates. *Acta Crystallographica Section B* **2017**, *73*, 931–940.

(146) Qi, X.-H.; Du, K.-Z.; Feng, M.-L.; Li, J.-R.; Du, C.-F.; Zhang, B.; Huang, X.-Y. A two-dimensionally microporous thiostannate with superior Cs^+ and Sr^{2+} ion-exchange property. *Journal of Materials Chemistry A* **2015**, *3*, 5665–5673.

(147) Han, J.; Zhang, L.; Li, S.; Zheng, W.; Jia, D.; Yuan, Y. Alcohol-solvothermal syntheses, crystal structures and photocatalytic properties of tin selenides with polyselenide ligands. *CrystEngComm* **2019**, *21*, 1642–1652.

(148) Zhang, R.-C.; Zhang, C.; Zhang, D.-J.; Wang, J.-J.; Zhang, Z.-F.; Ji, M.; An, Y.-L. Copper-Rich Framework Selenoarsenates Based on Icosahedral Cu_8Se_{13} Clusters. *Zeitschrift für anorganische und allgemeine Chemie* **2012**, *638*, 2503–2507.

(149) Luo, M.; Hu, D.; Yang, H.; Li, D.; Wu, T. PCU-type copper-rich open-framework chalcogenides: pushing up the length limit of the connection mode and the first mixed-metal $[Cu_7GeSe_{13}]$ cluster. *Inorganic Chemistry Frontiers* **2017**, *4*, 387–392.

(150) Schimek, G. L.; Kolis, J. W.; Long, G. J. Metal Hexaammine as a Bulky Cation: Structural and Property Studies of $[M(NH_3)_6]Cu_8Sb_3S_{13}$ (M = Mn, Fe, Ni) and $[Fe(NH_3)_6]AgES_4$ (E = As, Sb). *Chemistry of Materials* **1997**, *9*, 2776–2785.

(151) Zhang, Z.; Zhang, J.; Wu, T.; Bu, X.; Feng, P. Three-Dimensional Open Framework Built from CuS Icosahedral Clusters and Its Photocatalytic Property. *Journal of the American Chemical Society* **2008**, *130*, 15238–15239.

(152) Zhang, R.-C.; Yao, H.-G.; Ji, S.-H.; Liu, M.-C.; Ji, M.; An, Y.-L. Copper-Rich Framework Sulfides: $A_4Cu_8Ge_3S_{12}$ (A = K, Rb) with Cubic Perovskite Structure. *Inorganic Chemistry* **2010**, *49*, 6372–6374.

(153) Zhang, R.-C.; Zhang, C.; Ji, S.-H.; Ji, M.; An, Y.-L. Synthesis and characterization of $(H_2dab)_2Cu_8Ge_4S_{14}{\cdot}2\,H_2O$: An expanded framework based on icosahedral Cu_8S_{12} cluster. *Journal of Solid State Chemistry* **2012**, *186*, 94 – 98.

(154) Tang, S.; Zhou, J.; Liu, X.; Xiao, H.-P. A new 3-D cuprous thiogermanate with rare 3-D $[Cu\text{-}S\text{-}Cu]_n$ network. *Materials Today Communications* **2018**, *15*, 88 – 93.

(155) Zhang, R.-C.; Yao, H.-G.; Ji, S.-H.; Liu, M.-C.; Ji, M.; An, Y.-L. $(H_2en)_2Cu_8Sn_3S_{12}$: a trigonal CuS_3-based open-framework sulfide with interesting ion-exchange properties. *Chemical Communications* **2010**, *46*, 4550–4552.

(156) Behrens, M.; Ordolff, M.-E.; Näther, C.; Bensch, W.; Becker, K.-D.; Guillot-Deudon, C.; Lafond, A.; Cody, J. A. New Three-Dimensional Thiostannates Composed of Linked Cu_8S_{12} Clusters and the First Example of a Mixed-Metal Cu_7SnS_{12} Cluster. *Inorganic Chemistry* **2010**, *49*, 8305–8309.

(157) Yang, H.; Wang, L.; Hu, D.; Lin, J.; Luo, L.; Wang, H.; Wu, T. A novel copper-rich open-framework chalcogenide constructed from octahedral Cu4Se6 and icosahedral Cu_8Se_{13} nanoclusters. *Chemical Communications* **2016**, *52*, 4140–4143.

(158) Kaye, S. S.; Dailly, A.; Yaghi, O. M.; Long, J. R. Impact of Preparation and Handling on the Hydrogen Storage Properties of $Zn_4O(1,4-\text{benzenedicarboxylate})_3$ (MOF-5). *Journal of the American Chemical Society* **2007**, *129*, 14176–14177.

(159) Wang, Y.-L.; Zhang, B.; Li, W.-A.; Feng, M.-L.; Huang, X.-Y. Two new 3D heterometallic chalcogenides based on copper-rich selenogermanate clusters. *Inorganic Chemistry Communications* **2017**, *85*, 41 – 44, Special issue for the 7th National Conference on Structural Chemistry of Chinese Chemical Society (2016, Guangzhou).

(160) IZA, Database of Zeolite Structures - Zeolite Framework Types. `http://europe.iza-structure.org/IZA-SC/ftc_table.php`, 2017 (acessed June 1, 2020).

(161) Cheetham, A. K.; Férey, G.; Loiseau, T. Open-Framework Inorganic Materials. *Angewandte Chemie (International ed. in En-glish)* **1999**, *38*, 3268–3292.

(162) Lin, J.; Dong, Y.; Zhang, Q.; Hu, D.; Li, N.; Le Wang,; Liu, Y.; Wu, T. Interrupted chalcogenide-based zeolite-analogue semiconductor: atomically precise doping for tunable electro-/photoelectrochemical properties. *Angewandte Chemie (International ed. in English)* **2015**, *54*, 5103–5107.

(163) Xue, C.; Hu, D.; Zhang, Y.; Yang, H.; Wang, X.; Wang, W.; Wu, T. Two Unique Crystalline Semiconductor Zeolite Analogues Based on Indium Selenide Clusters. *Inorganic Chemistry* **2017**, *56*, 14763–14766.

(164) Cahill, C. L.; Parise, J. B. Synthesis and Structure of $MnGe_4S_{10}\cdot(C_6H_{14}N_2)\cdot 3\,H_2O$: A Novel Sulfide Framework Analogous to Zeolite Li-A(BW). *Chemistry of Materials* **1997**, *9*, 807–811.

(165) Loewenstein, W. The distribution of aluminum in the tetrahedra of silicates and aluminates. *American Mineralogist* **1954**, *39*, 92–96.

(166) Lin, Q.; Bu, X.; Mao, C.; Zhao, X.; Sasan, K.; Feng, P. Mimicking High-Silica Zeolites: Highly Stable Germanium- and Tin-Rich Zeolite-Type Chalcogenides. *Journal of the American Chemical Society* **2015**, *137*, 6184–6187.

(167) Chen, X.; Bu, X.; Lin, Q.; Mao, C.; Zhai, Q.; Wang, Y.; Feng, P. Selective Ion Exchange and Photocatalysis by Zeolite-Like Semiconducting Chalcogenide. *Chemistry – A European Journal* **2017**, *23*, 11913–11919.

(168) Wu, Z.; Wang, X.-L.; Hu, D.; Wu, S.; Liu, C.; Wang, X.; Zhou, R.; Li, D.-S.; Wu, T.

A new cluster-based chalcogenide zeolite analogue with a large inter-cluster bridging angle. *Inorganic Chemistry Frontiers* **2019**, *6*, 3063–3069.

(169) Chen, X.; Bu, X.; Wang, Y.; Lin, Q.; Feng, P. Charge- and Size-Complementary Multimetal-Induced Morphology and Phase Control in Zeolite-Type Metal Chalcogenides. *Chemistry – A European Journal* **2018**, *24*, 10812–10819.

(170) Dance, I. G. Formation, crystal structure, and reactions of catena-(μ-SPh)[(μ-SPh)$_6$Zn$_4$(CH$_3$OH)(SPh)], a model for zinc thiolate metalloenzymes. *Journal of the American Chemical Society* **1980**, *102*, 3445–3451.

(171) Casagrande, G. A.; Lang, E. S.; de Oliveira, G. M.; Hörner, M.; Broch, F. Dealing with 1,3-bis(4-nitrophenyl)triazene as intermediary ligand in the synthesis of polymeric (-Se)Hg-clusters: One-pot synthetic procedures and X-ray structural characterization of [(PhSe)$_7$Hg$_4$BrPy]$_n$. *Inorganica Chimica Acta* **2007**, *360*, 1776 – 1779.

(172) Dance, I. G.; Garbutt, R. G.; Craig, D. C.; Scudder, M. L.; Bailey, T. D. New non-molecular poly-adamantanoid crystal structures of Cd(SAr)2. Zeolitic Cd$_4$(SC$_6$H$_4$Me−4)8, and solvated Cd$_8$(SC$_6$H$_4$Br−4)16 (DMF)$_3$ (DMF = dimethylformamide), in relation to the molecular structures of aggregates in solution. *Journal of the Chemical Society, Chemical Communications* **1987**, 1164–1167.

(173) Dance, I. G.; Garbutt, R. G.; Craig, D. C.; Scudder, M. L. The different non-molecular polyadamantanoid crystal structures of cadmium benzenethiolate and 4-methylbenzenethiolate. Analogies with microporous aluminosilicate frameworks. *Inorganic Chemistry* **1987**, *26*, 4057–4064.

(174) Anjali, K.; Vittal, J. J. Polylinked adamantanoid structure of Cd(SePh)$_2$. *Inorganic Chemistry Communications* **2000**, *3*, 708 – 710.

(175) Zhang, Q.; Bu, X.; Zhang, J.; Wu, T.; Feng, P. Chiral Semiconductor Frameworks

from Cadmium Sulfide Clusters. *Journal of the American Chemical Society* **2007**, *129*, 8412–8413.

(176) Zhang, Q.; Lin, Z.; Bu, X.; Wu, T.; Feng, P. Solvothermal Conversion of Discrete Cubic Cadmium Thiolate Cluster into Supertetrahedral Cluster Decorating Quartz-Type Chiral Superlattice. *Chemistry of Materials* **2008**, *20*, 3239–3241.

(177) Zhang, Q.; Liu, Y.; Bu, X.; Wu, T.; Feng, P. A Rare (3,4)-Connected Chalcogenide Superlattice and Its Photoelectric Effect. *Angewandte Chemie (International ed. in English)* **2008**, *47*, 113–116.

(178) Zheng, N.; Lu, H.; Bu, X.; Feng, P. Metal-Chelate Dye-Controlled Organization of $Cd_{32}S_{14}(SPh)_{40}{}^{4-}$ Nanoclusters into Three-Dimensional Molecular and Covalent Open Architecture. *Journal of the American Chemical Society* **2006**, *128*, 4528–4529.

(179) Wu, T.; Bu, X.; Liao, P.; Wang, L.; Zheng, S.-T.; Ma, R.; Feng, P. Superbase Route to Supertetrahedral Chalcogenide Clusters. *Journal of the American Chemical Society* **2012**, *134*, 3619–3622.

(180) Vaqueiro, P.; Romero, M. L. $[Ga_{10}S_{16}(NC_7H_9)_4]^{2}$: a hybrid supertetrahedral nanocluster. *Chemical Communications* **2007**, 3282–3284.

(181) Batten, S. R.; Champness, N. R.; Chen, X.-M.; Garcia-Martinez, J.; Kitagawa, S.; Öhrström, L.; O'Keeffe, M.; Paik Suh, M.; Reedijk, J. Terminology of metal–organic frameworks and coordination polymers (IUPAC Recommendations 2013). *Pure and Applied Chemistry* **2013**, *85*, 1715–1724.

(182) Rowsell, J. L.; Yaghi, O. M. Metal–organic frameworks: a new class of porous materials. *Microporous and Mesoporous Materials* **2004**, *73*, 3 – 14.

(183) James, S. L. Metal-organic frameworks. *Chemical Society Reviews* **2003**, *32*, 276–288.

(184) Xie, J.; Bu, X.; Zheng, N.; Feng, P. One-dimensional coordination polymers containing penta-supertetrahedral sulfide clusters linked by dipyridyl ligands. *Chemical Communications* **2005**, 4916–4918.

(185) Zheng, N.; Bu, X.; Lu, H.; Chen, L.; Feng, P. One-Dimensional Assembly of Chalcogenide Nanoclusters with Bifunctional Covalent Linkers. *Journal of the American Chemical Society* **2005**, *127*, 14990–14991.

(186) Zhang, Q.; Bu, X.; Lin, Z.; Wu, T.; Feng, P. Organization of Tetrahedral Chalcogenide Clusters Using a Tetrahedral Quadridentate Linker. *Inorganic Chemistry* **2008**, *47*, 9724–9726.

(187) Zheng, N.; Bu, X.; Lauda, J.; Feng, P. Zero- and Two-Dimensional Organization of Tetrahedral Cadmium Chalcogenide Clusters with Bifunctional Covalent Linkers. *Chemistry of Materials* **2006**, *18*, 4307–4311.

(188) Xu, C.; Han, Y.-G.; Duan, T.; Zhang, Q.-F.; Leung, W.-H. Two-dimensional assembly of the type $Cd_{10}Te_4$ thiolate cluster with 4,4-trimethylenedipyridine. *Inorganic Chemistry Communications* **2009**, *12*, 1053 – 1056.

(189) Chen, Z.; Luo, D.; Luo, X.; Kang, M.; Lin, Z. Two-dimensional assembly of tetrahedral chalcogenide clusters with tetrakis(imidazolyl)borate ligands. *Dalton Transactions* **2012**, *41*, 3942–3944.

(190) Vaqueiro, P.; Romero, M. L. GalliumSulfide Supertetrahedral Clusters as Building Blocks of Covalent OrganicInorganic Networks. *Journal of the American Chemical Society* **2008**, *130*, 9630–9631.

(191) Vaqueiro, P.; M, R.; Rowan, B.; Richards, B. Arrays of Chiral Nanotubes and a Layered Coordination Polymer Containing Gallium–Sulfide Supertetrahedral Clusters. *Chemistry - A European Journal* **2010**, *16*, 4462–4465.

(192) Vaqueiro, P.; Makin, S.; Tong, Y.; Ewing, S. J. A new class of hybrid super-supertetrahedral cluster and its assembly into a five-fold interpenetrating network. *Dalton Transactions* **2017**, *46*, 3816–3819.

(193) Yang, H.; Zhang, J.; Luo, M.; Wang, W.; Lin, H.; Li, Y.; Li, D.; Feng, P.; Wu, T. The Largest Supertetrahedral Oxychalcogenide Nanocluster and Its Unique Assembly. *Journal of the American Chemical Society* **2018**, *140*, 11189–11192.

(194) Manos, M. J.; Jang, J. I.; Ketterson, J. B.; Kanatzidis, M. G. $[Zn(H_2O)_4][Zn_2Sn_3Se_9(MeNH_2)]$: a robust open framework chalcogenide with a large nonlinear optical response. *Chemical Communications* **2008**, 972–974.

(195) Wu, T.; Khazhakyan, R.; Wang, L.; Bu, X.; Zheng, S.; Chau, V.; Feng, P. Three-Dimensional Covalent Co-Assembly between Inorganic Supertetrahedral Clusters and Imidazolates. *Angewandte Chemie (International ed. in English)* **2011**, *50*, 2536–2539.

(196) Zhang, J.; Wang, W.; Xue, C.; Zhao, M.; Hu, D.; Lv, J.; Wang, X.; Li, D.; Wu, T. Metal Chalcogenide Imidazolate Frameworks with Hybrid Intercluster Bridging Mode and Unique Interrupted Topological Structure. *Inorganic Chemistry* **2018**, *57*, 9790–9793.

(197) Hou, Y.; Wu, T.; Le Wang,; Feng, P. Integration of supertetrahedral cluster with reduced graphene oxide sheets for enhanced photostability and photoelectrochemical properties. *Science China Chemistry* **2013**, *56*, 423–427.

(198) Li, Z.-Q.; Mo, C.-J.; Guo, Y.; Xu, N.-N.; Zhu, Q.-Y.; Dai, J. Discrete supertetrahedral CuInS nanoclusters and their application in fabrication of cluster-sensitized TiO_2 photoelectrodes. *Journal of Materials Chemistry A* **2017**, *5*, 8519–8525.

(199) Liu, D.; Huang, P.; Liu, Y.; Wu, Z.; Li, D.; Guo, J.; Wu, T. Cd/In-Codoped TiO_2 nanochips for high-efficiency photocatalytic dye degradation. *Dalton Transactions* **2018**, *47*, 6177–6183.

(200) Liu, D.; Liu, Y.; Huang, P.; Zhu, C.; Kang, Z.; Shu, J.; Chen, M.; Zhu, X.; Guo, J.; Zhuge, L.; Bu, X.; Feng, P.; Wu, T. Highly Tunable Heterojunctions from Multimetallic Sulfide Nanoparticles and Silver Nanowires. *Angewandte Chemie (International ed. in English)* **2018**, *57*, 5374–5378.

(201) Hu, R.; Wang, X.-L.; Zhang, J.; Hu, D.; Wu, J.; Zhou, R.; Li, L.; Li, M.; Li, D.-S.; Wu, T. Multi–Metal Nanocluster Assisted Cu–Ga–Sn Tri–Doping for Enhanced Photoelectrochemical Water Splitting of $BiVO_4$ Film. *Advanced Materials Interfaces* **2020**, 2000016.

(202) Mao, C.; Wang, Y.; Jiao, W.; Chen, X.; Lin, Q.; Deng, M.; Ling, Y.; Zhou, Y.; Bu, X.; Feng, P. Integrating Zeolite-Type Chalcogenide with Titanium Dioxide Nanowires for Enhanced Photoelectrochemical Activity. *Langmuir* **2017**, *33*, 13634–13639.

(203) Hu, D.-D.; Lin, J.; Zhang, Q.; Lu, J.-N.; Wang, X.-Y.; Wang, Y.-W.; Bu, F.; Ding, L.-F.; Wang, L.; Wu, T. Multi-Step Host–Guest Energy Transfer Between Inorganic Chalcogenide-Based Semiconductor Zeolite Material and Organic Dye Molecules. *Chemistry of Materials* **2015**, *27*, 4099–4104.

(204) Hu, D.-D.; Wang, L.; Lin, J.; Bu, F.; Wu, T. Tuning the efficiency of multi-step energy transfer in a host–guest antenna system based on a chalcogenide semiconductor zeolite through acidification and solvation of guests. *Journal of Materials Chemistry C* **2015**, *3*, 11747–11753.

(205) Hu, D.; Wang, X.; Yang, H.; Liu, D.; Wang, Y.; Guo, J.; Wu, T. Host-guest electrocatalyst with cage-confined cuprous sulfide nanoparticles in etched chalcogenide semiconductor zeolite for highly efficient oxygen reduction reaction. *Electrochimica Acta* **2018**, *282*, 877 – 885.

(206) Zheng, N.; Bu, X.; Wang, B.; Feng, P. Synthetic design of crystalline inorganic chalcogenides exhibiting fast-ion conductivity. *Nature* **2003**, *426*, 428–432.

(207) Zheng, N.; Bu, X.; Feng, P. $Na_5(In_4S)(InS_4)_3 \cdot 6\,H_2O$, a Zeolite-like Structure with Unusual SIn_4 Tetrahedra. *Journal of the American Chemical Society* **2005**, *127*, 5286–5287.

(208) Walden, P. Molecular weights and electrical conductivity of several fused salts. *Bulletin of the Imperial Academy of Sciences (Saint Petersburg)* **1914**, *1800*, 405–422.

(209) Rogers, R. D.; Seddon, K. R. Ionic Liquids–Solvents of the Future? *Science* **2003**, *302*, 792–793.

(210) Parnham, E. R.; Morris, R. E. Ionothermal Synthesis of Zeolites, Metal–Organic Frameworks, and Inorganic–Organic Hybrids. *Accounts of Chemical Research* **2007**, *40*, 1005–1013.

(211) Freudenmann, D.; Wolf, S.; Wolff, M.; Feldmann, C. Ionic liquids: new perspectives for inorganic synthesis? *Angewandte Chemie (International ed. in English)* **2011**, *50*, 11050–11060.

(212) Cooper, E. R.; Andrews, C. D.; Wheatley, P. S.; Webb, P. B.; Wormald, P.; Morris, R. E. Ionic liquids and eutectic mixtures as solvent and template in synthesis of zeolite analogues. *Nature* **2004**, *430*, 1012–1016.

(213) Xiong, W.-W.; Li, J.-R.; Hu, B.; Tan, B.; Li, R.-F.; Huang, X.-Y. Largest discrete supertetrahedral clusters synthesized in ionic liquids. *Chemical Science* **2012**, *3*, 1200–1204.

(214) Lin, Y.; Massa, W.; Dehnen, S. "Zeoball" $[Sn_{36}Ge_{24}Se_{132}]^{24-}$: A Molecular Anion with Zeolite-Related Composition and Spherical Shape. *Journal of the American Chemical Society* **2012**, *134*, 4497–4500.

(215) Shen, N.-N.; Hu, B.; Cheng, C.-C.; Zou, G.-D.; Hu, Q.-Q.; Du, C.-F.; Li, J.-R.; Huang, X.-Y. Discrete Supertetrahedral T3 InQ Clusters (Q = S, S/Se, Se, Se/Te):

Ionothermal Syntheses and Tunable Optical and Photodegradation Properties. *Crystal Growth & Design* **2018**, *18*, 962–968.

(216) Hao, M.; Hu, Q.; Zhang, Y.; Luo, M.; Wang, Y.; Hu, B.; Li, J.; Huang, X. Soluble Supertetrahedral Chalcogenido T4 Clusters: High Stability and Enhanced Hydrogen Evolution Activities. *Inorganic Chemistry* **2019**, *58*, 5126–5133.

(217) Discrete Supertetrahedral T5 Selenide Clusters and Their Se/S Solid Solutions: Ionic-Liquid-Assisted Precursor Route Syntheses and Photocatalytic Properties. *Chemistry (Weinheim an der Bergstrasse, Germany)* **2020**, *26*, 1624–1632.

(218) Santner, S.; Dehnen, S. $[M_4Sn_4Se_{17}]^{10-}$ Cluster Anions (M = Mn, Zn, Cd) in a Cs^+ Environment and as Ternary Precursors for Ionothermal Treatment. *Inorganic Chemistry* **2015**, *54*, 1188–1190.

(219) Li, J.-R.; Xie, Z.-L.; He, X.-W.; Li, L.-H.; Huang, X.-Y. Crystalline open-framework selenidostannates synthesized in ionic liquids. *Angewandte Chemie (International ed. in English)* **2011**, *50*, 11395–11399.

(220) Lin, Y.; Dehnen, S. $[BMIm]_4[Sn_9Se_{20}]$: Ionothermal Synthesis of a Selenidostannate with a 3D Open-Framework Structure. *Inorganic Chemistry* **2011**, *50*, 7913–7915.

(221) Lin, Y.; Xie, D.; Massa, W.; Mayrhofer, L.; Lippert, S.; Ewers, B.; Chernikov, A.; Koch, M.; Dehnen, S. Changes in the Structural Dimensionality of Selenidostannates in Ionic Liquids: Formation, Structures, Stability, and Photoconductivity. *Chemistry – A European Journal* **2013**, *19*, 8806–8813.

(222) Lin, Y.; Massa, W.; Dehnen, S. Controlling the Assembly of Chalcogenide Anions in Ionic Liquids: From Binary Ge/Se through Ternary Ge/Sn/Se to Binary Sn/Se Frameworks. *Chemistry – A European Journal* **2012**, *18*, 13427–13434.

(223) Li, J.-R.; Xiong, W.-W.; Xie, Z.-L.; Du, C.-F.; Zou, G.-D.; Huang, X.-Y. From selenidostannates to silver-selenidostannate: structural variation of chalcogenidometallates synthesized in ionic liquids. *Chemical Communications* **2013**, *49*, 181–183.

(224) Du, C.-F.; Li, J.-R.; Feng, M.-L.; Zou, G.-D.; Shen, N.-N.; Huang, X.-Y. Varied forms of lamellar $[Sn_3Se_7]n^{2n}$ anion: the competitive and synergistic structure-directing effects of metal–amine complex and imidazolium cations. *Dalton Transactions* **2015**, *44*, 7364–7372.

(225) Santner, S.; Sprenger, J. A. P.; Finze, M.; Dehnen, S. The Role of $[BF_4]$ and $[B(CN)_4]$ Anions in the Ionothermal Synthesis of Chalcogenidometalates. *Chemistry – A European Journal* **2018**, *24*, 3474–3480.

(226) Xiong, W.-W.; Zhang, G.; Zhang, Q. New strategies to prepare crystalline chalcogenides. *Inorganic Chemistry Frontiers* **2014**, *1*, 292–301.

(227) Xiong, W.; Zhang, Q. Surfactants as Promising Media for the Preparation of Crystalline Inorganic Materials. *Angewandte Chemie (International ed. in English)* **2015**, *54*, 11616–11623.

(228) Li, J.; Delmotte, L.; Kessler, H. Synthesis and characterization of a novel mesostructured layered tin(IV) sulfide. *Chemical Communications* **1996**, 1023–1024.

(229) Li, J.; Kessler, H.; Delmotte, L. Study of novel mesostructured materials based on tin(IV) sulfide Part 1.—Synthesis and characterization. *Journal of the Chemical Society, Faraday Transactions* **1997**, *93*, 665–668.

(230) Li, J.; Marler, B.; Kessler, H.; Soulard, M.; Kallus, S. Synthesis, Structure Analysis, and Characterization of a New Thiostannate, $(C_{12}H_{25}NH_3)_4[Sn_2S_6]\cdot 2\,H_2O$. *Inorganic Chemistry* **1997**, *36*, 4697–4701.

(231) Bonhomme, F.; Kanatzidis, M. G. Structurally Characterized Mesostructured Hybrid SurfactantInorganic Lamellar Phases Containing the Adamantane $[Ge_4S_{10}]^{4-}$ Anion: Synthesis and Properties. *Chemistry of Materials* **1998**, *10*, 1153–1159.

(232) MacLachlan, M. J.; Coombs, N.; Ozin, G. A. Non-aqueous supramolecular assembly of mesostructured metal germanium sulphides from $(Ge_4S_{10})^4$ clusters. *Nature* **1999**, *397*, 681–684.

(233) Rangan, K. K.; Kanatzidis, M. G. Mesolamellar thiogermanates $[CnH_2n_1{}^+NH_3]_4Ge_4S_{10}$. *Inorganica Chimica Acta* **2004**, *357*, 4036 – 4044.

(234) Wachhold, M.; Kanatzidis, M. G. Surfactant-Templated Inorganic Lamellar and Non-Lamellar Hybrid Phases Containing Adamantane $[Ge_4Se_{10}]^{4-}$ Anions. *Chemistry of Materials* **2000**, *12*, 2914–2923.

(235) Eichhöfer, A.; Hampe, O.; Blom, M. Synthesis, Structures, and Properties of a Series of $[Cd_8Se(SePh)_{12}Cl_4]^2$ Cluster Compounds with Different Counterions. *European Journal of Inorganic Chemistry* **2003**, *2003*, 1307–1314.

(236) Xiong, W.-W.; Athresh, E. U.; Ng, Y. T.; Ding, J.; Wu, T.; Zhang, Q. Growing Crystalline Chalcogenidoarsenates in Surfactants: From Zero-Dimensional Cluster to Three-Dimensional Framework. *Journal of the American Chemical Society* **2013**, *135*, 1256–1259.

(237) Xiong, W.-W.; Li, P.-Z.; Zhou, T.-H.; Tok, A. I. Y.; Xu, R.; Zhao, Y.; Zhang, Q. Kinetically Controlling Phase Transformations of Crystalline Mercury Selenidostannates through Surfactant Media. *Inorganic Chemistry* **2013**, *52*, 4148–4150.

(238) Gao, J.; Tay, Q.; Li, P.-Z.; Xiong, W.-W.; Zhao, Y.; Chen, Z.; Zhang, Q. Surfactant–Thermal Method to Synthesize a Novel Two-Dimensional Oxochalcogenide. *Chemistry – An Asian Journal* **2014**, *9*, 131–134.

(239) Zhang, G.; Li, P.; Ding, J.; Liu, Y.; Xiong, W.-W.; Nie, L.; Wu, T.; Zhao, Y.; Tok, A. I. Y.; Zhang, Q. Surfactant-Thermal Syntheses, Structures, and Magnetic Properties of Mn–Ge–Sulfides/Selenides. *Inorganic Chemistry* **2014**, *53*, 10248–10256.

(240) Shen, Y.; Liu, C.; Hou, P.; Zhi, M.; Zhou, C.; Chai, W.; Cheng, J.; Liu, Y.; Zhang, Q. Preparation of Porous Three-Dimensional Quaternary Thioantimonates(III) $ACuSb_2S_4$ (A=Rb, Cs) through a Surfactant-Thermal Method. *Chemistry – An Asian Journal* **2015**, *10*, 2604–2608.

(241) Xiong, W.; Miao, J.; Ye, K.; Wang, Y.; Liu, B.; Zhang, Q. Threading Chalcogenide Layers with Polymer Chains. *Angewandte Chemie (International ed. in English)* **2015**, *54*, 546–550.

(242) Suppan, P., Ed. *Chemistry and Light*; The Royal Society of Chemistry, 1994; pp 1–10.

(243) Coronado, J. M.; Fresno, F.; Hernández-Alonso, M. D.; Portela, R. *Design of Advanced Photocatalytic Materials for Energy and Environmental Applications*; Springer London: London, 2013.

(244) Whipple, D. T.; Kenis, P. J. A. Prospects of CO_2 Utilization via Direct Heterogeneous Electrochemical Reduction. *The Journal of Physical Chemistry Letters* **2010**, *1*, 3451–3458.

(245) Najafabadi, A. T. CO_2 chemical conversion to useful products: An engineering insight to the latest advances toward sustainability. *International Journal of Energy Research* **2013**, *37*, 485–499.

(246) Lewis, N. S.; Nocera, D. G. Powering the planet: Chemical challenges in solar energy utilization. *Proceedings of the National Academy of Sciences* **2006**, *103*, 15729–15735.

(247) Laursen, A. B.; Kegnæs, S.; Dahl, S.; Chorkendorff, I. Molybdenum sulfides—efficient

and viable materials for electro - and photoelectrocatalytic hydrogen evolution. *Energy & Environmental Science* **2012**, *5*, 5577–5591.

(248) Osterloh, F. E. Inorganic nanostructures for photoelectrochemical and photocatalytic water splitting. *Chemical Society Reviews* **2013**, *42*, 2294–2320.

(249) Reza Gholipour, M.; Dinh, C.-T.; Béland, F.; Do, T.-O. Nanocomposite heterojunctions as sunlight-driven photocatalysts for hydrogen production from water splitting. *Nanoscale* **2015**, *7*, 8187–8208.

(250) Serpone, N. Relative photonic efficiencies and quantum yields in heterogeneous photocatalysis. *Journal of Photochemistry and Photobiology A: Chemistry* **1997**, *104*, 1 – 12.

(251) Kong, D.; Zheng, Y.; Kobielusz, M.; Wang, Y.; Bai, Z.; Macyk, W.; Wang, X.; Tang, J. Recent advances in visible light-driven water oxidation and reduction in suspension systems. *Materials Today* **2018**, *21*, 897 – 924.

(252) Usubharatana, P.; McMartin, D.; Veawab, A.; Tontiwachwuthikul, P. Photocatalytic Process for CO_2 Emission Reduction from Industrial Flue Gas Streams. *Industrial & Engineering Chemistry Research* **2006**, *45*, 2558–2568.

(253) Maeda, K.; Domen, K. New Non-Oxide Photocatalysts Designed for Overall Water Splitting under Visible Light. *The Journal of Physical Chemistry C* **2007**, *111*, 7851–7861.

(254) Chang, X.; Wang, T.; Gong, J. CO_2 photo-reduction: insights into CO_2 activation and reaction on surfaces of photocatalysts. *Energy & Environmental Science* **2016**, *9*, 2177–2196.

(255) Millman, J.; Halkias, C. C. *Integrated Electronics: Analog and Digital Circuits and Systems*; McGraw-Hill, 1972.

(256) Dincer, I.; Zamfirescu, C. In *Sustainable Hydrogen Production*; Dincer, I., Zamfirescu, C., Eds.; Elsevier, 2016; pp 309 – 391.

(257) Sumanth Kumar, D.; Jai Kumar, B.; Mahesh, H. In *Synthesis of Inorganic Nanomaterials*; Mohan Bhagyaraj, S., Oluwafemi, O. S., Kalarikkal, N., Thomas, S., Eds.; Micro and Nano Technologies; Woodhead Publishing, 2018; pp 59 – 88.

(258) Tomkiewicz, M.; Fay, H. Photoelectrolysis of water with semiconductors. *Journal of Applied Physics* **1979**, *18*.

(259) Hernández-Alonso, M. D.; Fresno, F.; Suárez, S.; Coronado, J. M. Development of alternative photocatalysts to TiO_2: Challenges and opportunities. *Energy & Environmental Science* **2009**, *2*, 1231–1257.

(260) Matsumura, M.; Furukawa, S.; Saho, Y.; Tsubomura, H. Cadmium sulfide photocatalyzed hydrogen production from aqueous solutions of sulfite: effect of crystal structure and preparation method of the catalyst. *The Journal of Physical Chemistry* **1985**, *89*, 1327–1329.

(261) Kudo, A.; Nagane, A.; Tsuji, I.; Kato, H. H_2 Evolution from Aqueous Potassium Sulfite Solutions under Visible Light Irradiation over a Novel Sulfide Photocatalyst NaInS2 with a Layered Structure. *Chemistry Letters* **2002**, *31*, 882–883.

(262) Hao, M.-T.; Hu, Q.-Q.; Li, J.-R.; Huang, X.-Y. Ionothermal synthesis of $Zn_{1x}Cd_xS$ solid solutions with efficient photocatalytic H_2 production via elemental-direct-reactions. *Inorganic Chemistry Communications* **2018**, *93*, 20 – 24.

(263) Mikkelsen, M.; Jørgensen, M.; Krebs, F. C. The teraton challenge. A review of fixation and transformation of carbon dioxide. *Energy & Environmental Science* **2010**, *3*, 43–81.

(264) Jiang, Z.; Xiao, T.; Kuznetsov, V. L.; Edwards, P. P. Turning carbon dioxide into fuel. *Philosophical Transactions of the Royal Society A: Mathematical, Physical and Engineering Sciences* **2010**, *368*, 3343–3364.

(265) Orr, Jr., F. M. CO_2 capture and storage: are we ready? *Energy & Environmental Science* **2009**, *2*, 449–458.

(266) Bachu, S.; Celia, M. A. In *Carbon Sequestration and Its Role in the Global Carbon Cycle*; McPherson, B. J., Sundquist, E. T., Eds.; Geophysical Monograph Series; American Geophysical Union: Washington, D. C., 2009; Vol. 183; pp 203–216.

(267) Wang, W.-N.; Soulis, J.; Yang, Y. J.; Biswas, P. Comparison of CO_2 Photoreduction Systems: A Review. *Aerosol and Air Quality Research* **2014**, *14*, 533–549.

(268) Centi, G.; Perathoner, S. Opportunities and prospects in the chemical recycling of carbon dioxide to fuels. *Catalysis Today* **2009**, *148*, 191 – 205, Special Issue of the 10th International Conference on CO_2 Utilization, Tianijn, China, May 17-21, 2009.

(269) Inoue, T.; Jujoshima, A.; Konishi, S.; Honda, K. Photoelectrocatalytic reduction of carbon dioxide in aqueous suspensions of semiconductor powders. *Nature* **1979**, *277*, 637–638.

(270) Kumaravel, V.; Bartlett, J.; Pillai, S. C. Photoelectrochemical Conversion of Carbon Dioxide (CO_2) into Fuels and Value-Added Products. *ACS Energy Letters* **2020**, *5*, 486–519.

(271) Kumar, B.; Llorente, M.; Froehlich, J.; Dang, T.; Sathrum, A.; Kubiak, C. P. Photochemical and Photoelectrochemical Reduction of CO_2. *Annual Review of Physical Chemistry* **2012**, *63*, 541–569.

(272) Bernadet, S.; Tavernier, E.; Ta, D.-M.; Vallée, R. A. L.; Ravaine, S.; Fécant, A.;

Backov, R. Bulk Photodriven CO_2 Conversion through TiO_2@Si(HIPE) Monolithic Macrocellular Foams. *Advanced Functional Materials* **2019**, *29*, 1807767.

(273) Habisreutinger, S. N.; Schmidt-Mende, L.; Stolarczyk, J. K. Photocatalytic Reduction of CO_2 on TiO_2 and Other Semiconductors. *Angewandte Chemie International Edition* **2013**, *52*, 7372–7408.

(274) Goren, Z.; Willner, I.; Nelson, A. J.; Frank, A. J. Selective photoreduction of carbon dioxide/bicarbonate to formate by aqueous suspensions and colloids of palladium-titania. *The Journal of Physical Chemistry* **1990**, *94*, 3784–3790.

(275) Li, K.; Peng, B.; Peng, T. Recent Advances in Heterogeneous Photocatalytic CO_2 Conversion to Solar Fuels. *ACS Catalysis* **2016**, *6*, 7485–7527.

(276) Indrakanti, V. P.; Kubicki, J. D.; Schobert, H. H. Photoinduced activation of CO_2 on Ti-based heterogeneous catalysts: Current state, chemical physics-based insights and outlook. *Energy & Environmental Science* **2009**, *2*, 745–758.

(277) Halmann, M.; Katzir, V.; Borgarello, E.; Kiwi, J. Photoassisted carbon dioxide reduction on aqueous suspensions of titanium dioxide. *Solar Energy Materials* **1984**, *10*, 85 – 91.

(278) Tennakone, K. Photoreduction of carbonic acid by mercury coated n-titanium dioxide. *Solar Energy Materials* **1984**, *10*, 235 – 238.

(279) feng Xie, T.; jun Wang, D.; jie Zhu, L.; jin Li, T.; jun Xu, Y. Application of surface photovoltage technique in photocatalysis studies on modified TiO_2 photo-catalysts for photo-reduction of CO_2. *Materials Chemistry and Physics* **2001**, *70*, 103 – 106.

(280) Tseng, I.-H.; Chang, W.-C.; Wu, J. C. Photoreduction of CO_2 using sol–gel derived titania and titania-supported copper catalysts. *Applied Catalysis B: Environmental* **2002**, *37*, 37 – 48.

(281) Tseng, I.-H.; Wu, J. C.; Chou, H.-Y. Effects of sol–gel procedures on the photocatalysis of Cu/TiO_2 in CO_2 photoreduction. *Journal of Catalysis* **2004**, *221*, 432 – 440.

(282) Liu, S.; Yu, J.; Jaroniec, M. Tunable Photocatalytic Selectivity of Hollow TiO_2 Microspheres Composed of Anatase Polyhedra with Exposed 001 Facets. *Journal of the American Chemical Society* **2010**, *132*, 11914–11916.

(283) Cheng, H.; Huang, B.; Liu, Y.; Wang, Z.; Qin, X.; Zhang, X.; Dai, Y. An anion exchange approach to Bi2WO6 hollow microspheres with efficient visible light photocatalytic reduction of CO_2 to methanol. *Chemical Communications* **2012**, *48*, 9729–9731.

(284) Liu, Q.; Zhou, Y.; Kou, J.; Chen, X.; Tian, Z.; Gao, J.; Yan, S.; Zou, Z. High-Yield Synthesis of Ultralong and Ultrathin Zn_2GeO_4 Nanoribbons toward Improved Photocatalytic Reduction of CO_2 into Renewable Hydrocarbon Fuel. *Journal of the American Chemical Society* **2010**, *132*, 14385–14387.

(285) Li, P.; Zhou, Y.; Zhao, Z.; Xu, Q.; Wang, X.; Xiao, M.; Zou, Z. Hexahedron Prism-Anchored Octahedronal CeO_2: Crystal Facet-Based Homojunction Promoting Efficient Solar Fuel Synthesis. *Journal of the American Chemical Society* **2015**, *137*, 9547–9550.

(286) Wang, S.; Guan, B. Y.; Lu, Y.; Lou, X. W. ormation of Hierarchical $In_2S_3In_2S_3$ Heterostructured Nanotubes for Efficient and Stable Visible Light CO_2 Reduction. *Journal of the American Chemical Society* **2017**, *139*, 17305–17308.

(287) Wu, H.-L.; Li, X.-B.; Tung, C.-H.; Wu, L.-Z. Semiconductor Quantum Dots: An Emerging Candidate for CO_2 Photoreduction. *Advanced materials (Deerfield Beach, Fla.)* **2019**, *31*, 1900709.

(288) Hiragond, C.; Ali, S.; Saurav, S. Hierarchical Nanostructured Photocatalysts for CO_2 Photoreduction. *Catalysts* **2019**, *9*, 370.

(289) Yan, Y.; Crisp, R. W.; Gu, J.; Chernomordik, B. D.; Pach, G. F.; Marshall, A. R.; Turner, J. A.; Beard, M. C. Multiple exciton generation for photoelectrochemical hydrogen evolution reactions with quantum yields exceeding 100%. *Nature Energy* **2017**, *2*.

(290) Zhang, P.; Wang, S.; Guan, B. Y.; Lou, X. W. Fabrication of CdS hierarchical multicavity hollow particles for efficient visible light CO_2 reduction. *Energy & Environmental Science* **2019**, *12*, 164–168.

(291) Jin, J.; Yu, J.; Guo, D.; Cui, C.; Ho, W. A Hierarchical Z-Scheme CdS-WO_3 Photocatalyst with Enhanced CO_2 Reduction Activity. *Small (Weinheim an der Bergstrasse, Germany)* **2015**, *11*, 5262–5271.

(292) Xu, F.; Zhang, J.; Zhu, B.; Yu, J.; Xu, J. $CuInS_2$ sensitized TiO_2 hybrid nanofibers for improved photocatalytic CO_2 reduction. *Applied Catalysis B: Environmental* **2018**, *230*, 194 – 202.

(293) Xu, F.; Zhu, B.; Cheng, B.; Yu, J.; Xu, J. 1D/2D TiO_2 /MoS_2 Hybrid Nanostructures for Enhanced Photocatalytic CO_2 Reduction. *Advanced Optical Materials* **2018**, *6*, 1800911.

(294) Wang, S.; Guan, B. Y.; Lou, X. W. D. Construction of $ZnIn_2S_4$–In_2O_3 Hierarchical Tubular Heterostructures for Efficient CO_2 Photoreduction. *Journal of the American Chemical Society* **2018**, *140*, 5037–5040.

(295) Jung, H.; Cho, K. M.; Kim, K. H.; Yoo, H.-W.; Al-Saggaf, A.; Gereige, I.; Jung, H.-T. Highly Efficient and Stable CO_2 Reduction Photocatalyst with a Hierarchical Structure of Mesoporous TiO_2 on 3D Graphene with Few-Layered MoS_2. *ACS Sustainable Chemistry & Engineering* **2018**, *6*, 5718–5724.

(296) Low, J.; Cao, S.; Yu, J.; Wageh, S. Two-dimensional layered composite photocatalysts. *Chemical Communications* **2014**, *50*, 10768–10777.

(297) Jiao, X.; Chen, Z.; Li, X.; Sun, Y.; Gao, S.; Yan, W.; Wang, C.; Zhang, Q.; Lin, Y.; Luo, Y.; Xie, Y. Defect-Mediated Electron–Hole Separation in One-Unit-Cell $ZnIn_2S_4$ Layers for Boosted Solar-Driven CO_2 Reduction. *Journal of the American Chemical Society* **2017**, *139*, 7586–7594.

(298) Yuan, J.; Hao, C. Solar-driven photoelectrochemical reduction of carbon dioxide to methanol at $CuInS_2$ thin film photocathode. *Solar Energy Materials and Solar Cells* **2013**, *108*, 170 – 174, Selected publications from the 22nd Space Photovoltaic Research and Technology (SPRAT) Conference.

(299) Chen, J.; Xin, F.; Yin, X.; Xiang, T.; Wang, Y. Synthesis of hexagonal and cubic $ZnIn_2S_4$ nanosheets for the photocatalytic reduction of CO_2 with methanol. *RSC Advances* **2015**, *5*, 3833–3839.

(300) Li, X.; Sun, Y.; Xu, J.; Shao, Y.; Wu, J.; Xu, X.; Pan, Y.; Ju, H.; Zhu, J.; Xie, Y. Selective visible-light-driven photocatalytic CO_2 reduction to CH_4 mediated by atomically thin $CuIn_5S_8$ layers. *Nature Energy* **2019**, *4*, 690–699.

(301) Sasan, K.; Lin, Q.; Mao, C.; Feng, P. Open framework metal chalcogenides as efficient photocatalysts for reduction of CO_2 into renewable hydrocarbon fuel. *Nanoscale* **2016**, *8*, 10913–10916.

(302) Augugliaro, V.; Litter, M.; Palmisano, L.; Soria, J. The combination of heterogeneous photocatalysis with chemical and physical operations: A tool for improving the photoprocess performance. *Journal of Photochemistry and Photobiology C: Photochemistry Reviews* **2006**, *7*, 127 – 144.

(303) Gaya, U. I.; Abdullah, A. H. Heterogeneous photocatalytic degradation of organic contaminants over titanium dioxide: A review of fundamentals, progress and problems. *Journal of Photochemistry and Photobiology C: Photochemistry Reviews* **2008**, *9*, 1 – 12.

(304) Zhao, J.; Yang, X. Photocatalytic oxidation for indoor air purification: a literature review. *Building and Environment* **2003**, *38*, 645 – 654.

(305) Huang, D.; Chen, S.; Zeng, G.; Gong, X.; Zhou, C.; Cheng, M.; Xue, W.; Yan, X.; Li, J. Artificial Z-scheme photocatalytic system: What have been done and where to go? *Coordination Chemistry Reviews* **2019**, *385*, 44 – 80.

(306) Li, J.; Jiménez-Calvo, P.; Paineau, E.; Ghazzal, M. N. Metal Chalcogenides Based Heterojunctions and Novel Nanostructures for Photocatalytic Hydrogen Evolution. *Catalysts* **2020**, *10*.